Master's Thesis
MsC Degree in Aeronautical Engineering

Design of a Plasma Actuator Based on Dielectric Barrier Discharge (DBD)

Author: **Mª Scherezade Balsera Barquero**

Tutors: *José Cotrino Bautista*, Chair in Physiscs

Ana María Gómez Ramírez, PhD in Physics

Antonio Franco Espín, PhD in Aeronautical Engineering

Dept. Aerospace Engineering and Fluid Mechanics

Higher Technical School of Engineering

University of Seville

Sevilla, 2018

Master's Thesis
MsC Degree in Aeronautical Engineering

Design of a Plasma Actuator Based on Dielectric Barrier Discharge (DBD)

Author:

Mª Scherezade Balsera Barquero

Tutors:

José Cotrino Bautista, Chair in Physiscs

Ana María Gómez Ramírez, PhD in Physics

Antonio Franco Espín, PhD in Aeronautical Engineering

Dept. Aerospace Engineering and Fluid Mechanics
Higher Technical School of Engineering
University of Seville

Sevilla, 2018

Master's Thesis: Design of a Plasma Actuator Based on Dielectric Barrier Discharge (DBD)

Author: **Mª Scherezade Balsera Barquero**

Tutors: *José Cotrino Bautista*, Chair in Physiscs

Ana María Gómez Ramírez, PhD in Physics

Antonio Franco Espín, PhD in Aeronautical Engineering

The tribunal appointed to judge the work indicated above, which is composed of the following professors:

President:

Vocal/s:

Secretary:

agree to grant her the qualification of:

The secretary of the tribunal

Date:

Acknowledgement

First of all, thanks to the Surface Nanotechnology Area of the Isla de la Cartuja Scientific Research Center for having allowed me to use its facilities and equipment for the development of this Master's Thesis, and thanks to all its researchers I met because I have enjoyed a lot contemplating the work ambient of research world. Special thanks to the Professor José Cotrino Bautista, for accepting being my tutor almost a year ago when I went to the Faculty of Physics to ask him if I could develop a project with plasma, transmitting his knowledge with a facilitating role and proactive attitude; and of course, to Paula de Navascués Garvín, for her support; I learned a lot from you, Paula. Thank you very much to you both. I have been enthusiasted with every step that the work went through.

Two years ago I wrote the acknowledgments of my Final Bachelor's Degree Project from this same table, excited for a new stage, but also aware of the effort that a master's degree of this size would require; and at that moment, I promised myself that during those two years I would squeeze the time to the maximum, and at the same time that I am moving a little further towards my dream of building spaceship engines, I was not going to abandon any of the other aspects of life that are also part of what I am. Today, proud, I can say now that during the two years that this Master's Degree has taken –that brought me to new classrooms, new streets and new people– that I achieved it. So, thanks for the engineering knowledge and all the opportunities for personal and professional growth provided and taken, for having felt part of this university, for having known great professionals (both proffessors and colleagues), and because these years have led me to have better criteria and to feel more confident with my ability to work. Again, I have enjoyed a lot learning and doing. It was an honor for me to have been able to make the speeches for both Aerospace Engineering and Aeronautical Engineering, because they are my sincere thanks to life and my reconciliation with all the futures that come, came or will come.

To Sevilla, for all the hearts and minds that it has given me the opportunity to meet, really thanks; from the full days in Cartuja to the nightly promenade along the bank of the Guadalquivir, from which we have built years with only hours rediscovering ourselves. Thank you, Luis, for your support 'to the vacuum and back'; always I will have a memories-stop in my Elves Place. Thanks to my family, for a support and motivation full of love; to her, our angel, to my four "frústrate" siblings, Almudena, Carolina, Inés y Pedro Antonio, to my grandmother Inés and, without doubt, to my mother, Toni. Absolutamente gracias, mamá, como siempre.

Good luck, Scherezade.

Abstract

Related with recent investigations, plasma actuator or plasma controller has been the most promising flow control device, and specifically the Dielectric Barrier Discharge flow controller (usually called DBD plasma actuator). The popularity of these devices comes from the advantages offered by a lower weight and size, absence of moving parts that would mean, for example, less drag and possible reduction in maintenance.

The experimental study carried out during the last months has been exposed in this document, through which a a large number of different devices have been built, seeking to identify which factors contribute to a maximization of the efficiency in terms of different parameters, of plasma generation devices through Dielectric Barrier Discharge (DBD). For this purpose, the operation and performance of the different configurations of the DBD plasma actuator were carried out, having into account frequency, pressure, substrate materials and geometrical configuration of the electrodes; and they have been characterized and quantified from a fundamentally electrical point of view. In addition, optical spectroscopic analyzes of the plasma generated were done.

The use of ferroelectric materials such as lithium niobate allows to provide new approaches to traditional studies. Also, it has been able to successfully compare the conclusions derived from this work with other published studies.

Keywords

DielectricBarrierDischarge, Plasma, Actuator, Capacitance, microplasma

Index

Notation

v_{T_e}	Average quadratic velocity
k	Boltzmann constant
Q	Charge
I	Current
α	Degree of Ionization
n	Density
$\overrightarrow{v_d}$	Drag or drift velocity
$\overrightarrow{E}$	Electric field
s	Electrode longitude
$\nu_{e,i}$	Electron-ion collision frequency
$\nu_{e,n}$	Electron-neutral collision frequency
ν_e	Electron plasma frequency
a	Exposed electrode width
f	Frequency
p	Gas pressure
b	Ground electrode width
h	Height between exposed-ground electrodes
Z	Impedance
T	Kinetic temperature
T'	Kinetic temperature expressed in eV
λ_D	Length of Debye
m	Mass
μ	Mobility
Λ	Plasma Parameter
L	Plasma size

ε	Permittivity
ϕ	Phase difference
P	Power
X_{bd}	Referred to “breakdown”
X_e	Referred to electrons
X_i	Referred to ions
X_n	Referred to neutral particles
ε_r	Relative Permittivity or Dielectric constant
R	Resistance
γ_{es}	Secondary electron emission coefficient in the cathode
S	Surface/A of the dielectric
t	Time/Thickness
ε_0	Vacuum permittivity
V	Voltage
λ	Wavelength

1 Introduction

Laws of physics never stop surprising us as we go deeper into their knowledge, while it offers us new and fascinating challenges to embark on after each advance, especially to scientists and engineers.

Within these innumerable fascinating fields of study, both technological and purely scientific, to which physics open its doors, lies the generation of artificial plasmas and all the practical possibilities that their properties allow. Thus, this work will focus on taking advantage of certain properties to incorporate them into aeronautical engineering, specifically the control of aerodynamic flow; regarding which it is remarkable the number of investigations and relevant developments have taken place in recent years. Related with those investigations, plasma actuator or plasma controller has been the most promising flow control device, and in particular the Dielectric Barrier Discharge flow controller (usually called DBD plasma actuator).

1.1 Objective

As a theoretical concept, the DBD plasma actuator stands out as a good alternative to, for example, the use of mobile parts in the wing for the control of surrounding flow; however, it is not yet used as an application for real use. That is why, despite the fact that there are numerous publications about it, it is still necessary to continue delving into the analysis of its performance, effectiveness and efficiency; since there are still limits to improve and barriers to overcome. This has been the reason that has led to this master's thesis to choose this line of research as a topic, pretending to contribute to the advances in this field.

The questions that are asked must be answered in a more precise and systematic way, for which different paths can be followed. As can be seen from the reference literature, the importance of offering systematic and quantitative answers regarding the operation of plasma actuators arises from the existing need that requires objective parameters that allow comparing the different designs that are studied between the different groups of research, alluding to the advantages that could be derived from the use of specific dimensionless parameters for the DBD actuator, since without them the comparison between the different published studies becomes more complex. In turn, the advance

in numerical models on plasmas so that the simulations are more detailed and realistic, while considering the operational conditions of the DBD flow controllers, represents an important line of research in which to advance.

Throughout this work, the characterization and quantification of the operation and yield of the DBD controller is examined in detail, through the electrical and spectroscopic magnitudes, thus employing a macroscopic and optical vision respectively of the concept as a tool to quantify its performance. The experimental study has been developed by varying the frequency of the discharge in a range of low frequencies (1-15 kHz): the type of dielectric material used as a substrate or barrier, the geometrical configuration of the electrodes (specially to study the influence of the gap between active and encapsulated electrode) and the pressure, having experimented with near than twenty different devices that have been manufactured for that purpose. So, summarizing, these are the objectives of this project:

1. Review of existing academic literature on this issue.
2. Learn how to develop a DBD actuator.
3. Build and test different DBD actuator designs varying electrodes geometry, dielectric material, frequency and pressure.
4. Use different programs to analyze the voltage and current signals of the generated DBD plasma.

All measurements will be saved in the voltage value in which it is noticeable to the naked eye the appearance of plasma in the devices. This point will be called interchangeably **"breakdown" value** or ignition value of the plasma.

It is important to note that in this document when referring to the concept of "**efficiency**", this is related to the voltage necessary to achieve the ignition of the plasma; the more efficient the device will be, the lower the voltage it needs to produce plasma.

1.2 Methodology

After presenting a broad study about the theoretical basis that support this experimental project, this document presents everything related to manufacturing and experimentation with different devices, including reasons, results and conclusions about each step, in order to give response to the claims presented in Section 1.1. As explained in the previous section, in this work one can find both electrical and spectroscopic analysis of these DBD plasma actuators, and the study has been developed according to the frequency of the input signal (in a range from 1 kHz to 15 kHz), the pressure of the ambient (from ambient conditions to values of reduced pressure of 20 mbar), the type of substrate or barrier dielectric material used in the device (quartz, alumina and lithium niobate) and the geometrical configuration of its electrodes (with special attention in the influence of gap). To achieve the proposed objectives, the experiments have been framed within four different phases of study, in which particular approaches are had into account.These phases and their purposes are the following:

- ***Phase 1**: Basis functional study of DBD actuator with the aim of generating the largest possible amount of surface covered with plasma*

  In this first phase it has been studied, mainly, the efficiency of different configurations of a DBD Actuator with, as explained, the aim of generating the largest possible amount of surface covered with plasma, on the dielectric layer. For this purpose, reactors with three different electrode configurations (A, B y C) have been designed, manufactured and powered, and in addition, the effect on two different dielectric materials has been checked: quartz (SiO_2) and lithium niobate ($LiNbO_3$). At the end, 4 devices in total have been developed and tested: Experiments 1 to 4 –see Table 3.1–.

- ***Phase 2**: Influence of dimension of gap*

  To this goal, reactors that have been fed they share the same configuration regarding: the shape, number and function of the electrodes used, composed of an active electrode with a narrow band on the upper face and another with the same characteristics on the lower face but in this case connected to ground, that is, Type D configuration. This configuration of electrodes has been mounted on 3 different types of substrates, thus having 3 different device species, to which the size of the gap between both electrodes has been varied; for each device, 4 measurements have been made according to the gap: 5 mm, 2,5 mm, 1 mm and canceling the gap. The substrates used were: quartz (SiO_2), alumina ($Al2O_3$) and lithium niobate ($LiNbO_3$). In total, 12 different devices have been built and tested: Experiments 5 to 16 –see Table 3.1–.

- ***Phase 3**: Active muti-electrode configurations*

  Phase 3 is presented as an evolution of phase 2. In it, active multi-electrode configurations are studied, as a result of a series of type D configurations adjacent to each other, it means, alternating conductive and insulating bands. At the end, 3 devices in total have been developed and tested: Experiments 17 to 19 –see Table 3.1–.

- ***Phase 4**: Experimentation with airflow and at reduced pressure*

  All the experiments from Phase 1 to 3 have been tested in atmospheric pressure and calm atmosphere (laboratory conditions), except finally in Phase 4, in which the multi-band device on lithium niobate had been, on the one hand faced with an air flow and on the other hand tested at reduced pressure. Experiments 20 and 21, respectively –see Table 3.1–.

The fact of sometimes maintaining the same geometric structure and varying the substrate material, as well as, conversely, maintaining the same barrier material and studying different electrode configurations, makes possible to establish comparisons between the different results. The chosen mode of comparative analysis is based on electrical and spectroscopic characterization, for which the necessary equipment circuits are assembled and explained in the Section 3.4.

The electrical characterization will be carried out from measurements of current and voltage as a function of time obtained for each of the experiments tested as a function of frequency. Both signals have been analyzed, and from which the rest of the electrical magnitudes have been calculated and the appropriate graphs have been constructed.

Regarding the spectroscopic characterization, it has been done by using a monochromator to, in this way, collect the optical emission spectrum of the air plasma excited by the surface DBD discharge; and the objective is to identify the composition of the plasma generated.

Respect to the way to expose the results, they have been collected in the same chapter (Chapter 4), and explained differentiating by operational parameter of study. Finally, in Chapter 5, about conclusions, the results obtained during this master‘s thesis are compared to other published studies (or completing conclusions with them), as well as they have been related to Paschen representations.

Excel Spreadsheets, Matlab and OriginPro have been used to process and visualize the data.

1.3 Structure of the document

This document is divided into five chapters and three appendices, whose content is briefly explained in the following enumeration:

- **Chapter 1: Introduction**

  Include objectives –Section 1.1–, methodology –Section 1.2– and structure of the document –Section 1.3–.

- **Chapter 2: Theoretical basis**

  In this chapter, as an introduction, a summary of the main characteristics that define, firstly, the plasma state will be presented –Section 2.1–, to later describe the operation of an aerodynamic flow controller through Dielectric Barrier Discharge –Section 2.2– and, finally, specify what are the general terms of the electrical and spectroscopic analysis that will be carried out –Section 2.3–.

  With this knowledge base, it is tried to familiarize ourselves with the classifications of different types of DBD plasma controller, and thus be able to understand their different applications based on quantifiable parameters.

- **Chapter 3: Design and Construction of DBD plasma controllers**

  In this chapter, specifically in Section 3.1, are explained all the study phases –and consequently, its devices– and the reasons why the different configurations were carried out; that is, the design and construction of the DBD Plasma Actuator. Each one of these devices used will be presented in order to characterize them to understand the differences between the data obtained from their analysis, which will be shown in Chapter 4. Also, in Section 3.2 and 3.3 a series of considerations regarding the manufacturing of the devices and about the experimentation are collected respectively; and, finally the experimental procedure and its necessary resources and considerations will be shown in Section 3.4, including electrical and spectroscopic procedures and equipment.

- **Chapter 4: Analysis and Results**

  In this chapter the results obtained after carrying out all the experiments and their respective analysis are presented, from Phase 1 to 4, including comparisons according to the substrate material, the geometric

configuration of the devices and influence of pressure and frequency. The results are exposed differentiating by operational parameter of study.

- **Chapter 5: Conclusions**

  In this last chapter are presented the conclusions of this work according to the objectives presented in Section 1.1: influence of dielectric material, geometrical electrode configuration, pressure and frequency in the plasma ignition, and conclusions about the spectroscopic analysis.

Appendices

Finally, appendices A, B and C, respectively, include representations in reference to Paschen's curves, a summary of some interesting data from others SDBD studies and possible lines with which to continue this investigation.

2 Theoretical Basis

In this chapter, a summary of the main characteristics that define, the plasma state will be presented –Section 2.1–, to later describe the operation of an aerodynamic flow controller through Dielectric Barrier Discharge –Section 2.2– and, finally, specify what are the general terms of the electrical and spectroscopic analysis that will be carried out –Section 2.3–.

With this knowledge base, it is tried to familiarize ourselves with the classifications of different types of DBD plasma controller, and thus be able to understand their different applications based on quantifiable parameters such as frequency, gap or pressure.

2.1 Plasma physics

Physics has taught us that gases containing electrically charged particles offer an excellent way of manipulating and transforming materials in a controlled manner. Plasmas are the object of study of the academic field of Plasma Science or Plasma Physics, including sub-disciplines such as the following fields of active research:

- *Plasma theory* (Plasma equilibria and stability, Plasma interactions with waves and beams, Guiding center, Adiabatic invariant, Debye sheath, Coulomb collision, ...),
- *Plasma in nature* (Astrophysical plasma, Northern and southern (polar) lights, The Earth's ionosphere, Interplanetary medium, Planetary magnetospheres, Space plasma, ...),
- *Industrial plasmas* (Plasma chemistry, Plasma processing, Plasma spray, Plasma display, Plasma sources, Dusty plasmas, ...),
- *Plasma diagnostics* (Thomson scattering, Langmuir probe, Ball-pen probe, Faraday cup, Spectroscopy, Interferometry, Ionospheric heating, Incoherent scatter radar, ...) or

- *Plasma applications* (Dielectric Barrier Discharge, Enhanced oil recovery, Fusion power, Ion implantation, Ion thruster, MAGPIE (Implosion experiments), Plasma ashing, Food processing, Plasma arc waste disposal, recycling, Plasma acceleration, Plasma medicine, Plasma window, ...).

In this Section, a general review of plasma physics will be carried out by answering a series of questions that present both its definition and its main characteristics that allow us to understand how plasma is classified. These questions are three:

1. What is plasma? –Section 2.1.1–.
2. What are the main characteristic magnitudes of the plasma state?
3. How can different plasma states be classified?

Through question 2 you will be responding to question 3 in the aspects that interest us, so both will be answered in Section 2.1.2.

2.1.1 What is plasma?

Langmuir, in his works initiated in the twenties to develop valves that allowed the passage of high currents, introduced in 1929 the word *plasma* to describe ionized gases. Everything seems to indicate that 99 % of the visible matter of Universe is in plasma state. He described the plasma he observed as follows:

"Except near the electrodes, where there are sheaths containing very few electrons, the ionized gas contains ions and electrons in about equal numbers so that the resultant space charge is very small. We shall use the name plasma to describe this region containing balanced charges of ions and electrons."[2]. The term **"plasma" refers to total or partially ionized gases, that presents collective behavior, corresponding to the fourth state of matter**[3].

This overall behavior is due to the long range of electric forces and the existence of mobile charges can cause a slight local loss of spatial neutrality, which causes electric fields to which the loads are subject. Also as a consequence of the movement of them, magnetic fields are produced that will exert dynamic actions on the charges.[4] As to how this state is reached, the transition from gas to plasma takes place in a smooth way, whereby the plasma state is generally constituted by a gas of electrons, ions and neutral particles. At a macroscopic scale, plasmas present quasi-neutrality[1][6]; a quasi-neutral state refers to the concentration of positive and negative charges is approximately equivalent. These particles are unbound, but it doesn't mean that they are free in the sense of not experiencing forces, because moving charged particles generate an electric current within a magnetic field, and any movement of

[1] There are also **non-neutral or unstable plasmas**. The strength and range of the electric force and the good conductivity of plasmas usually ensure that the densities of positive and negative charges in any sizeable region are equal ("quasineutrality"). A plasma with a significant excess of charge density, or, in the extreme case, is composed of a single species, is called a non-neutral plasma. In such a plasma, electric fields play a dominant role. Examples are charged particle beams, an electron cloud in a Penning trap and positron plasmas.[5]

a charged plasma particle affects and is affected by the fields created by the other charges. In turn this fact governs collective behavior with many degrees of variation.

So, plasma is a state of matter in which an ionized gaseous substance becomes highly electrically conductive to the point that long-range electric and magnetic fields dominate the behavior of the matter[7][8]. Most of matter in the visible Universe is in a plasma state; unlike other states of matter, plasma is rare on the Earth's surface under normal conditions, and is mostly artificially generated from neutral gases.

Three **factors define a plasma: the plasma approximation, bulk interactions and plasma frequency**[9], but they will be discussed in Section 2.1.2. Thus, regarding ionization, ionized gases cover a wide range of thermodynamic properties and regimes depending on the values that can be associated with important properties that characterize them, such as electronic density, n_e, ion density, n_i, and temperature of the electrons, T_e; and these different regimes to which reference is made, can be achieved both naturally and by industrial processes. It is important, therefore, to develop a characterization of types of plasmas, so that they can be identifiable and, therefore, also lead us to develop the most desired configuration of DBD controller through the representative parameters of each different plasma.

It is important to be aware that in spite of being able to define relatively simple mathematical models that characterize plasma physics, in reality, the behavior of the plasma can be extraordinarily varied and subtle, and the appearance of unexpected behaviors from a simple model it leads us to develop **complex systems**. These systems are, in some way, at the limit between ordered and disordered behavior, since they can not normally be described by simple and fluid mathematical functions, nor by sheer randomness. The spontaneous formation of interesting spatial features on a wide range of length scales is one manifestation of plasma complexity. Examples of complexity and complex structures in plasmas include: filamentation (striations or string-like structures also known as Birkeland currents), Dusty plasma/grain plasma, non-neutral plasma –already described– or impermeable plasma[10]; however, it is not the purpose of this work to delve into these aspects.

Derived from nature of this state of matter, there are quite **interesting properties**. Because they are charged, plasmas can be manipulated with electric and magnetic fields, and can be used to effect technologically useful physical and chemical transformations in controllable ways. two of them will be highlighted right now, such as being able to control the direction/confinement of the plasma through electromagnetic fields; and the generation of the "sheath" effect in the contact zone between plasma and solids. Respect to the first, the literature [4] says that the name "plasma" seems to be related to the possibility of shaping ("plasmar" in Spanish) using electric and magnetic fields, thus avoiding the need for a container or container, as is the case with fluids; this first property has many applications, for example, the concept applied by ionic propellers, which can dispense with physical nozzles by replacing them with an electromagnetic field that directs the output flow, thus avoiding temperature limitations on the flow that the materials of nozzles require to be able to resist. Regarding the second property, it will be explained in a little more detail below.

Plasma-wall interaction: Sheath effect

The "sheath effect" refers to the effect that comes from the called plasma-wall interaction, referred to the phenomena take place as a result of the contact of the plasma with a solid body, not only on the contact surface but also inside the plasma (recycling, transfer of matter and energy, ...) as the solid (diffusion, structural changes, ...). So, in general, for artificially generated plasmas, the phenomenon known as "**plasma recycling**" occurs, which occurs when plasma is in contact with solid matter. This solid matter acts as a sink for the plasma, so that ions and electrons precipitate on the solid and recombine, thus emerging as neutral atoms, which return to ionize in the plasma, usually by collision with electrons. In this way, while the solid acts as a sink for the plasma, it also feeds the source that generates new plasma in its vicinity, with neutral atoms.

This phenomenon occurs because in a plasma the electrons usually have a greater mobility in comparison with the ions, due to the difference of masses that exist between them –the electrons have a temperature on the order of magnitude or greater than that of the ions and are much lighter too–. This fact causes the electrons to spread rapidly (at least they are faster than the ions by a factor of $\sqrt{m_i/m_e}$ where m_i is the ion mass and m_e is the electron mass), generating at the same time an electric polarization field that separates the charges that, in the absence of another force, will make the flow of electrons come back restoring the quasi-neutrality of the plasma. Here, this means the electronic diffusion is limited by the diffusion of ions; process that receives the name of ambipolar diffusion. [12]

At the interface to a material surface, therefore, the electrons will fly out of the plasma, charging the surface negative relative to the bulk plasma. Due to Debye shielding, the scale length of the transition region will be the Debye length, λ_D. As the potential increases, more and more electrons are reflected by the sheath potential. An equilibrium is finally reached when the potential difference is a few times the electron temperature –see Fig. 2.1– .[13] [14]

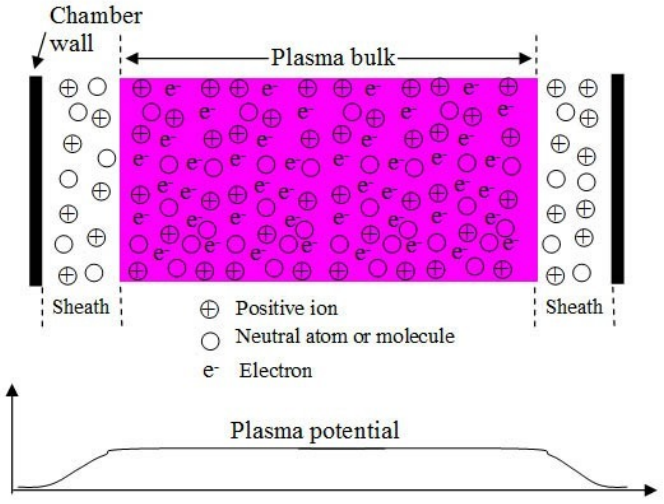

figure 2.1 Plasma and plasma sheath.
Source of the image: [11].

It means, due to this mobility difference, electrons will be the first species to reach a surface exposed to plasma. This causes the appearance of a gradient of electric potential in the plasma in contact with the surface, a gradient that is rapidly attenuated by the effect of protecting of charges at distances in the order of the length of Debye –see Section 2.1.2– [15]. **This region in which the potential decays from its value in the plasma to the floating potential of the surface is called** a sheath (or **Debye/electrostatic sheath** [2] to differentiate it from magnetic sheath) and, therefore, is formed between plasmas and electrodes or walls, been the transition between them[3], which has different advantages to apply in different fields of science.

2.1.2 What are the main characteristic magnitudes of the plasma state? How can different plasma states be classified?

In this Section will be constructed through the enumeration of the most important parameters from the point of view of which determines each type of plasma according to projects that have extensively studied the classification of the fourth state of matter. In Notation (page IX) there is a list of all physical properties and constants that are going to be mentioned in this work.

Previously, it was be exposed that three are the factors that define plasma: the plasma aproximation, bulk interactions and plasma frequency; and, also, were mentioned properties as electronic density, ion density and temperature of electrons as three fundamental properties for classification of plasmas, directly related to the first ones. Right now, these three first fundamental factors will be briefly described as an introduction to the enumeration that will be the goal of this Section, since the following three magnitudes establish the said factors: **Debye length**, **mean kinetic temperature** and **charge density** –or electronic density–.

1. *The plasma approximation*: The plasma approximation applies when the plasma parameter, Λ[4],[23] representing the number of charge carriers within the Debye sphere surrounding a given charged particle, is sufficiently

[2] Plasmas are complicated because motions of electrons and ions are determined by the electric and magnetic fields but also change the fields by the currents they carry.

The **magnetic sheath** is a plasma-wall interaction effect. It says that in presence of a magnetic field, the particles describe Larmor's orbits. In this case, electrons are more mobile than ions, but in the direction of the magnetic field, so that the sheath is also formed. Now there is a magnetic sheath zone and an electrostatic sheath zone. The magnetic sheath is determined by the change in the trajectories of ions in the direction of the surface.[16]

[3] Similar physics is involved **between two plasma regions** that have different characteristics; the transition between these regions is known as a double layer, and features one positive, and one negative layer, i.e., a **double layer is a structure in a plasma consisting of two parallel layers of opposite electrical charge**. The sheets of charge, which are not necessarily planar, produce localised excursions of electric potential, resulting in a relatively strong electric field between the layers and weaker but more extensive compensating fields outside, which restore the global potential.Ions and electrons within the double layer are accelerated, decelerated, or deflected by the electric field, depending on their direction of motion.[17]

Double layers can be created in discharge tubes, where sustained energy is provided within the layer for electron acceleration by an external power source. Double layers are claimed to have been observed in the aurora and are invoked in astrophysical applications. Similarly, a double layer in the auroral region requires some external driver to produce electron acceleration.[18][19]

Electrostatic double layers are especially common in current-carrying plasmas, and are very thin (typically ten Debye lengths).[20]

[4] The **plasma parameter, Λ,** is a dimensionless number, usually interpreted to be the argument of the Coulomb logarithm, which is the ratio of the maximum impact parameter to the classical distance of closest approach in Coulomb scattering. In this case,

high as to shield the electrostatic influence of the particle outside of the sphere.[44][45]

2. *Bulk interactions*: The Debye screening length (defined below) is short compared to the physical size of the plasma. This criterion means that interactions in the bulk of the plasma are more important than those at its edges, where boundary effects may take place. In consequence, When this criterion is satisfied, the plasma is quasineutral.[27]

3. *Plasma frequency*: A gradient in space-charge fields is formed when a plasma is disturbed from equilibrium, resulting in collective wave-like oscillatory particle motions that work to restore the original macroscopic neutrality. In consequence, the plasma frequency is the time-scale used to describe the collective natural frequency of such oscillations, and these these oscillations are inherently related to the stability of a plasma's charge neutrality. [28]

   The electron plasma frequency, ν_e, (that it measures plasma oscillations of the electrons) is large compared to the electron-neutral collision frequency, $\nu_{e,n}$, (measuring frequency of collisions between electrons and neutral particles); so, when this occurs making that this condition were valid: electrostatic interactions dominate over the processes of ordinary gas kinetics.[29]

   The proper frequency of plasma oscillations due to the collective character, called plasma frequency, is directly proportional to the square root of the concentration of the charged species and inversely proportional to the square root of the mass, consequently, its values for electrons and ions are quite different.

   If plasma is subjected to a frequency disturbance lower than the plasma frequency of the charged particles (electrons and ions), they will respond trying to maintain the neutrality of the whole.The presence of magnetic fields causes causes anisotropic behavior in the plasma.[24] [25]

In a general way, the parameters that characterize plasmas will be the average concentration of electrons that it supposed equal to that of ions (monopositive), and the concentration of neutrons, or equivalently the degree of ionization, and on the other hand the energy distributions and the average energies or the equivalent temperature. Once the foregoing is stated, the magnitudes that allow the establishment of categories or conclusions as those referred to so far are are listed after this paragraph.

---

the plasma parameter is given by equation 2.1, indicates the average number of particles contained in a sphere whose radius is the length of Debye (Debye sphere) –page 13–. [23]

$$\Lambda = 4\pi n_e \lambda_D^3 \tag{2.1}$$

where n_e is the electronic density and λ_D the Debye length.

The definition of plasma, according to which the electromagnetic interaction of a particle with the multitude of distant particles dominates over the interaction with the few nearby neighbors, can be written in terms of the plasma parameter as $\Lambda \gg 1$.[22][23]

- **Debye length, λ_D**:

  As previously mentioned, the characteristic of *quasineutrality* is often associated with plasmas, however, this happens on a macroscopic scale, while on a microscopic scale this characteristic does not necessarily have to occur; this means that although large-scale equiparity occurs, spatial charges located within the plasma may appear.

  The characteristic magnitude that allows comparing these two scales is the length of Debye, λ_D, also called Debye radius or Debye's shielding distance (equation 2.2, which for cold plasmas becomes equation 2.3) named after the Dutch physicist and physical chemist Peter Debye, is a measure of a charge carrier's net electrostatic effect in solution and how far its electrostatic effect persists. It is the scale through which mobile charge carriers –for example, electrons– generate a shielding of electric fields in plasmas and other conductors. In other words, the length of Debye, related to the volumetric concentration of loads and temperature, is the distance over which a significant load separation can occur.

$$\lambda_D = \sqrt{\frac{n_e e^2}{\varepsilon_0}\left(\frac{1}{kT_e}+\frac{1}{kT_i}\right)}^{-1} \tag{2.2}$$

$$\lambda_D = \sqrt{\frac{\varepsilon_0 kT_e}{n_e e^2}} \tag{2.3}$$

  where ε_0 is vacuum permittivity, k is the *Boltzmann constant*, T_e and T_i is, respectively, kinetic temperature of the electrons and of the ions, n_e is electronic density y e is the elementary charge. See Section Notation, IX to know the values, whenever needed, even if no explicit reference is made.

  The length of Debye thus defines the spatial range of a plasma, which can compromise the charge balance. Thus, the plasma is considered quasi-neutral when the plasma size, L, is greater than the length of Debye, λ_D.

  Also, as already mentioned in Section 2.1, it also characterizes the thickness of the sheaths, which are formed between plasmas and electrodes or walls. I.e., the Debye sheath or electrostatic sheath, is a layer in a plasma which has a greater density of positive ions, and hence an overall excess positive charge, that balances an opposite negative charge on the surface of a material with which it is in contact –see Fig. 2.1–. This layer is several Debye lengths thick, anad it depends on various characteristics of plasma like temperature, density, etc.[15]

  Analogous to the definition given for the concept, similarly, a **Debye sphere** is the volume whose radius is a length of Debye, within which there is a sphere of influence, and out of which the charges are "shielded"[5].[48]

[5] A **screen/shielding effect** is one that can attenuate a force or interaction. From a perspective of atomic physics, the screen effect on outermost electrons of an atom is described as the attenuation of net attractive force on the electron, due to the presence of other electrons in lower layers and of the same energy level. The screen effect, then, is a barrier of electrons of the same level, which exert repulsive forces on higher level electrons, thus decreasing the probability of finding these electrons at lower levels. Each level produces screen queue effect; the greater the number of electrons, the greater the screen effect.

Regarding the view of quantum physics, this effect is the interference that exists between the last orbit of an atom and its nucleus.[47]

In summary, *"the length of Debye is a measure of the shielding that makes a plasma of an electrostatic alteration such as an electrode. In its proximity a space charge or pod region is generated. To be able to consider that a plasma exists, it must be fulfilled that its dimensions are much greater than the length of Debye, otherwise we are in a situation of ionized gas. An equivalent way of talking about a Plasma is to indicate that the number of particles within a sphere whose radius is the Debye length is very high."* [30]

- **Mean Kinetic temperature,** T_e:

  Plasmas do not have to be homogeneous, that is, the concentrations and temperatures are the same at all points; often, there are inhomogeneities, which implies the existence of diffusion processes associated with the gradients of these characteristic magnitudes.

  Usually, the particles of a certain kind of plasma located at a given point do not have the same speed: on the contrary, there is a distribution that in thermal equilibrium is described by Maxwell-Boltzmann distribution; the higher the temperature, the greater the dispersion of the speeds[6]. So, unlike neutral gases, where there is a single value of temperature for the entire volume, in the ionized gases different species can have different temperatures[7]; but for plasmas in thermodynamic equilibrium, all electrons, ions and neutrons have the same temperature, T_e, that it means that there is not significant energy flows within the plasma. Respect to **non-equilibrium plasmas** the temperature is in the order of $T_e' \approx 1-10eV$, while the temperature of ions and neutrals does not exceed room temperature significantly.[31][33][34]

  Based on the relative temperatures of the electrons, ions and neutrals, plasmas are classified as "thermal" or "non-thermal" (also referred to as "cold plasmas"):

  - *Thermal plasmas*: electrons and heavy particles are at the same temperature, it means all of them are in thermal equilibrium with each other ($T_e = T_i = T_{gas}$).
  - *Non-Thermal plasmas*: are non-equilibrium ionized gases, with two temperatures: ions and neutrals stay at a low temperature (sometimes room temperature), whereas electrons are much hotter ($T_e \gg T_i = T_{gas}$). So, they can be defined on this category either the ion and electron temperatures being different, or if the distribution of velocities of the two species does not satisfy the Maxwell-Boltzmann distribution.

[6] One measure of such dispersion is the **average quadratic velocity** which, at equilibrium, is also called thermal velocity. It is frequent, although formally incorrect like the specific literature indicates, to also speak of thermal speed and temperature in plasmas far from the thermodynamic equilibrium. [Citation needed] In this case, the temperature that would correspond to a determined average quadratic speed is mentioned. The thermal speed of electrons is $v_{T_e} = \sqrt{kT_e/m_e}$, where k is the Boltzmann constant and m_e is the electron mass.

In most cases, electrons are fairly close to thermal equilibrium, even when there is a significant deviation from the Maxwell energy distribution function (for example, due to UV radiation, energetic particles or strong electric fields). However, due to the large difference in mass between the neutral atoms and electrons, the electrons reach thermal equilibrium between them, much faster than they come into equilibrium with atoms or neutral atoms; why the temperature of the united-states can be very different from the temperature of the electron, and the temperature of the system is usually lower than that of the electron, it is very common in weakly ionized technological plasmas, where human beings are often close by of the room temperature[31]

[7] In this situation of **non-thermodynamic equilibrium**, we speak of electronic temperature and ionic temperature. An additional complication arises from using different temperatures for the (massive) ions and neutrals: gas temperature, which reflects the translational energy, excitation temperature, which indicates the location of the excited particles (interna energy), the temperatures of ionization and dissociation, which characterize these processes, and the radiation temperature that quantifies the radiated energy, this is the exchange with the environment by emission of photons.[35]

Interesting for this work, cold plasmas are industrially produced in electric discharges by applying a potential difference (voltage) of direct current (DC) to a gas under reduced pressure; or also using alternating current (AC) voltages, either RF (radio frequency assigned to industrial use 13.56 MHz), or microwave (frequency assigned 2.45 GHz). In the case of variable voltages with time, it can be resorted to applying them directly to electrodes in contact with the gas or inductive or capacitive coupling without electrodes.

As for the unit of measurement of temperature, kinetic temperature T' is usually used in electronvolts instead of in Kelvins, this unit –a measure of energy– thus becoming, informally, a measure of the thermal kinetic energy per particle. This conversion –equation 2.4 - is used because high temperatures are usually needed to maintain the plasma ionization:

$$T' \equiv kT \tag{2.4}$$

where T' is kinetic temperature expressed in electronvolts, T is kinetic temperature expressed in Kelvins and k is the Boltzmann constant.

- **Charge density or electronic density,** n_e:

  For plasma to exist, ionisation is necessary, the term "plasma density" by itself usually refers to the "electron density". So, *the charge density, n, measures the quantity of charges within a particular volume of gas*, that it the same that the electron density (n_e), that is how many free electrons, not bound to an atom, there are in a given volume; since all plasmas have some degree of ionization, this means that there are electrons that have been stripped from atoms, and are moving around, while the atoms are converted into ions.

  The **degree of ionization,** α, of a plasma is the proportion of atoms that have lost or gained electrons, and is controlled by the electron and ion temperatures and electron-ion vs. electron-neutral collision frequencies; i.e., is determined by temperature of electrons in relation to ionization energy (and more weakly by the density of charge), governed by Saha ionization equation (also known as the Saha–Langmuir equation)[8]

[8] **Saha equation** –equation 2.5, for a gas composed of a single atomic species– describes the degree of ionization for any gas in thermal equilibrium as a function of the temperature, density, and ionization energies of the atoms. The Saha equation only holds for weakly ionized plasmas, for which the Debye length is large. Saha equation is useful for determining the ratio of particle densities for two different ionization levels.[39][23]

$$\frac{n_{i+1}n_e}{n_i} = \frac{2}{\lambda^3}\frac{g_{i+1}}{g_i}\exp\left[-\frac{(\varepsilon_{i+1}-\varepsilon_i)}{kT}\right] \tag{2.5}$$

where n_i is the density of atoms in the i-th state of ionization (that is with i electrons removed), g_i is the degeneracy of states for the i-ions, ε_i is the energy required to remove i electrons from a neutral atom, creating an i-level ion, n_e is the electron density λ is the thermal de Broglie wavelength of an electron, m_e is the mass of an electron T is the temperature of the gas, k is the Boltzmann constant and h is the Planck's constant.

The expression $(\varepsilon_{i+1}-\varepsilon_i)$ is the energy required to remove the $(i+1)^{th}$ electron. In the case where only one level of ionization is important, one has $n_1 = n_e$ and defining the total density n as $n = n_0 + n_1$, the Saha equation simplifies to equation 2.6.

$$\frac{n_e^2}{n-n_e} = \frac{2}{\lambda^3}\frac{g_1}{g_0}\exp\left[\frac{-\varepsilon}{kT}\right] \tag{2.6}$$

where ε is the energy of ionization.[49]

Thus, generally a criterion widely used to classify plasmas is its kinetic temperature and its density of charged particles, as can be seen in Fig. 2.2 developed from the diagrams of Boeuf[43], Braithwaite[36], Jolibois[37] and Smirnov[38]. The formula for α is in equation 2.7, only depends on ion density, n_i and neutral-particles density, n_n. [41]

$$\alpha = \frac{n_i}{n_i + n_n} \tag{2.7}$$

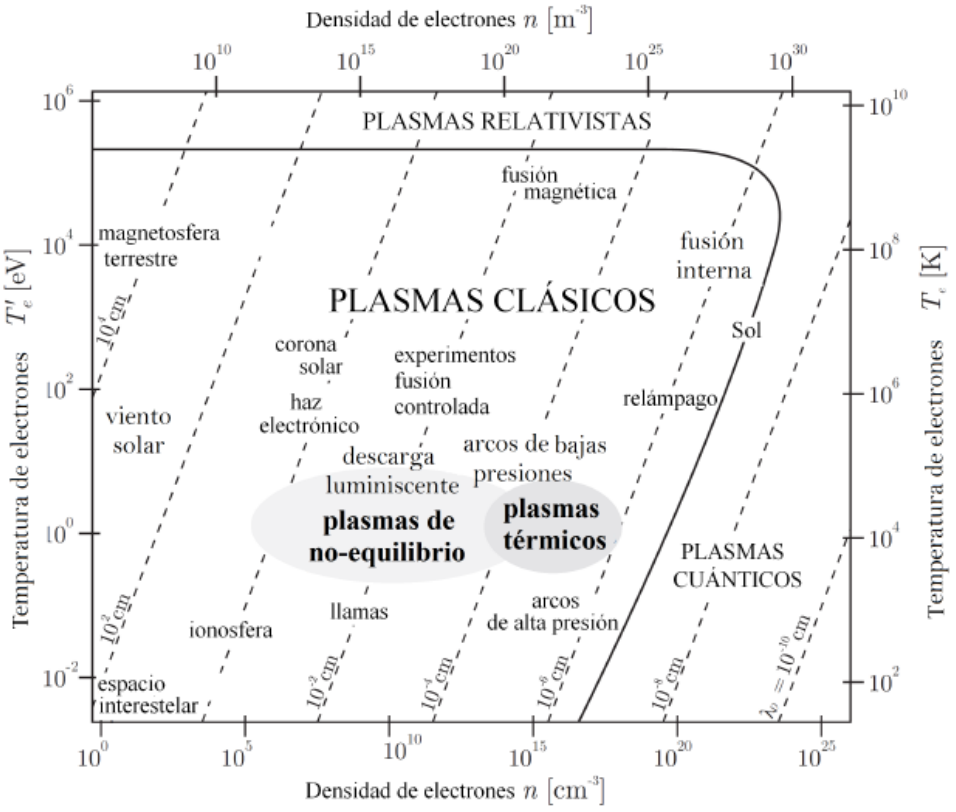

figure 2.2 **Classification of plasmas characterized by electronic density, n_e, and electronic temperature, T_e.** *Source of the image: [43][36][37][38].*

One can differentiate between fully ionized plasmas, partially or weakly ionized gases. In a plasma, the electron-ion collision frequency, $\nu_{e,i}$, is much greater than the electron-neutral collision frequency, $\nu_{e,n}$. Therefore, with a weak degree of ionization the electron-ion collision frequency can equal the electron-neutral collision frequency: $\nu_{e,i} = \nu_{e,n}$, being the limit separates a fully ionized plasma from a weakly ionized plasma.

- *Fully ionized plasmas:* the term was introduced by Lyman Spitzer, and it means that the plasma is in a Coulomb-collision dominated regime, i.e., $\nu_{e,i} > \nu_{e,n}$, which can correspond to a degree of ionization as low as 0.01%.[42]
- *Partially ionized plasmas:* the plasma is not dominated by Coulomb collisions, i.e. when $\nu_{e,i} < \nu_{e,n}$, this means that the screening of the Coulomb interaction of ions and electrons by other ions and electrons is negligible

($\alpha \ll 1$). In this case, it can be assumed as a hypothesis that collisions mainly occur between charged particles and neutral atoms, and that collisions between charged particles can be practically disregarded.

Most of technological (engineered) plasmas are weakly ionized gases.

Relating the density to the speed or **frequency of collision**, logically, the amount of movement that is transferred in the collisions per unit of time increases with the number of molecules in a specific volume of the gas; and in addition, the collision frequency, ν_m, is proportional to the density, n_n, and consequently to the gas pressure, p, nevertheless, the dependency with the collision speed can be neglected in first approximation –relation is in equation 2.8–. [50] [51]

$$\nu_m \propto n_n \propto p \tag{2.8}$$

By comparing different collisions with each other, loads will surely be accelerated in random directions. In this way, provided an uniform external electric field, $\overrightarrow{E}$, this random movement will be governed by a systematic movement in the direction of the field, which is known as drift. If this movement is averaged over numerous collisions, the drag or drift velocity, $\overrightarrow{v_d}$, is obtained –equation 2.9–.

$$\overrightarrow{v_d} = \begin{cases} -\mu \overrightarrow{E} & \text{for positive particles} \\ \\ -\mu \overrightarrow{E} & \text{for negative particles} \end{cases} \tag{2.9}$$

where μ is mobility like $\mu = e/m\nu_m$, valid for any value of the electric field, since it is assumed that in first approximation the mobility is only a function of the collision frequency[33][51]. Because the mass, and its corresponding inertia, are larger in ions than in electrons, the mobility of the ions is several orders of magnitude less than the mobility of the electrons: $\mu_i \ll \mu_e$.

As one has seen, different approaches can be used to classify Plasmas.

2.2 DBD Plasma Actuator

In recent times, the development of plasmas artificially (industrially), the so-called **technological plasmas**, has become a reality with many future possibilities in very varied applications (surface engineering, biomedical, environmental, manufacturing, propulsive, energy sources, ...). This vast field of possibilities is favored by, as one has already seen, the amount of possible alternatives in which plasma can present itself, with a wide range of temperatures and pressures.

Most artificial plasmas are generated by application of electric and/or magnetic fields through a gas, causing its ionization, or to a solid to achieve an ionizing sublimation. Different energetic approaches are applied to achieve this objective. In general, plasma generated in a laboratory setting and for industrial use can be categorized by[52]:

- The type of power source used to generate the plasma
- The pressure they operate at
- The degree of ionisation within the plasma
- The temperature relationships within the plasma
- The electrode configuration used to generate the plasma
- The magnetization of the particles within the plasma

The work objective of this project is focused on the generation of technological plasma through Dielectric Barrier Discharge (hereinafter “DBD”) reactors –see page 7–, studying the influence of gap, pressure, frequency and material; for possible aerodynamic flow control purposes. So, in this part of the document a review of the physics of discharges on gases will be shown to understand how plasma is generated –Section 2.2.1– to later expose, specifically, the bases of generation of plasma by Dielectric Barrier Discharge –Section 2.2.2–, and finally go on to explain the general concept of the device and its applications –Section 2.2.3–.

2.2.1 Electrical discharges in gases

In this Section, basic ideas about the mechanism and discharge status are exposed, to understand the operation of the plasma flow controller generated by gas discharge.

Three parts are going to be distinguished: basic aspects –Section 2.2–, voltage-current characteristics –Section 2.2– and breakdown voltage and Paschen curve –Section 2.2–.

Basic aspects of discharges in gases

Electric discharge in gases occurs when electric current flows through a gaseous medium due to ionization of the gas. Depending on several factors, the discharge may radiate visible light (glow discharge).

First investigations on discharges in gases were mainly concentrated in low pressure discharge tubes, whose scheme can be seen in Fig. 2.3. Unlike them, plasma controllers are devices that work with alternating current, AC, and in a range of frequencies between 50Hz and 30 kHz, with an inhomogeneous and at least two-dimensional electric field. This implies more complexity in the corresponding download mechanisms and therefore does not allow an exact definition of the properties of the download. Despite this difference, some aspects of the direct current case DC discharge mechanism can also be used for a description of the fundamental aspects of the AC case. [0][54].

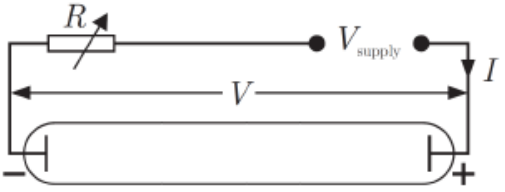

figure 2.3 **Discharge tubes.** Low pressure discharge tubes are the famous fluorescent tubes today. *Source of the image: [53].*

The fact that plasma controllers can operate at non-reduced pressure offers a lot of possibilities.

Voltage-Current characteristics of discharges in gases

The increase in voltage between the two electrodes in a low pressure discharge tube leads to a non-linear voltage-current relationship –see Fig. 2.4–. There are three types of discharge regimes, these are: Dark Discharge (dark current mode), Glow Discharge (normal glow mode) and Arc Discharges (arc mode). [55][56][0]

1. ***Dark current mode:*** Apart from the exception of the corona discharge, this discharge regime remains invisible to the naked eye and is therefore called dark discharge.

    - **A-B:** During the background ionization stage of the process the electric field applied along the axis of the discharge tube sweeps out the ions and electrons created by ionization from background radiation. Background radiation from cosmic rays, radioactive minerals, or other sources, produces a constant and measurable degree of ionization in air at atmospheric pressure. The ions and electrons migrate to the electrodes in the applied electric field producing a weak electric current. Increasing voltage sweeps out an increasing fraction of these ions and electrons. I.e., at low voltage there are very few charges that contribute to current flow. In this regime an increasing number of the charges generated are accelerated towards the electrodes as the voltage increases.

    - **B-C:** Once all the charges produced reach the electrodes, there is a stagnation in the current in the saturation regime, in which the energy levels are too low to create new secondary loads. Because if the voltage between the electrodes is increased far enough, eventually all the available electrons and ions are swept away, and the current saturates. So, in the saturation region, the current remain constant while

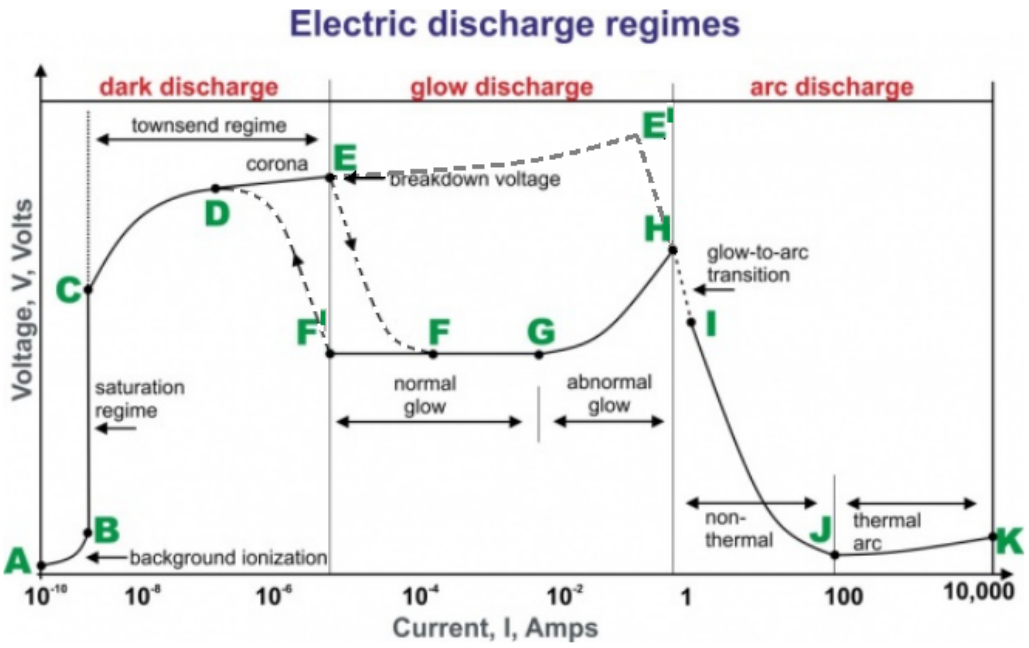

figure 2.4 **Typical V/I plot of a glow discharge (DC).** The main characteristics of the discharge such as the breakdown voltage, the voltage current characteristic and the structure of the discharge depend on the geometry of the electrodes, the gas used, the pressure and the electrode material.[55][56] *Source of the image: [102].*

the voltage is increased. This current depends linearly on the radiation source strength, a regime useful in some radiation counters.

- **C-D:** If voltage across the low pressure discharge tube is increased beyond point C, the current will rise exponentially. The electric field is now high enough so the electrons initially present in the gas can acquire enough energy before reaching the anode to ionize a neutral atom. As the electric field becomes even stronger, the secondary electron may also ionize another neutral atom leading to an avalanche of electron and ion production. The region of exponentially increasing current is called the Townsend discharge; and in this regime the electric field is high enough so that the primary charges partially ionize the gas; and, like it has been said, due to these new charges acquire enough field energy to ionize the gas, avalanche discharges appear, leading to an exponential growth of the current as the voltage increases.

- **D-E:** Corona (crown) discharges may appear in the later stages of the Townsend regime, where between D and E a localized increase of the field exceeds the breakdown point of the gas. These local concentrations are caused by peaks, side edges or roughness of the electrodes.

  Definetly, corona discharges occur in Townsend dark discharges in regions of high electric field near sharp points, edges, or wires in gases prior to electrical breakdown; and if coronal cuurents are high enough, corona discharges can be technically “glow discharges”, visible to the eye. However, for low

currents, the entire corona is dark, as appropriate for the dark discharges[9]. E (Electrical breakdown) occurs in Townsend regime with the addition of secondary electrons emitted from the cathode due to ion or photon impact. At the breakdown, or sparking potential,the current might increase by a factor of 104 to 108, and is usually limited only by the internal resistance of the power supply connected between the plates.

2. ***Normal glow mode:***

   - **E-F:** Once the breakdown voltage is reached at point E, an electrical break occurs followed by a DISCONTINUOUS transition from E to F to the glow discharge regime. The large potential difference between the electrodes drops due to the significant increase in the current flow, and therefore the plasma becomes visible.
   - **F – G:** After reaching point F, the gas enters the normal glow/luminiscent region, in which the voltage is almost independent of the current over several orders of magnitude in the discharge current, and current increases. The electrode current density is independent of total current in this regime. This means that the plasma is in contact with only a small part of the cathode surface at low currents. As the current is increased from F to G, the fraction of the cathode occupied by the plasma increases, until plasma covers the entire cathode surface at point G.
   - **G – H:** In the abnormal glow regime above point G, the voltage increases significantly with the increasing total current in order to force the cathode current density above its natural value and provide the desired current, because once the cathode is completely covered, a considerably high voltage rise is needed to achieve an abnormally high current density (and this result is achieved in electrodes heated in succession and in an incandescent cathode at point H). Go on from C and moving to the left to lower currents, a form of hysteresis-cycle is observed in the voltage-current characteristic curve: the discharge maintains itself at considerably lower currents and current densities than at point F and only then makes a transition back to Townsend regime; it means, the luminescent discharge is maintained below F, once it has been established.

   At point F'the transition back to the Townsend regime occurs without going through the Townsend discharge or crown again.

3. ***Arc mode:***

   - **H-I:** The electrodes at point H become sufficiently hot that the cathode emits electrons thermionically. In consequence, if the DC power supply has a sufficiently low internal resistance, the discharge will undergo a glow-to-arc transition (H-I).
   - **I-J:** The transition is followed by a regime of non-thermal arcs (I-J), where the voltage required for the discharge decays rapidly due to the additional loads of the thermionic emission: the arc regime, from I

[9] **Related phenomena** include the silent electrical discharge, an inaudible form of filamentary discharge, and the brush discharge, a luminous discharge in a non-uniform electric field where many corona discharges are active at the same time and form streamers through the gas.

through K is one where the discharge voltage decreases as the current increases, until large currents are achieved at point J, and after that the voltage increases slowly as the current increases.

- **J-K:**Since this influence grows with the heating of the electrons, the effect corresponds to a characteristic negative resistance. Beyond the local voltage minimum at point J, the voltage-intensity curve again reaches the thermal arc regime (J-K) towards thermal equilibrium at point K.

As we already know, the above discussion introduces the main characteristics that describe a low pressure discharge. For levels of atmospheric pressure and more inhomogeneous electric fields, direct breakdowns by arcs can occur, which can be maintained with sufficient current applied (indicated in Fig. 2.4 by dotted lines and by the point E').

Depending on the geometrical conditions and the gas, it is possible that there is a direct transition from the Townsend discharge or corona to the arc discharge (E'-I).[57]

Breakdown voltage and Paschen curve

The measurements of the experiments carried out have been saved at the ignition voltage appreciable by the naked eye. Theorically, the ***breakdown voltage***, V_{bd}, (ignition/breakdown potential), signaled with point E in Fig. 2.4, is a system instability resulting from discharge and high voltage, and is crucial since before that point (period CE) the discharge is only possible through the emission of secondary electrons. Beyond point E the ionization avalanche provides a sufficient amount of electrons to maintain a self-sustaining discharge. [58]

The interest of this project is that said breakdown voltage, and its corresponding electric firing field, depend both on the material of the electrode, the geometry and the distance between electrodes, and on the species of gas and pressure, as well as on the the characteristics of the substrate used in the case in question, DBD actuators.

At the end of the 19th century, Paschen formulated a law with the same name (equation 2.10) in which it was established that for a given gas, the ignition voltage is only a function of the product pg (where g the distance between electrodes) and the secondary electron emission coefficient in the cathode γ_{es}. [62][135] –see Fig. 2.5–. For all gases there is a minimum ignition voltage, depending on pg, which corresponds to the Stoletow benchmark of better efficiency, which implies a minimum power consumption of the discharge.

$$V_{bd} = \frac{Bpg}{ln(Apg) - ln[ln(1 + \frac{1}{\gamma_{es}})]} \tag{2.10}$$

where p is pressure in pascals, g distance between electrodes in meters, is the coefficient of emission of secondary electrons in the cathode, A is the ionization of saturation in the gas at a particular value of E/p, and B is related to ionization and excitation energies. The values A and B are determined experimentally, and what is obtained is that they are approximately constant in a strict range of values of E/p for a given gas. For example, For example, in the case of air with values of E/p between 450 and 7500 V(kPa cm)$^{-1}$, we have values for the constants of $A = 112.50$ (kPa cm)$^{-1}$, and $B = 2737.50$ V(kPa cm)$^{-1}$.[135] [62]

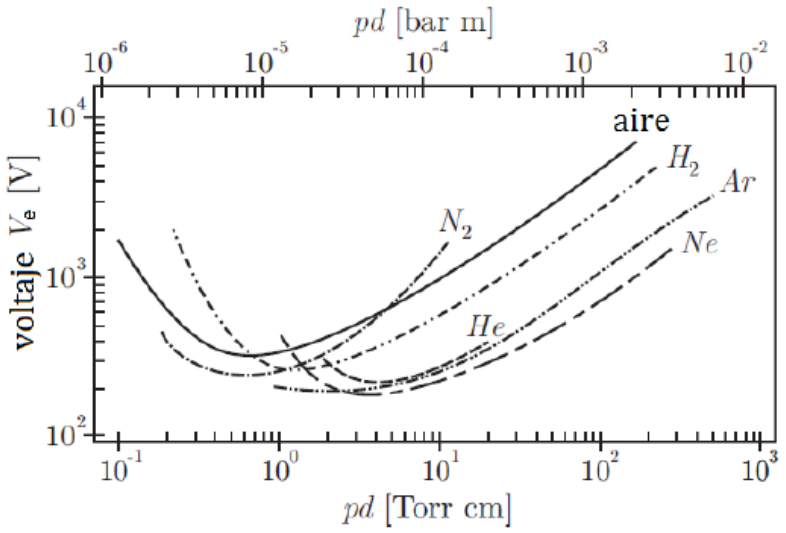

figure 2.5 **Paschen curves for different gases**. The parameter d refers to the distance between electrodes, in the present document it is represented as g. *Source of the image: [60].* .

2.2.2 Dielectric Barrier Discharge Plasmas Theory: Characterization

Dielectric Barrier Discharge (DBD) –see Fig. 2.6– is a non-thermal electrical discharge generated by the application of high voltages across small gaps wherein a non-conducting coating prevents the transition of the plasma discharge into an arc[10]. It is characterized by having at least one layer of an insulating dielectric barrier located between the electrodes. When a high voltage is applied between the electrodes some arcs are randomly generated among them caused by the accumulation of charges on the surface of the dielectric material –Section 2.2–, this generates thousands of discharges in microseconds which provides the degree of ionization required to sustain a discharge of plasma.

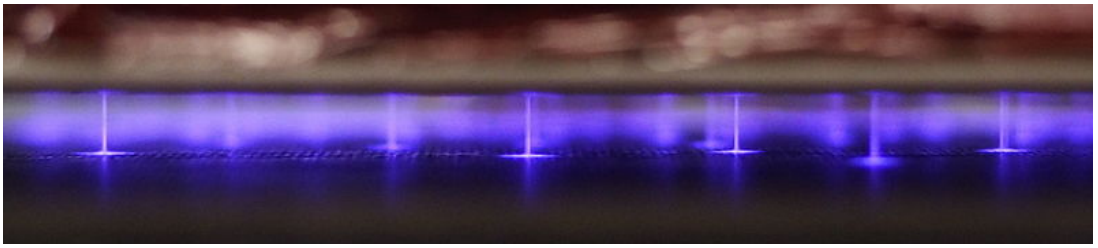

figure 2.6 **Filamentous Dielectric Barrier Discharge.** The photograph shows an atmospheric DBD discharge occurring in between two steel electrode plates, each covered with a dielectric (mica) sheet. The filaments are columns of conducting plasma, and the foot of each filament is representative of the surface accumulated charge. The discharge is taking place in normal atmospheric air, at about 30 kHz, with a discharge gap of about 4 mm. The "foot" of the discharge is the charge accumulation on the barrier surface.*Source of the image: [78]* .

Because the DC current can not pass this dielectric barrier, it is required to operate in AC[11] for the operation

[10] An **electric arc**, or arc discharge, is an electrical breakdown of a gas that produces an ongoing electrical discharge.

[11] The process normally uses high voltage alternating current, ranging from lower RF to microwave frequencies. However, other methods were developed to extend the frequency range all the way down to the DC. One method was to use a high resistivity layer to cover one of the electrodes. This is known as the resistive barrier discharge. [75][76]

of the DBD device. In addition, this fact offers the advantage of locating the electrodes, or at least one of them, separated from the discharge, that is to say without being in contact with it [63]. This can be very beneficial when, for example, highly aggressive gases are used.

So, plasma controllers used in this project act at AC voltages, that is, the electric field periodically changes sign, so when the AC voltage is applied, a discharge appears on the surface of the dielectric. Therefore, in the operation, the discharge appears every half cycle of the applied AC voltage.

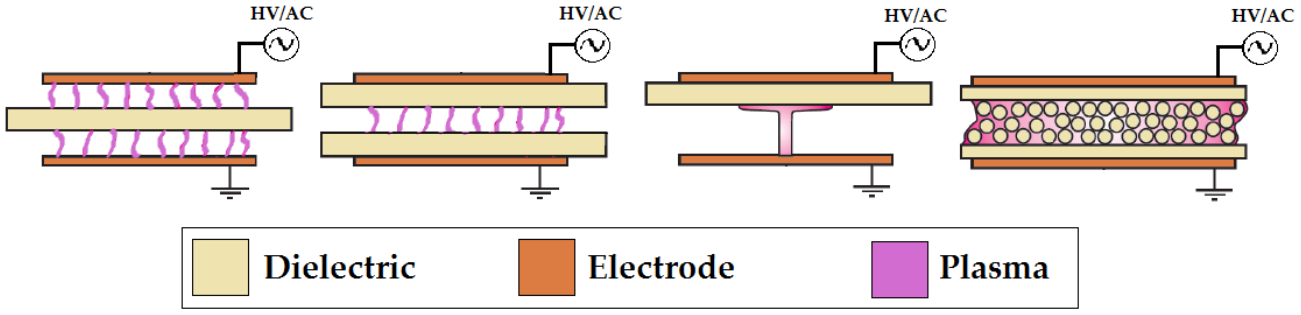

figure 2.7 **Examples of typical configurations of Dielectric Barrier Discharge in volume (VD).** *Source of the image: Own image .*

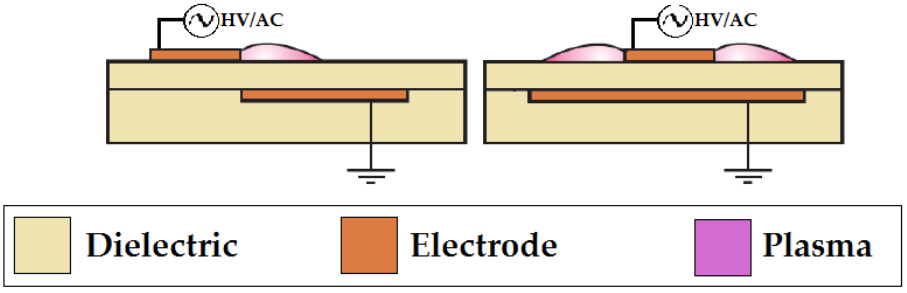

figure 2.8 **Examples of typical configurations of Dielectric Barrier Discharge in surface (SD).** *Source of the image: Own image .*

Unlike most other non-equilibrium discharges, the Dielectric Barrier Discharge can operate at high pressures, in a range of $10^{-1} - 10^{1}$ bar.

Also, there are both class types Volume Discharge (VD) and Surface Discharge (SD), like you can see in Fig. 2.7 and 2.8, respectively. The main difference between these two configurations is that in the VD discharge the rupture occurs through the gas in the space between electrodes, while in the SD discharge the rupture grows periodically on the dielectric. Note that the presence of a dielectric layer is essential for the formation of a surface discharge, since the insulation prevents the flow of current.[74] The figures that have been referred show diagrams with typical constructions of a DBD device, wherein one, usually, of the two electrodes is covered with a dielectric barrier material. The lines between the dielectric and the electrode are representative of the discharge filaments, which are normally visible to the naked eye. This work is based on **surface discharges**.

The first technological application of the Dielectric Barrier Discharge was made by Ernst Werner von Siemens in 1857[64], who observed luminescence between two coaxial glass tubes while **generating ozone**. Originally DBD discharge was called silent (inaudible) –but experiments reveal that the geration of plasma DBD, the ionization of a gas, does sound– discharge and also known as ozone production discharge or partial discharge. It is the most profitable technique to produce it. [65][66][66].

With respect to its **applications**, currently Dielectric Barrier Discharges constitute a scientific field of great interest, whose success is demonstrated in the wide variety of industrial applications based on this type of plasma, especially focused on the generation of ozone, decontamination of gases, fluorescent lamps, laser discharge, surface treatment, synthetic facrics and plastics, plasma medicine[12] or also used in the design of low temperature plasma jets[13].[68][69][71]

Interest in plasma actuators as active flow control devices is growing rapidly due to their lack of mechanical parts, light weight and high response frequency.[77] In consequence, due to the direct relationship with my studies, this Master's Thesis will focus on the **applications of DBD devices as flow controllers**, and Section 2.2 contains a list of historical advances regarding this discipline.

Dielectric and ferroelectric materials

A dielectric (or dielectric material) **is an electrical insulator –low electrical conductivity/specific conductance ($\sigma \ll 1$)– that can be polarized by an applied electric field**. Thus, all dielectric materials are insulators but not all insulating materials are dielectric. The term dielectric, which means "through", was coined by William Whewell (from $dia- + electric$) in response to a request from Michael Faraday. [153][152]

Although the term "insulator" implies in itself having low electrical conductivity; A "dielectric" material refers to materials with a high degree of polarizability. That is, **the term insulation is used to indicate electrical obstruction, while the adjective dielectric is used to indicate the energy storage capacity of the material, through polarization.** The concept of polarizability is expressed through the magnitude: relative permittivity, ε_r[14], also is called as dielectric constant. Scheme shown in Fig. 2.9.

When a dielectric is placed in an electric field, electric charges do not flow through the material as they do in an electrical conductor but only slightly shift from their average equilibrium positions causing dielectric polarization. Because of dielectric polarization, positive charges are displaced in the direction of the field and negative charges shift in the opposite direction. This creates an internal electric field that reduces the overall field within the dielectric

[12] The Dielectric Barrier Discharge was used in the mid-1990s to show that low temperature atmospheric pressure plasma is effective in inactivating bacterial cells. This work and later experiments using mammalian cells led to the establishment of a new field of research known as plasma medicine. [72]

[13] These plasma jets are produced by fast propagating guided ionisation waves known as plasma bullets.[73]

[14] **Relative permittivity** is its (absolute) permittivity, ε, expressed as a ratio relative to the permittivity of vacuum, ε_0.

Permittivity is a material property that affects the Coulomb force between two point charges in the material. Relative permittivity is the factor by which the electric field between the charges is decreased relative to vacuum.

Likewise, relative permittivity is the ratio of the capacitance of a capacitor using that material as a dielectric, compared with a similar capacitor that has vacuum as its dielectric. Relative permittivity is also commonly known as dielectric constant.

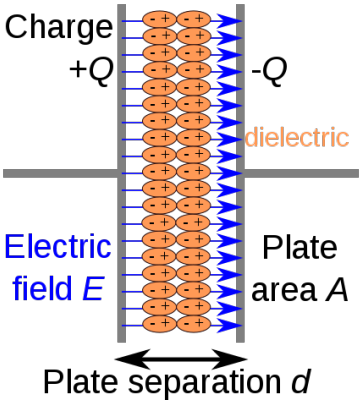

figure 2.9 **Capacitor schematic with dielectric.** *Source of the image: [80]* .

itself. If a dielectric is composed of weakly bonded molecules, those molecules not only become polarized, but also reorient so that their symmetry axes align to the field.[79]

In this work we have experimented with the dielectric materials listed in Table 2.1 as a barrier for the DBD actuators, and they are: quartz, alumina, lithium niobate and teflon.

To familiarize ourselves with the existing literature, it is also useful to understand the ownership of **ferroelectric materials**. Ferroelectricity is a property of non-centrosymmetric dielectric materials. The observable physical effect is that the material presents a polarization even after having removed the electric field. It can be explained based on a residual supply of permanent dipoles. Consequently, ferroelectricity is a characteristic of certain materials that have a spontaneous electric polarization that can be reversed by the application of an external electric field.[83] [84] lithium niobate is a ferroelectric material, suitable for a variety of applications; its versatility is made possible by the excellent electro-optic, nonlinear, and piezoelectric properties of the intrinsic material. [86]

Table 2.1 **Dielectric constants of materials used in DBD devices in this work.**
Note: It is important to consider values "in the order of" those presented in the table, since the dielectric constants have a strong dependence on parameters such as temperature. .

Dielectric	**Formula**	ε_r **at 20ºC/1MHz**
Air	-	1
Quartz	SiO_2	~ 3
Alumina	Al_2O_3	~ 5
lithium niobate	$LiNbO_3$	~ 1000

Piezoelectricity is a phenomenon that occurs in certain crystals that, when subjected to mechanical stress, in their mass acquire an electrical polarization and a difference of potential and electrical charges appears on their surface. This phenomenon also occurs in reverse: they deform under the action of internal forces when subjected to an electric field. The piezoelectric effect is normally reversible: by not subjecting the crystals to an external voltage or electric field, they recover their shape.

Piezoelectric materials are natural or synthetic crystals that lack a center of symmetry. Compression or shearing causes dissociation of the centers of gravity of the electric charges, both positive and negative. As a result, elementary dipoles appear in the mass and, by influence, on opposite surfaces arise charges of opposite sign.[144]

There are certain phenomena that appear in low symmetry networks such as ferroelectricity, piezoelectricity or pyroelectricity. A crystal with a structure in which the positive ions do not have a symmetrical arrangement with respect to the negative ones can give rise to a net dipole moment and therefore to a spontaneous polarization in the absence of a field.

We define a ferroelectric crystal as the one that shows a dipole moment, spontaneous polarization, in the absence of external electric field, and below a certain temperature and it is also possible to reverse the direction of polarization by applying electric field.

As the frequency increases, this effect becomes increasingly greater until the crystals do not support the stresses that are produced and therefore break; said ruptures may be due to defects of the crystalline network produced during the manufacture of the material.

So, in the phenomenon of piezoelectricity, when applying a mechanical tension changes the electrical polarization of the material generating an electric field (appearance of charges on the surfaces of the material). As shown in the figure, the mechanical stress changes the center of gravity of negative charges and positive, producing a change in the dipole moment.[145]

2.2.3 Fundamentals of operation of a DBD Plasma actuator

Plasma actuators, in general, involve the use of non-thermal atmospheric pressure plasmas, i.e., plasmas that are not in thermodynamic equilibrium. As already stated, the formation of the SDBD plasma is based on the Townsend mechanism; this is an electron avalanche process involving the multiplication of an initial set of free electrons through cascade ionization. [94] Completing, the behavior of this type of plasma is defined by these charge mechanisms in alternating half-cycles, that is, by the AC voltage power source; so that when alternating voltage is applied, a plasma discharge appears on the surface of the dielectric above the encapsulated electrode, causing an injection of momentum into the surrounding air during each half-cycle of the applied AC.

The following will be presented in different subsections: injection of momentum, advantages, characteristics of the discharge process and usual values.

Injection of momentum

Flow control concerns the ability to manipulate a flow for a desired change, and there are two large categories of devices: Active and Passive flow control. Active flow control devices involve the addition of energy to a system via an actuator, and this actuator (integrated in a control loop) requires auxiliary power. [91]. On the other hand, Passive flow control devices require no such support, and are largely mechanical in nature. In particular, within active flow control, in recent years, DBD plasma actuators are presented as a promising proposal (eventhough reserach is relatively recent, with preliminary studies first initiated in the early 1950s in Europe and the USA), in relation to its advantages: low weight, robustness, lower power consumption, simplicity, and ability for real time control at high frequencies. [28][94]

The injection of momentum is characterized as a macroscopic EHD[15] *process or plasma body force that can be measured, and is transferred to the neutral continuum through collisions between charged and neutral particles. In fact, while the plasma appears to be a relatively uniform diffuse discharge, measurements have indicated that it is highly ordered in space, and time, as already seen.* [88]

Advantages

DBD plasma actuator, as other mechanisms like mechanical flaps on an airplane wing, uses blowing (or an injection of momentun at the near-wall region) to induce an modify a flow congiguration. And, nowdays, the investigation is centred in achieve goals such as greater lift enhancement and drag reduction, noise suppression, transition and separation delays, through efficient and profitable devices that reduce the environmental impact and allow, at the same time, energy saving.[89]

Contributing to its natural preference over other traditional mechanical flow control devices, **DBD plasma actuator's advantages include its reduced size and weight, which is particularly important in aviation applications, as well as an absence of moving parts, robustness, increased reliability, inexpensiveness, fast time-response, and the ability to be applied onto surfaces without requiring holes or cavities**. On this way, this type of devices are presented sucha an efficient conversion of input electric energy into output fluid momentum, of great significance, and the straightforward nature of simulating the effects of the device using numerical flow solvers is also an asset: completely welcomed in an aeronautical industry future based on a more electric aircraft. [88] [90] [94] [95] [92]

Is important to know the DBD is widely preferred due to its ability to sustain a large volume discharge at atmospheric pressure without the discharge collapsing into a constricted arc [95], due to the inherently self-limiting configuration of the DBD plasma actuator, a behavior dictated by the build-up of charges on the dielectric surface.[28]

[15] **EHD**: Electrohydrodynamic.

Characteristics of the discharge process

Fundamentally, all plasma controllers are characterized by the **transfer of momentum from the accelerated ions and electrons to the surrounding neutral gas by collisions between particles**; this moment transferred to the air flow is called volumetric force.

AC voltages are generally preferred as they provide for a more stable plasma discharge in the presence of a dielectric barrier; nevertheless, other methods have been developed to enable the use of DC voltages to provide for stable plasma discharges in the presence of a dielectric barrier. [122] [123] As already explained, **due to the use of AC current, during the operation of the developed plasma controllers, the luminescent discharge appears every half cycle of the applied AC voltage**. Although at first it may seem that the plasma appears as a relatively uniform diffuse discharge, this statement is erroneous (already seen in Fig. 2.6), since optical measurements indicate that the discharge is highly structured in space and time, as can be seen , again, in the examples contained in Fig. 2.10 and 2.11 –in Fig. 2.12 one can see a example picture of the type of discharge observed in the laboratory–. The temporal nature of the controller indicates that the plasma is in fact a single barrier discharge. [85]

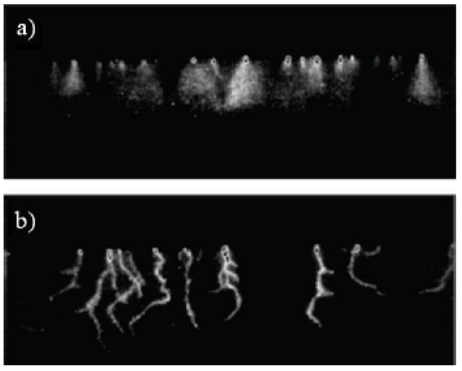

figure 2.10 **High-speed photographs (5 ms exposure) of the micro-discharges generated** in the first (a) and in the second (b) discharge cycle of the plasma controller, the asymmetric structure between both cycles can be observed. *Source of the image: [85]. .*

So, in particular, the configuration most used in plasma actuators are the SDBD configurations, single Dielectric Barrier Discharge, that it consists of two electrodes is exposed to the airflow while the other is encapsulated within the dielectric material. The electrodes are long and thin, arranged in a span-wise direction on the aerodynamic surface, and connected to a DC or AC voltage power source (high voltage), and, usually, the encapsulated electrode is usually grounded. [88] Up to the present time, several investigations are developed based on them. A simple scheme of the SDBD asymmetric configuration described is found in the Fig. 2.13.

The DBD device can maintain its discharge–see Fig. 2.10–. This maintenance of the Dielectric Barrier Discharge requires applying alternating current. In Fig. 2.14 there is a surface discharge configuration illustrating the two cycles that make up its operation.

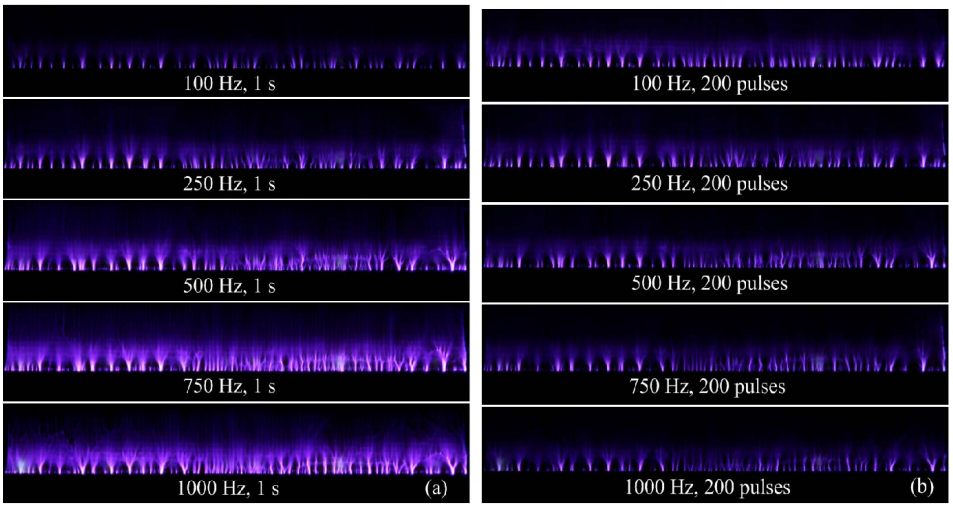

figure 2.11 **DBD discharge images.** Discharge images at different PRFs, exposure times for (a) 1 s; (b) 200 pulses (electrode width 8 mm, electrode gap 2 mm, applied voltage 18 kV). *Source of the image: [85].* .

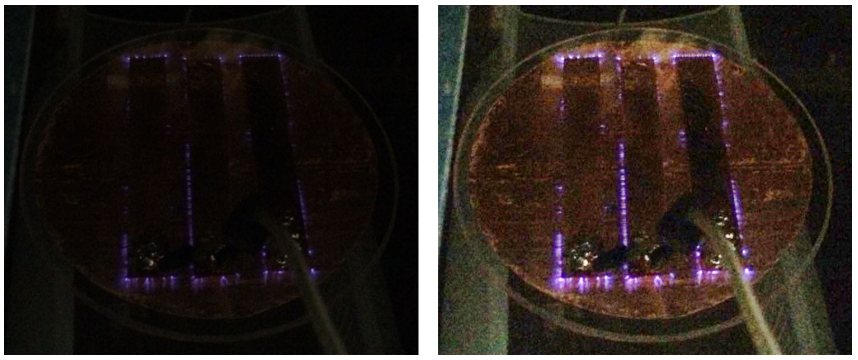

figure 2.12 **DBD discharge images.** DBD discharge during the experiments carried out. As can be seen, the images are repeated, in the case of that on the right they are digitally manipulated with a different color balance, to ensure that the printing of the document allows observing the discharges..

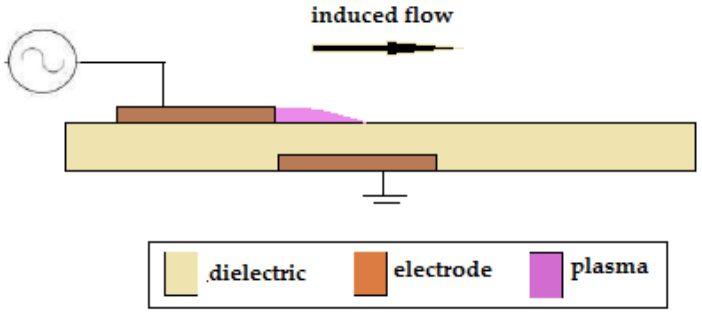

figure 2.13 **Schematic of the profile of an asymmetric SDBD plasma actuator.** An AC voltage of a peak value of 5-20 kV is usually applied to the electrodes at a frequency range from 3-15 kHz.[88] [91] This results in the formation of a plasma discharge above the encapsulated electrode on the surface of the dielectric, due to the ionization of air, aptly providing the device its moniker as a plasma actuator. The color of the plasma depends on the gas. *Source of the image: Own image.*.

Now, the two cycles of the discharge are going to be explained:

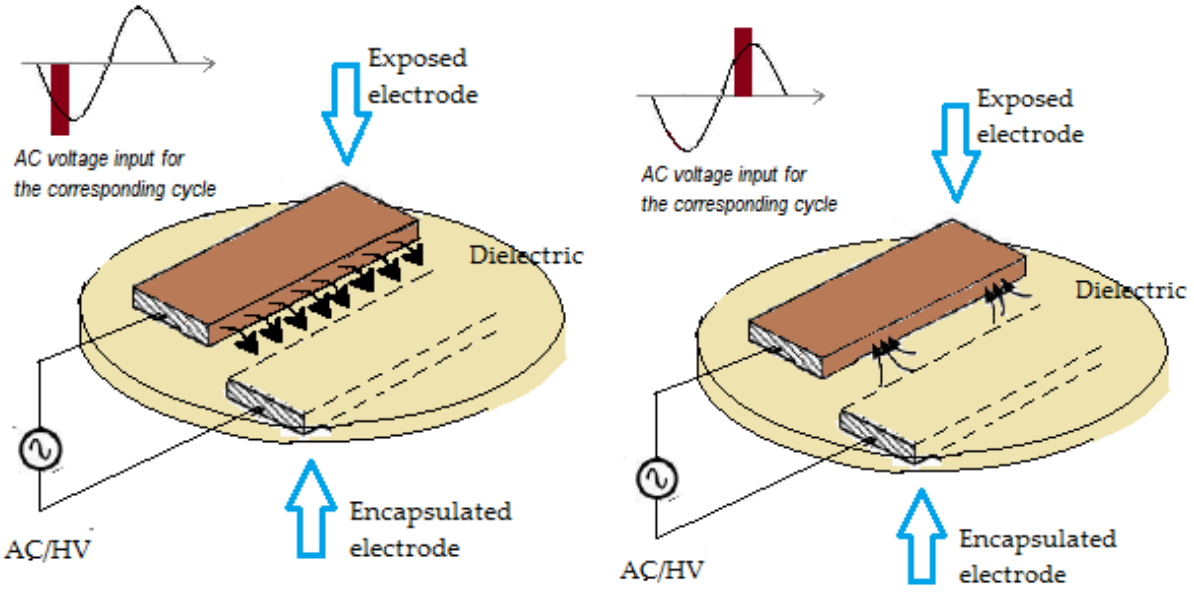

(a) Forward-Phase Charge Cycle: Deposition of electrons on the dieletric layer..

(b) Backward-Phase Charge Cycle: Deposition of electrons onto the exposed electrode..

figure 2.14 **SDBD Diagram of the accumulation of charge in the surface** of the dielectric during the first half cycle (a) and the second half cycle (b)..

- **Forward-Phase Charge Cycle (First half cycle of the discharge):** the exposed electrode is at a more negative potential than the surface of the dielectric, behaving like the cathode in the discharge. In this case, assuming that the potential difference is sufficiently high, the exposed electrode can emit electrons. Because the discharge ends in a dielectric surface, the accumulation of the surface charge opposes the applied voltage, and the discharge is turned off, unless the applied voltage is continuously increased. see Fig. 2.14.a.
- **Backward-Phase Charge Cycle (Second half cycle of the discharge):** the behavior of the discharge is similar in the half cycle opposite: a positive slope applied in the voltage used to maintain the discharge is required. In this half cycle, the charge available for discharge is limited to that deposited during the previous cycle on the surface of the dielectric, where now the surface plays the role of cathode, as can be seen in Fig. 2.14.b.

This self-limiting behavior due to the accumulation of charge in the surface of the dielectric affects the spatial and temporal structure of the plasma.

The **quasi-neutrality** that defines the plasma has already been highlighted, that is to say, that its net charge is null. Taking into account that in the ionization of the gas that gives rise to the plasma, as many electrons as ions are generated (both being the charged components of the plasma); these respond to the external electric field so that the electrons move towards the positive electrode as the positive ions move towards the negative electrode, resulting in a

Table 2.2 Characteristics and typical parameters of the SDBD plasma controller.

Definition range	
$\sim$ Atmospheric pressure	$p = 10^{-1} - 10^{1} bar$
Weakly ionized gas	$\alpha = 10^{-4} - 10^{-3}$
Non-equilibrium plasma	$T_e' = 1 - 10eV$
	$T_i \approx T_n \approx 300K = 0.0259eV$
Range of Usual Values	
Operating voltage	$V = 1 - 50kV$
Frequency of operation	$f = 0.5 - 25kHz$
Wave type	sinusoidal, square, triangular

load imbalance at the edges of the plasma. This imbalance generates an electric field opposite to the applied external field. Thus, the redistribution of charges continues until the net electric field in the plasma is neutralized.[0][28]

Usual values

See Table 2.2.

Thus, the discharge rate of the plasma controllers is generally classified as a luminescent discharge (slightly filamentary) in the group of non-equilibrium plasmas, where the temperature of the electrons is approximately two orders of magnitude higher than that of the electrons ($T_e' = 1 - 10eV$, $T_i \approx T_n \approx 300K = 0{,}0259eV$). According to the low degree of ionization ($\alpha = 10^{-4} - 10^{-3}$), the DBD plasma controllers produce a thin volume of weakly ionized gas, where the density of charged species is approximately $n = 10^{1}6m^{-3}$.[0]

In this work the experiments have been developed in electrical values usual in the industry for this type of devices. Generally, an AC voltage of a peak value of 5-20 kV is usually applied to the electrodes (although it is normal to move in a 1-50 kV range) at a frequency range from 3-15 kHz (analogously, literature can be found that extends this range to $0{,}5 - 25kV$). The AC signal is usually a sinusoidal, square or triangular wave. [88]-[91];[0]

Regarding the pressure of the gas to which the actuator is used, this usually corresponds to reduced pressure ($10^{-1} bar$) that represents cruise characteristics[98][99], or raised to $10^{1} bar$ to reproduce the internal conditions of compressors and turbines.[100] In this work, the central focus will be on experiments at atmospheric pressure (sea level: 1013 mbar).

2.2.4 DBD applications as flow control devices

There are two ways through which to manipulate desire a flow: actively or passively. One knows that with the term "active", it is understood a flow control device that involves the need to apply energy to the system through an actuator, which needs auxiliary power as well as a control method. There are numerous investigations related to plasma controllers, fruit of a growing interest of the scientific world and the industry in the development of both plasma applications and micro-scale technologies. Consequently, you can access a variety of experimental tests or models of representation that support the path of the potential of plasma devices to become a reality for active flow control in a field as promising as aerodynamics. In order to manipulate a free airflow, three are the main objectives to act on: laminar-to-turbulent transition (delaying it to reduce drag, for example), separation (for take-off, landings...) and turbulence (for reducing noise for example).

The main concept is that the body force acting on the flow –see Section 2.3–, as produced by the plasma DBD actuator, is used to change the Kutta condition on the rounded trailing edge of the profile and with that the circulation and corresponding lift. Such a configuration reduces the weight and complexity issues typically associated with classical blowing circulation control concepts and many other concepts aiming at load control[1]. Specifically "in the middle of the 1990s, Roth's group perfected and developed a new atmospheric pressure DBD, a surface DBD, established in air between at least two electrodes placed asymmetrically on each side of a dielectric; they protected it by a patent in 1994 and called it 'One Atmosphere Uniform Glow Discharge Plasma' (OAUGDPTM)." It waas presented for the first time for airflow control in 1998 [149], [147] and published in a journal in 2000 [148]. It was revealed that the discharge induces a secondary airflow of several m/s tangentially to the wall, an that consequent force increases with the applied voltage, modifying the free air stream, which causes a change in the drag.

Going back to half a century ago in history, where one of the first discharge-based flow control articles was published in 1968 by Velko and Ketcham [136], who demonstrated the effect of electric fields on fluid boundary layers through corona discharge cables, which were placed at a short distance from the surface of the flat plate. It also highlights the advances made in the 90s by the research group of John R. Roth at the University of Tennessee; they developed a new way of generating uniform supeficial Dielectric Barrier Discharge, which was called uniform discharge of luminescent plasma at one atmosphere (OAUGDP). At the end of the century, Roth published the first results based on OAUGDP [137].

At present, this subject arouses great interest in the scientific world, and the generation of plasma by barrier discharge is proposed in a variety of aerodynamic applications, as it is the case that concerns the replacement of moving parts for flow control where, in addition, a fast response time is needed. Some other applications successfully tested in the laboratory are the elevation of the wing section [135], control of the separation of the blades of a low pressure turbine [138], control of the aerodynamic flow at the tip of a turbine [139], generation of unstable vortex [140], separation control at the tip of a wing profile [141], application to the aerodynamics of a train [124], etc. In the final chapter of this work, in which the main conclusions of the study are summarized, some other studies are shown that can be compared with the present work, or that analyze the same concept from different perspectives or

models (as experimental as computational), as well as possible future research lines.

Important dissertations also are the projects related with the study of the single-dielectric barrier discharge aerodynamic plasma actuator, developed in [88] and [95] by Orlov et al., where the physics of the plasma discharge was studied through the time-resolved light intensity measurements of the plasma illumination, and plasma characteristics were obtained and analyzed for a range of applied voltage amplitudes and a.c. frequencies. Based on this data, electro-static and lumped-element circuit models were developed, and, in this way, the time-dependent charge distribution was used to provide boundary conditions to the electric field equation that was used to calculate the actuator body force vector; and it was applied on airfoils.

Finally, some very interesting theses, in addition to those that are appearing referenced throughout the work, or that can be found in the historical summary on the plasma actuators made by Moreau [94], are the following. For example, “Plasma Flaps and Slats: An Application of Weakly Ionized Plasma Actuators” [150], “Environmental Impacts on Dielectric Barrier Discharge Plasma Actuators” [151] , application related with anti-icing, for example, in “Experimental study of an anti-icing method over an airfoil based on pulsed dielectric barrier discharge plasma”[152] or “An experimental study of icing control using DBD plasma actuator ” [153], about plasma actuators manufacturing to reduce degradation[154] or, different, for separation control in oscillating profiles[155]. It is also interesting to pay attention to the publications developed in the framework of the Delft University of Technology about plasma actuators in recent years.

2.3 Mechanical, Electrical and Spectroscopic Analysis

It is intended to model the plasma actuator in such a way that its effectiveness in controlling flow separation is as successful as possible. For this, most experiments have focused on the modification of the physical dimensions and macroscopic parameters of the plasma actuator system. There are many parameters involved, so controlling in detail the dynamic behavior of the system becomes extremely complicated in short time scales. However, the macroscopic behavior of the device is highly influenced by its microscopic structure, and the fact that the scales of measurement of the device elements and the discharges move in small units (the devices are usually several millimeters in height and the discharge is composed of multiple micro-shocks of short duration, of the order of nanoseconds that vary significantly over the period of the AC voltage source) –see Chapter 3–, causes that directly measure these properties microscopic is also of great difficulty, properties such as charge density or electric field.

In this work the DBD devices are going to be characterized, above all, through an electrical analysis, and for this **it is going to study aspects such as the influence of the configuration of the electrodes, the dielectric material or the gap,** whose results are presented in the following chapters. In the consulted bibliography, as it has been summarized in Section 2.2, there have been very diverse studies in which other parameters have been varied; that is why it is recommended that the reader go to different bibliography to deepen in the understanding of this type of reactors.

An efficient alternative to measure these micro-properties is numerical modeling, thus, numerical modeling and simulations are useful and flexible tools for modeling the development of Dielectric Barrier Discharge controllers in spatial and temporal dimensions, in addition to being able to continuously monitor the evolution of complex flow control systems. But, like it has been explained, this is not the objective of this work –see Section 1.1–.

In this part of the document, firstly, fundamental concepts about plasma body force are collected in Section 2.3; accordingly to the power characterization, in Section 2.3 the aspects of the electrical analysis that correspond to this work are explained; likewise, spectroscopic analysis is included, whose bases are found in Section 2.3.

2.3.1 Ionic wind

The ionized air that appears on the dielectric surface is the basic mechanism that gives it the ability to manipulate or induce a flow configuration to the DBD plasma actuator or controller, since in the presence of the electric field produced by the geometry of the electrode, a force of body that acts on the environment, not charged air; because it has already been seen that the collision processes lead to a transfer of momentum between the particles involved, because as the charged particles move under the Coulombian forces of the electric field, between the exposed electrode and the surface of the dielectric, they collide with the neutral particles that make up the gas, transferring amount of movement, these collisions being called “Lorentzian collisions”. This effect is classically termed as an

electric wind, directed from the exposed electrode toward the dielectric surface, that modifies the boundary layer, and allowing for the active manipulation of the airflow [93][94][95]; the act of producing a mechanical output or kinetic energy, for an electrical input or electric energy, without the use of mechanical moving parts, classifies the plasma actuator as a Micro-Electro-Mechanical-System (MEMS). [94]

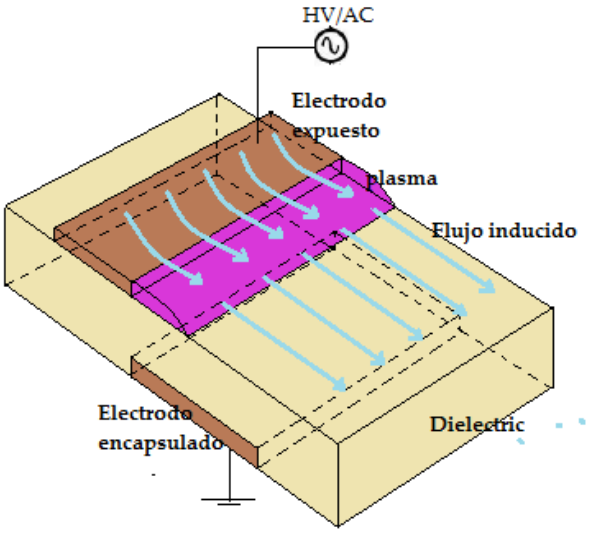

figure 2.15 **Scheme of the flow controller where the direction of flow induced can be seen.** .

Thus, **ion wind** –ionic wind, coronal wind or electric wind– **describe the airflow induced by electrostatic forces linked to corona discharge arising at the tips of some sharp conductors** (such as points or blades) **subjected to high voltage relative to ground**, as each collision contributes to the force exerted on the gas and in this way flow velocities are induced on the surface of the electrodes. The induced flow is characterized by a tangential velocity from the exposed electrode towards the encapsulated electrode –see Fig. 2.15–. Ion wind (this motion induced in the gas, created by the Coulombian forces acting on the ions and electrodes, and the Lorentzian collisions between the particles) **is an electrohydrodynamic phenomenon**; and Ion wind generators can also be considered electrohydrodynamic thrusters. [97] [32]

As already mentioned, the DBD controllers generate an EHD force or plasma body force that depends entirely on the electric field, $\vec{E}(\vec{r},t)$, defined by the geometry of the electrode and the charged particles density, $\vec{n_i}(\vec{r},t)$,as a function of position $\vec{r}$ and time t, integrated into the plasma volume V –see equations 2.11 and, summed over all species, 2.12–.[28]

$$\vec{F}_i(t) = \int_v q_i n_i(\vec{r},t)\vec{E}(\vec{r},t)\mathrm{d}t \tag{2.11}$$

$$\vec{F}_{EHD}(t) = \sum_i \vec{F}_i(t) \tag{2.12}$$

The phenomenon of electric wind, is referred to the “movement of gas induced by the repulsion of ions from the

vecinity of a high voltage electrode" [46], and it was firstly reported at the beginning of XVIII century and Faraday explained it more than a hundred years later. So, this wind, as Moreau says in [94], "is due to the collisions between the ions that drift and the neutral particles in the electrode gap region, because as the electron velocity is much higher than the ion one, one can neglect the role of electrons because their mass is very low compared with the ion one." Expression 2.3[46] contains the firs relation for electric wind:

$$v_G = k\sqrt{\frac{i}{\rho\mu}}$$

In consequence, plasma actuators consist of using the discharge-induced electric wind within the boundary layer to change its properties, and in this way transform the airflow actively. During this project, the most usual configuration also has been built and tested, composed of two electrodes flush-mounted at the wall of a flat plate (simulating the wing profile), between which a high voltage is applied, generating a non-thermal surface plasma. When discharge is on and is established, the airflow is deviated tangentially very close to the wall and accelerated within its boundary layer as consequence of the depression induced at the anode by the electric wind.[94] In these conditions of the devices that are going to be exposed in this worl, and above the ignition voltage, a plasma sheet appears on both sides of the dielectric, consisting of an electric wind on both sides of the dielectric substrate. As one can check in this document, electrical and mechanical ..as bibliography tell us[94]– characteristics of this plasma depend strongly on different parameters, such as electrode width, electrode gap, dielectric thickness or the nature of the dielectric.

Over the years, various body force models have been proposed, and these models can be classified into two categories: Phenomenological (or Simplified), and First- Principles-Based models. Phenomenological models involve approaches with reduced complexity providing reasonable qualitative correspondence with experimental observations. In reference [28], is explain to us that such models are limited in their ability to accurately pre- dict, and explain the physics involved. Meanwhile, First-Principles-Based models distinctly address the necessary knowledge required towards understanding the fundamental physical processes involved. [91]-[96]

This work will not have simulation studies, but the reader can go to, for example, the reference [28] to know the conclusions drawn from the analysis developed to understand the plasma actuators through: a fluid electrostatic model by Orlov[88], and a hybrid PIC model formulated by the author. Both models are based on first-principles, whose objective will be to provide a comparative study of the two models in their application to the SDBD plasma actuator flow problem focusing specifically on the formation of the plasma body force.

2.3.2 Electrical characterization: Accumulated charge and Consumed power

The yield of a plasma controller is mainly characterized by the electrical power that is consumed during the discharge. The plasma parameters, such as electron density, sheath thickness and sheath voltage, are not easy to be probed experimentally, while the electrical characteristics, such as impedance, resistance and reactance, are relatively convenient to be measured, and there are several studies that that relate both parameters through theoretical models. [146]

In Section 3.4 the schematization of the experimental procedure will be presented, while in the present part of the work the underlying theory is indicated. As a result of the experiment, the oscilloscope returns two output files with the electrical conditions of the storage point, that is, the breakdown point of the plasma; These correspond to the current and voltage signal that the device is experiencing at that moment, and which contain as many signal periods as specified on the screen –see Fig. 4.1 and 4.2– ; the signal can be saved either averaged or not averaged. Thus, one has two files that contain the discretization of $V_{bd}(t)$ e $I_{bd}(t)$, and from them all the electrical parameters that are presented in this Section are calculated/obtained. Voltage and current are defined as follows:

- **Voltage, electric potential difference, electric pressure or electric tension** (formally denoted ΔV or ΔU, but more often simply as V or U, for instance in the context of Ohm's or Kirchhoff's circuit laws) is the difference in electric potential between two points. The voltage between two points is equal to the work done per unit of charge against a static electric field to move a test charge between two points. This is measured in units of volts (V) (a joule per coulomb); moving 1 coulomb of charge across 1 volt of electric potential requires 1 joule of work.[126]

- **Electric current**, I is a flow of electric charge. In electric circuits this charge is often carried by moving electrons in a wire. It can also be carried by ions in an electrolyte, or by both ions and electrons such as in an ionised gas (plasma).[127]

  The SI unit for measuring an electric current is the ampere (A), which is the flow of electric charge across a surface at the rate of one coulomb per second.

- **Phase difference or Phase shift** as it is also called of a Sinusoidal Waveform is the angle ϕ, in degrees or radians that the waveform has shifted from a certain reference point along the horizontal zero axis. In other words phase shift is the lateral difference between two or more waveforms along a common axis and sinusoidal waveforms of the same frequency can have a phase difference.[108]

  The three main components in an AC circuit which can affect the relationship between the voltage and current waveforms, and then their phase difference, by defining the total impedance of the circuit are the resistor, the capacitor and the inductor. The generated current in plasma reactor is sinusoidal with a phase shift ϕ with respect to the voltage signal–see Fig. 4.1 and 4.2–, because there are not only resistive elements, and we are interested in moving away from a behavior of the device as if it were a capacitor[16]. Related to this, for the further development of the power concept, it is important to know that the intensity has two components. Active component of the intensity, $I_a = Icos\ \phi$, is defined to the component of it that is in phase with the voltage, and reactive component, $I_r = Isen\phi$, to which it is in quadrature with it –see Fig. 2.16.a–; so in order

[16] **Why is there a phase shift between current and voltage in an AC circuit?**

Related to the impedance associated with the passage of current in the case of capacitors and coils. The capacitor, when it is initially discharged, offers little resistance to current flow; However, as time goes by, it becomes charged and thus increases the resistance to the passage of current. When it is fully charged, its behavior is as if it were an open circuit.

The fact of using alternating current causes that it also generates the same effect when the capacitor is discharged, at the beginning of the negative half cycle. When the voltage enters in a negative half-cycle, the capacitor still has remains from the charge of the first half cycle. This is what causes 90 to be lagged.

In the case of the coils, the behavior is completely opposite to that of the capacitor. In a coil, its first behavior is of high impedance, and with the passage of time, this resistance begins to decrease

for us to calculate the total consumed power, it is needed to know the phase difference between the sinusoidal waveforms of the voltage and current.

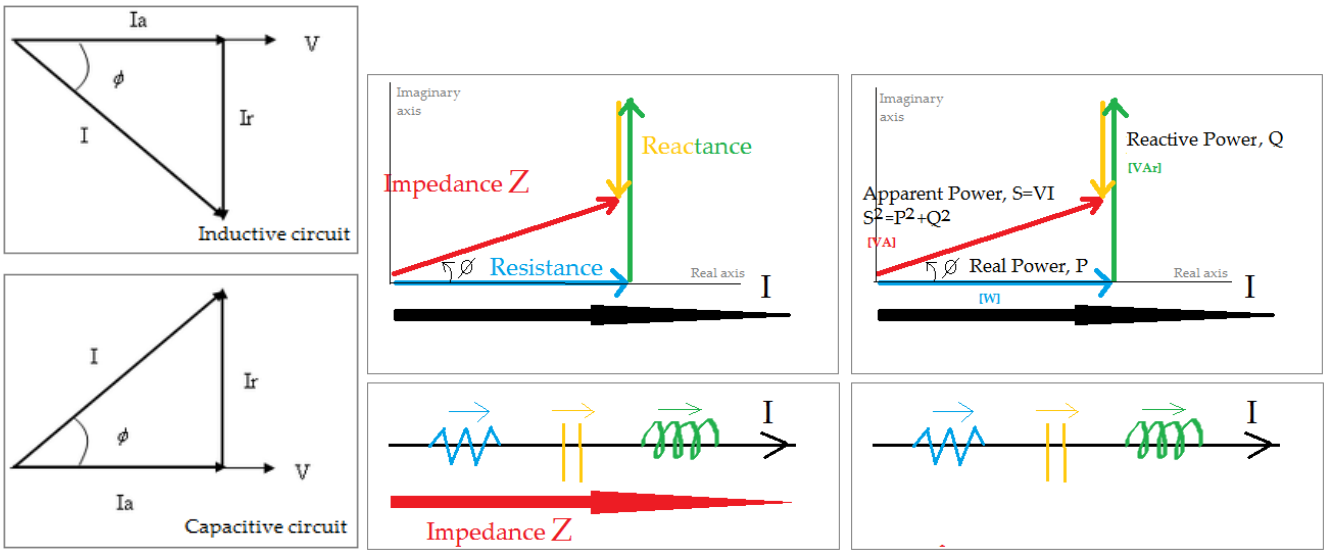

(a) Current triangle.. **(b)** Impedance triangle.. **(c)** Power triangle..

figure 2.16 **RLC circuit in AC: complex current, complex impedance and complex power.**
A phasor is a graphic representation of a complex number that is used to represent an oscillation, so that the phasor sum of several phasors can represent the magnitude and phase of the oscillation resulting from the superposition of several oscillations in an interference process..

The signals that are received from the oscilloscope in a discrete manner, are first centered so that the calculations of the integrals in which they are later involved are more precise; for this the following assumption is taken: the average of each of the signals during a period must be zero. In addition, after that they are smoothed through the *smooth* Matlab function.

Ohm's law is a basic law of electrical circuits. It establishes that the potential difference V that is applied between the ends of a given conductor is proportional to the intensity of the current I that circulates through said conductor. Ohm completed the law introducing the notion of electric resistance R; which is the proportionality factor that appears in the relationship between V and I:

$$V = R \cdot I \tag{2.13}$$

where V corresponds to the potential difference, R to the resistance e I to the intensity of the current. The units of these three magnitudes in the international system of units are, respectively, volts (V), ohms (Ω) and amps (A).

Some parameters used in this projects are explained in the following sections:

- Voltage and Current, peak-to-peak and RMS values
- Accumulated Charge
- Lissajous Figures and Zero Charge

- Impedance Components
- Consumed Power
- Power Factor and Phase Shift

Voltage and Current, peak-to-peak and RMS values

The amplitude of a periodic variable is a measure of its change over a single period (such as time or spatial period). There are various definitions of amplitude (peak-to-peak amplitude, peak amplitude, semi-amplitude, root mean square amplitude (RMS) or pulse amplitude), which are all functions of the magnitude of the difference between the parameter's extreme values. In general, the use of peak amplitude is simple and unambiguous only for symmetric periodic waves.[129]

- ***Peak-to-peak amplitude*** is the change between peak (highest amplitude value) and trough (lowest amplitude value, which can be negative). With appropriate circuitry, peak-to-peak amplitudes of electric oscillations can be measured by meters or by viewing the waveform on an oscilloscope.
- ***Peak amplitude***, useful in telecommunications and other areas where the measurand is a signal that swings above and below a reference value but is not sinusoidal; if the reference is zero, this is the maximum absolute value of the signal; if the reference is a mean value (DC component), the peak amplitude is the maximum absolute value of the difference from that reference.
- ***Peak amplitude, semi-amplitude or amplitude*** means 1/2 (half) of the peak-to-peak amplitude.
- ***Root mean square (RMS) amplitude:***

  The quadratic mean value of an electric quantity is called the effective value. The concept of effective value is used especially to study the periodic waveforms, despite being applicable to all waveforms, constant or not. It is sometimes referred to as RMS (from the English, root mean square).

  So, this value is used especially in electrical engineering, and is defined as the square root of the mean over time of the square of the vertical distance of the graph from the rest state, i.e. the RMS of the AC waveform (with no DC component). For complicated waveforms, especially non-repeating signals like noise, the RMS amplitude is usually used because it is both unambiguous and has physical significance. For example, the average power transmitted by an acoustic or electromagnetic wave or by an electrical signal is proportional to the square of the RMS amplitude (and not, in general, to the square of the peak amplitude).

  For alternating current electric power, the universal practice is to specify RMS values of a sinusoidal waveform. One property of root mean square voltages and currents is that they produce the same heating effect as direct current in a given resistance.

The peak-to-peak value is used, for example, when choosing rectifiers for power supplies, or when estimating the maximum voltage that insulation must withstand.

$$V_{RMS} = \frac{V_{peak}}{\sqrt{2}} \tag{2.14}$$

$$I_{RMS} = \frac{I_{peak}}{\sqrt{2}} \tag{2.15}$$

- ***Pulse amplitude***, in telecommunication, is the magnitude of a pulse parameter, such as the voltage level, current level, field intensity, or power level. Pulse amplitude is measured with respect to a specified reference and therefore should be modified by qualifiers, such as average, instantaneous, peak, or root-mean-square.

Accumulated Charge

Electric charge, Q, is the physical property of matter that causes it to experience a force when placed in an electromagnetic field. There are two types of electric charges, that is, positive and negative (commonly carried by protons and electrons respectively). Electric charge is a conserved property: the net charge of an isolated system, the amount of positive charge minus the amount of negative charge, cannot change. An object with an absence of net charge is referred to as neutral. [130]

The coulomb (C) is the International System of Units (SI) unit of electric charge. It is the charge transported by a constant current of one ampere in one second.

In this paper the concept of accumulated electric charge Q_a will be used and, specifically, of **accumulated centered charge** Q_c (although for simplification the subscript can be eliminated from now on), whose mathematical expressions are as follows, equation 2.16 and 2.17, respectively:

$$Q_a(t) = \sum_t I(t) \cdot \mathrm{d}t \tag{2.16}$$

where the summation has been calculated in Matlab through the *cumsum()* function, and the time differential $\mathrm{d}t$ is calculated as the time interval between two measurements, directly from the outputs of the oscilloscope, and

$$Q_c(t) = Q_a(t) - \frac{max\{Q_a(t)\} + min\{Q_a(t)\}}{2} \tag{2.17}$$

and finally, $Q_c(t)$ is smoothed through the *smooth()* function, which smooths the data in the column vector, what is in function's parentheses, using a moving average filter, being the default span for the moving average 5.

Lissajous figures and Zero charge

The representation known as "**Lissajous figures**" (also known as Lissajous Curve or Bowditch curve) are of vital importance in this type of electrical analysis; these are provided by the trajectories followed by the system in the two-dimensional space in its magnitudes of voltage and stored charge, because in mathematics it is the graph of a system of parametric equations (equations 2.19) which describe in general, the superposition of two simple harmonic movements in perpendicular directions (and a complex harmonic motion in classical mechanics). This family of curves was investigated by Nathaniel Bowditch in 1815, and later in more detail by Jules Antoine Lissajous in 1857.

$$x = Asin\ (at+\alpha) \tag{2.18}$$

$$y = Bsin\ (bt+\beta) \tag{2.19}$$

where A and B are the corresponding amplitudes of these signales, a is w_x, b is w_y (frequencies of both movements) and $\delta = \alpha - \beta$, the phase difference, usually in the literature.

Eliminating the time in the previous expressions you get an equation of the trajectory of the type:

$$f(x,y,\delta) = cte \tag{2.20}$$

Regarding properties of shape, visually, the ratio a/b determines the number of "lobes" of the figure, so, the appearance of the figure is highly sensitive to this ratio. For a ratio of 1, the figure is an ellipse, with special cases including circles ($A = B, \delta = \pi/2$ radians) and lines ($\delta = 0$); and another simple figure is the parabola ($b/a = 2, \delta = \pi/4$). Other ratios produce more complicated curves, which are closed only if a/b is rational, and the visual form of these curves is often suggestive of a three-dimensional knot, and indeed many kinds of knots, including those known as Lissajous knots, project to the plane as Lissajous figures.

Respect to the specfic value of the ratio, for example, a ratio of $3/1$ or $1/3$ produces a figure with three major lobes, or similarly, a ratio of $5/4$ produces a figure with five horizontal lobes and four vertical lobes. Rational ratios produce closed (connected) or "still" figures, while irrational ratios produce figures that appear to rotate.

By last, the ratio A/B determines the relative width-to-height ratio of the curve. That is, for example, a ratio of $2/1$ produces a figure that is twice as wide as it is high. Finally, the value of δ determines the apparent "rotation" angle of the figure, viewed as if it were actually a three-dimensional curve. For example, $\delta = 0$ produces x and y components that are exactly in phase, so the resulting figure appears as an apparent three-dimensional figure viewed from straight on (0). In contrast, any non-zero δ produces a figure that appears to be rotated, either as a left–right or an up–down rotation (depending on the ratio a/b).[101]

Although originally the Lissajous figures are formed with the representation of current $I(t)$ in front of voltage $V(t)$, it is very useful to develop them from the representation of charge $Q(t)$ versus voltage $v(t)$, since this way one has that the area enclosed in the figure is directly related to the amount of accumulated charge. In addition,

the literature consulted indicates that as the frequency of the discharge signal increases, all materials experience a tendency to decrease their maximum accumulated charge. In this work, this trend will be verified. This enclosed area multiplied by the (respective) frequency is defined as the average power:

$$\overline{p} = f \cdot Area[Q,V] \tag{2.21}$$

where Q is referred to, as it was explained above, the accumulated centered charge.

From the previous Lissajous figure $Q(t)$ vs. $V(t)$, it can also be highlighted a significant value, such as the zero charge Q_0, representative of the amount of accumulated charge at null voltage. For an ideal DBD plasma, its Lissajous figure takes the form of the Fig. 2.17, being the faces of the parallelogram being more horizontal those in which the plasma is off. However, in this work the form is more elliptical, as in many other documents that have been consulted.

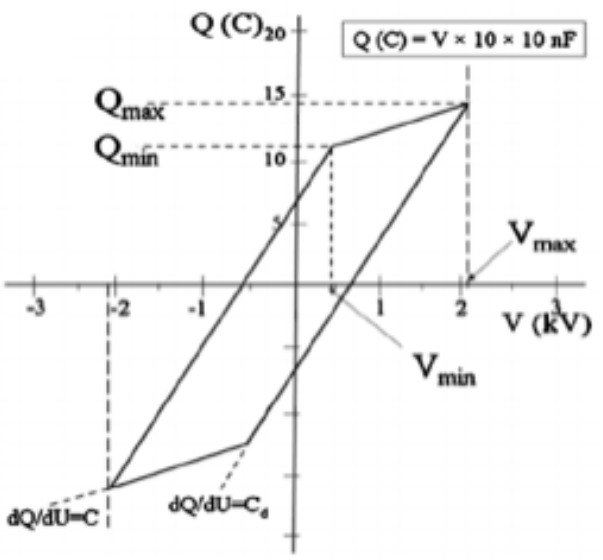

figure 2.17 **Lissajous Figures for an ideal DBD plasma: Example.**.

Impedance components

Electrical impedance Z is the measure of the opposition that a circuit presents to a current when a voltage is applied. The term complex impedance may be used interchangeably in AC. [118] So, quantitatively, the impedance of a two-terminal circuit element is the ratio of the complex representation ($Z = V/I = X_R + jX_I$)f the sinusoidal voltage.

Impedance extends the concept of resistance to AC circuits (which have both resistive and reactive components) due to its resistance and reactance that are combined together to give a total impedance, possesing both magnitude and phase, unlike resistance, which has only magnitude; but impedance is not equal to the algebraic sum of the resistive and reactive ohmic values because pure resistance and pure reactance are 90º out-of-phase with each other. When a circuit is driven with direct current (DC), there is no distinction between impedance and resistance; the latter can be thought of as impedance with zero phase angle.

This geometric relationship between resistance, reactance and impedance can be represented visually by the use of an impedance triangle, with the impedance being the hypotenuse as determined by Pythagoras theorem, as it can be seen in Fig. 2.16.b.

The notion of impedance is useful for performing AC analysis of electrical networks, because it allows relating sinusoidal voltages and currents by a simple linear law. So, impedance is a complex number, with the same units as resistance, for which the SI unit is the ohm (Ω). Its symbol is usually Z, and it may be represented by writing its magnitude ($|z|$ and phase θ.

Regarding the calculation of the impedance, first, to simplify calculations, sinusoidal voltage and current waves are commonly represented as complex-valued functions of time denoted as V and I:

$$V = |V|e^{j(\omega t+\phi_V)} \tag{2.22}$$

$$I = |I|e^{j(\omega t+\phi_I)} \tag{2.23}$$

The impedance of a bipolar circuit is defined as the ratio of these quantities:

$$Z = \frac{V}{I} = \frac{|V|}{|I|}e^{j(\omega t+\phi_I)} \tag{2.24}$$

Hence, denoting $\theta = \phi_V - \phi_I$, one has

$$|V| = |I| \cdot |Z| \tag{2.25}$$

$$\phi_V = \theta + \phi_I \tag{2.26}$$

where the last equation defines the phase relationship.

Consumed power

The **electric power**[17] P, as a function of the operating voltage, V, is an established measure to describe electrical characteristics of the plasma controller. Electric power is the rate, per unit time, at which electrical energy is transferred by an electric circuit. The SI unit of power is the watt (W), one joule per second. This magnitude, in terms of average value, is defined as the frequency multiplied by the area enclosed in the Lissajous figures $Q(t)$ vs. $V(t)$, for each frequency. However, as an instantaneous value the Ohm's law is used for calculation, so that for each moment the power is:

$$P = \text{work done per unit time} = \frac{VQ}{t} = VI \Rightarrow P(t) = V(t) \cdot I(t) \tag{2.27}$$

[17] General concepts extracted from: [110][111][112].

and following this definition from Ohm's law, we obtain this average expression for a period, whose result must coincide with the area enclosed in the figure of Lissajous multiplied by frequency for the corresponding frequency:

$$\overline{P} = \frac{1}{T}\int_{t=0}^{T} V(t)\cdot I(t)\mathrm{d}t \tag{2.28}$$

However, taking these arguments to specific theory of alternating current AC, in the case of sinusoidal alternating current, the average electrical power developed by a two-terminal device is a function of the effective values or mean square values, of the potential difference between the terminals and the current that passes through the device.

In an AC circuit, the voltage and current waveforms are sinusoidal, i.e., their amplitudes are constantly changing over time. Since is is known that power is voltage times the current ($P = V \cdot I$), maximum power will occur when the two voltage and current waveforms are lined up with each other, that is, their peaks and zero crossover points occur at the same time. It happens when the two waveforms are said to be "in-phase". But if not, then, remembering the current components, the product of the intensity, and those of its active and reactive components, by the voltage results in the **apparent** (S), **active** (P) and **reactive** (Q) powers, respectively.

- ***Apparent Power***, S: is the magnitude of the complex power in an AC circuit, being the module of the vector sum of its components. It is measured in volt-ampere (VA),

  $$S = V \cdot I \Rightarrow S = V_{RMS} \cdot I_{rms} \Rightarrow S^2 = P^2 + Q^2 \tag{2.29}$$

  This power is not really the "useful" power, except when the power factor is the unit ($cos\ \phi = 1$) –explained later in this enumeration–, and indicates that the power supply of a circuit must not only satisfy the energy consumed by the resistive elements, but also considers which will "store" the coils and capacitors.

- ***Active Power***, P: is used as useful power. It is also called average consumed power or absorbed, real or true power; and is due to resistive devices. It is the power capable of transforming electrical energy into work; this power is, therefore, the one actually consumed by the circuits. It is measured in watts (W).

  If a sinusoidal voltage of the form $V(t) = |V| \cdot \sin(\omega t)$, this will cause in the case of an inductive character circuit a current $I(t) = |I| \cdot \sin(\omega t - \phi)$ offset by an angle with respect to the applied voltage ϕ, where, for the purely resistive case, the phase angle can be taken as zero. The instantaneous power will be given as the product of the previous expressions:

  $$P(t) = |V| \cdot |I| \cdot \sin(\omega t - \phi) \cdot \sin(\omega t) = |V| \cdot |I| \frac{cos\ \phi - cos\ (2\omega t - \phi)}{2} \tag{2.30}$$

  and replacing the peak values with the effective ones:

  $$P(t) = V_{RMS} I_{RMS} cos\ \phi - V_{RMS} I_{RMS} cos\ (2\omega t - \phi) \tag{2.31}$$

  This gives a constant power component and another variable with time for the complex power of an electric circuit of alternating current, being the first value called *active power* and the second *fluctuating power*.

Summarizing and according to its expression, the law of Ohm and the triangle of impedance –see Fig. 2.16.b–:

$$P = V \cdot I_a \Rightarrow P = I_{RMS} \cos\ \phi \cdot V_{RMS} = I_{RMS} Z \cdot I_{RMS} \cos\ \phi = I_{RMS}^2 \cdot Z \cdot \cos\phi = I_{RM\ S}^2 \cdot R \tag{2.32}$$

where it can be verified that the power is due is due to the resistive elements.

Then real power, P, in an AC circuit is the same as power, P, in a DC circuit. As resistances do not produce any phase shift between voltage and current waveforms, all the power is delivered directly to the resistance and converted to heat, light and work. Then consumed power by a resistance is real power which is fundamentally the circuits average power.

- ***Reactive Power**, Q* is not consumed or generated in the strict sense, although by convention can be found terms like “reactive power generated” and/or “reactive consumed power”. In linear circuits only appears when there are coils or capacitors; so, therefore, all that power developed in inductive circuits is inductive reactive power, and capacitive reactive power is all that power developed in a capacitive circuit.

$$Q = V \cdot I_r = V \cdot Isen\phi \tag{2.33}$$

Power factor and phase shift

In a purely resistive circuit, both voltage and current signals are in phase with each other, so the actual consumed power is the same as the apparent power, since the phase shift is zero. In this way the power factor is of value one, since $cos\ (\phi = 0) = 1$. This result implies that the number of watts of consumed power is the same as the number of volt-amperes consumed, that is, a unit value for the power factor is equivalent to a percentage of 100 % in which there are no energy losses; since in a conceptual way the reactive power is a power of “ roundtrip ” in that when there are capacitors and coils, they remain continuously storing and returning energy, but there are losses in these "trips".

That is, the **power factor** of an alternating current circuit is defined as the ratio between the active power, P, and the apparent power, S; giving a measure of the capacity of a charge to absorb active power. For this reason, $cos\ \phi = 1$ in purely resistive loads; and in ideal inductive and capacitive elements without resistance $cos\ \phi = 0$ (that is the number of watts consumed is zero but there is still a voltage and current supplying the reactive charge), because there is no phase difference between the voltage and the current in a resistive circuit, the phase shift between the two waveforms will be zero.

$$PF = \frac{P}{S} = cos\ \phi \tag{2.34}$$

where in impedance calculations phase shift ϕ was referred as θ. Those losses of the trip that were discussed are those that should be avoided by compensating the inductive reactive power with the capacitive one, as close to the consumption as possible. In this way it is achieved that the energy does not fluctuate and part of it is not lost along the way; this is called power factor compensation, which should be as close to 1 as possible.

To find the corresponding value of the real power the rms voltage and current values are multiplied by the cosine of the phase angle, θ as shown.

2.3.3 Spectroscopic analysis

Electromagnetic radiation is composed of a series of particles called photons. These particles travel at the speed of light, and their energy is shown in equation 2.35. The electric and magnetic fields of radiation, especially the electric one, which is the most intense, interact with matter, due to the electrical nature that it possesses. The main phenomena originated by the light-matter interaction are: reflection, dispersion, transmission and absorption.

The energy of a photon of an electromagnetic wave or its corresponding frequency is equivalent to the energy difference between two quantum states of the substance studied. The basic equation of spectroscopy is as follows:

$$\Delta E = h \cdot \nu \tag{2.35}$$

where h is the Planck constant, ν is the frequency of the light beam or electromagnetic wave associated with that how much of light –that is, the oscillation frequency of the electric and magnetic fields associated with said photon, which oscillate transversely to the propagation direction of the wave– and ΔE is the energy difference. The energy differences between quantum states depend on the elemental composition of the test or the structure of the molecule, depending on the case in which we are.

So, **what is spectroscopy?** spectroscopy is the study of the interaction between electromagnetic radiation and matter, with absorption or emission of radiant energy. The purpose of spectroscopy is to obtain information about a test or a radiant body.

Electromagnetic radiation is attributed to energy differences in the transitions of electrons from one atomic level to another. There are three cases of interaction with matter: elastic shock, inelastic shock and absorption or resonant emission of photons; spectroscopy is related in most cases to the third interaction, being understood by it all phenomena of absorption and emission of radiation by matter, studying in what frequency or wavelength a substance can absorb or emit energy in the form of a quantum of light.

Although the emission lines are caused by a transition between quantized energy states, and can be very sharp at first glance, they have a finite width; that is, they are composed of more than one wavelength of light. In general, the distribution of intensity as a function of frequency or wavelength is called **spectrum**. In addition to visible light ($\lambda = 700 - 400nm.$), spectroscopy now covers a large part of the electromagnetic spectrum. Visible light is physically identical to all electromagnetic radiation. It is visible to the human being, because the eye detects this narrow radiation band of the complete electromagnetic spectrum. This band is the dominant radiation that the Sun emits.

The molecules in gaseous state, absorb radiation, at least, in 3 regions of the spectrum, microwave, IR and

UV-visible. A molecule absorbs a photon only if the energy of the incident radiation exactly matches the separation between two energy levels of the molecule. This condition is necessary, although not sufficient, since another set of requirements must be fulfilled (selection rules).[113]

Molecules are small accumulators of energy, and can modify their energy by collisions with other molecules, or by emission or absorption of radiation.

There is a set of spectroscopies called emission – often called **Optical emission spectroscopy** , due to the nature of the light that is emitted–, in which the molecules are previously excited, analyzing then the radiation they emit upon returning to their ground state, and this is the case that occupies this work as can be known. In this work the molecules have been excited by the passage of electrical current. Then, also called field spectroscopy or emission spectroscopy, optical spectroscopy for the study of plasmas is a characterization technique that allows to know the properties of a plasma. So, Emission optical spectrometry is a spectroscopic technique that analyzes the wavelengths of photons emitted by atoms or molecules during their transition from an excited state to a state of lower energy. Each element emits a characteristic set of discrete wavelengths according to its electronic structure. By observing these wavelengths, the elemental composition of the sample can be determined. Emission spectrometry was developed at the end of the 19th century, and theoretical efforts to explain the atomic emission spectra led to quantum mechanics.

Thus, the **spectral analysis** is based on detecting the absorption or emission of electromagnetic radiation at certain wavelengths, in relation to the energy levels involved in a quantum transition. By means of a spectrophotometer the spectrum of the light is measured (intensity of the light absorbed, reflected or emitted as a function of the frequency or of the wavelength); and the spectra differ considerably from element to element.

Previous concepts

Quantum mechanics is a discipline of physics responsible for providing a fundamental description of nature at small spatial scales. Quantum mechanics can not predict the exact location of a particle in space, only the probability of finding it in different places; and, in consequence, there is the term “atomic orbital” is a mathematical function that describes the wave-like behavior of either one electron or a pair of electrons in an atom. This function can be used to calculate the probability of finding any electron of an atom in any specific region around the atom’s nucleus; it may also refer to the physical region or space where the electron can be calculated to be present, as defined by the particular mathematical form of the orbital.[131]

Each orbital in an atom is characterized by a unique set of values of the three quantum numbers n, l and m, which respectively correspond to the electron’s energy, angular momentum, and an angular momentum vector component, the magnetic quantum number. Each such orbital can be occupied by a maximum of two electrons, each with its own spin quantum number s. The simple names s orbital, p orbital, d orbital and f orbital refer to orbitals with angular momentum quantum number l equal to 0, 1, 2 and 3 respectively. These names, together with the value of n, are used to describe the electron configurations of atoms.

The ground state of a quantum mechanical system represents its lowest possible energy state; also known as the zero point energy of the system. By excited or vibrational state is understood any state with energy superior to that of the ground state.

If there is more than one fundamental state, it is understood that they are degenerate. According to the third principle of thermodynamics a system at absolute zero temperature is in its ground state, since its entropy is determined by the degeneracy of the ground state. Many systems, such as a perfect crystal structure, have a unique ground state, and therefore have zero entropy when they are at absolute zero –it is also possible for the state of greatest excitation to have absolute zero temperature in the systems that exhibit negative temperature–.

The ground state in physics opened the doors of quantum mechanics at the beginning of the 20th century, when the Bose Einstein Condensate was predicted; since when the atoms lose their individual identity at extremely low temperatures, it is established that the atoms are at the same quantum level. In this, as can be understood, energy is a fundamental pillar, since at very low temperatures atoms are also at their lowest energy level, while at normal temperatures atoms are at different energy levels, i.e., in an excited (vibrational) state.

Electronic and Vibrational Structure of the N_2

The developed experiments have been carried out with air, being the composition of this one of 78 % of nitrogen, 21 % of oxygen and the remaining 1 % is composed of gases such as carbon dioxide, argon, neon, helium, hydrogen, others gases and water vapor. That is why it is mainly interesting to know the spectroscopic properties of N_2. This high concentration is the result of the balance between the fixation of atmospheric nitrogen by bacterial, electrical (lightning) and chemical (industrial) action and its release through the decomposition of organic matter by bacteria or by combustion.[18]

The nitrogen atom is a chemical element with atomic number 7 and the first element of group 15 of the periodic table. [114]

Firstly, homonuclear molecules/species are composed of only one element. They may consist of several atoms, depending on the properties of the element, and some of these may have several allotropes[19].

Noble gases are exceptional cases of monoatomic molecules, because they rarely form bonds. However, most homonuclear molecules are diatomic: hydrogen (H_2), oxygen (O_2), nitrogen (N_2) and all halogens; however, not all diatomic molecules are homonuclear.[115]

- **Electronic structure:**

  The usefulness of homonuclear diatomic molecules comes from the fact that they provide an excellent basis for understanding the composition of molecular orbitals by means of combinations of atomic orbitals: wave functions superimposed linearly or constructively (union orbitals) or destructive form (antibonding orbitals),

[18] Information of this section extracted meanly from [133].

[19] **Allotrope:** each of two or more different physical forms in which an element can exist. For example, graphite, charcoal, and diamond are all allotropes of carbon.

which are governed by the symmetry of the molecule and the degree of superposition atomic. [35] Regarding atomic orbitals, they can be mixed in symmetric (σ) or antisymmetric (π) molecular orbitals under rotations with respect to the internuclear axis; and, likewise, molecular orbitals can be symmetric (g) or antisymmetric (u) under inversion with respect to the center of mass of the molecule.

The most external energy level in an atom is known as the valence band, with the electrons placed in this layer named as valence electrons. These electrons are involved mainly in the formation of bonds and in the chemical reaction with other atoms, thus being responsible for different chemical and physical properties of the element. In the case of nitrogen, as its atomic number 7, its electronic configuration is 1s2 2s2 2p3, having as valencies 1,2,+3,-3,4,5 to achieve a stable configuration with its full valence band.

In the case of nitrogen N_2, the orbitals of the 1s electrons do not overlap, however the remaining 10 valence electrons occupy molecular orbitals that are the result of the mixture of the 2s and 2p orbitals, including s-p interactions due to their proximity, as we can see in Fig. 2.18.a.

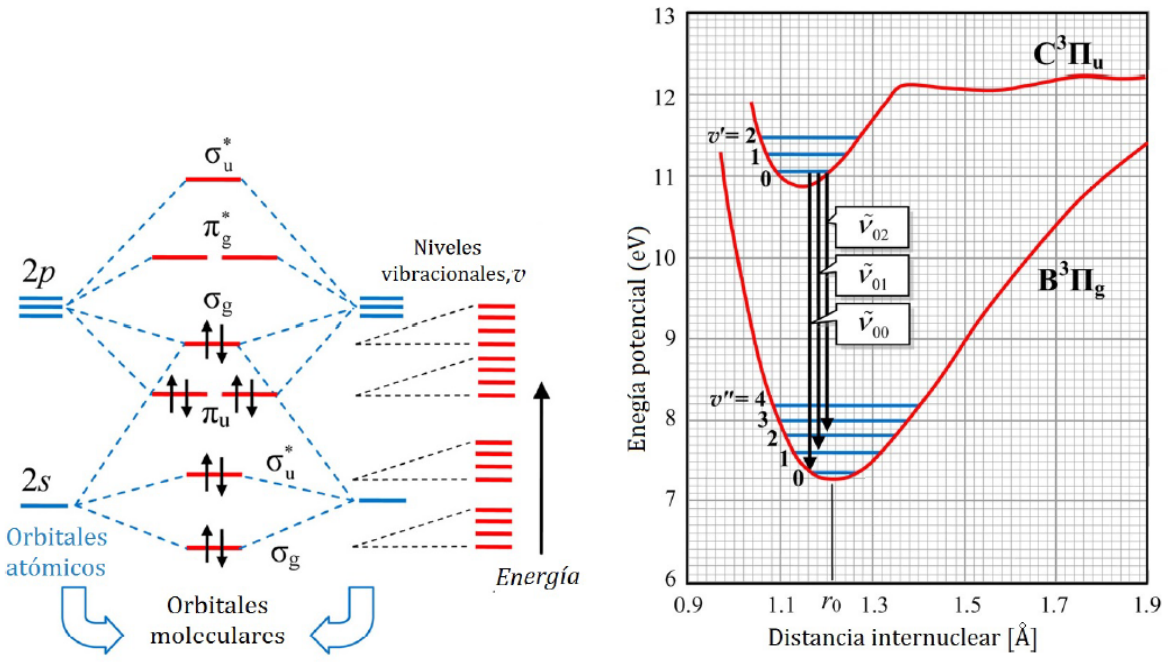

(a) Electronic configuration..

(b) Vibrational states..

figure 2.18 **Electronic and Vibrational structure of N_2 molecule.**
Regarding a), nitrogen molecules perform vibrations according to the particular occupation of the electrons in the binding or anti-binding molecular orbitals determining the length and strength of the bond. The energy levels of the corresponding quantized vibrations of the molecule, described by the vibrational quantum number of the molecule v, are superimposed on the levels of electronic energy. *Source of the image: [0]*
Respect to b), the red lines represent the curves of potential energy of the vibrational states $C^3\Pi$ and $B^3\Pi$. They are the transitions responsible for the most intense peaks that are observed in the spectrum, and which are represented with the number $\nu_{0v''}$. *Source of the image: [116]* .

- **Vibrational structure:**

  In addition, the discrete energy structure of the molecular electron can be divided in a superposed spectrum of vibrational states. Due to the fact that each electronic state is characterized by different lengths and link strengths (by different electronic distributions), the molecular oscillator will have a variety of potential energy curves associated with the different vibrational states, each with a range of vibrational levels spaced differently, organisationally represented by quantum numbers: $v = 0,1,2...$

  The designation negative and positive groups (or bands) refer to the occurrence of these bands in the negative glow or the positive column, respectively, of an electric discharge. The positive groups are due to the neutral molecule, the negative groups to the singly positively charged molecular ion.[134]

  In the present work, the Second Positive System of vibrational states of nitrogen will be studied: $C^3\Pi_u$ and $B^3\Pi_g$, whose potential energy curves are illustrated in Fig. 2.18.b.

  So, to observe the vibrational levels, the nitrogen molecule must be first excited into metastable radiative states, such as via a transition from the molecular ground state X^1R_g into $C^3\Pi_u$.

  As already explained in Section 2.2, the discharges in gases get to excite the species causing collisions between electrons and ions, and as a consequence, the species decay energetically through the emission of light forming glow discharges. If that potential difference is maintained so that the plasma self-sustains, new accelerated free electrons will be enveloped in new impacts by excitation and ionizations.

  Nitrogen is easily excited at one of its v' levels of the C $^3\Pi_u$ state. The discharge region may also contain other species of molecular nitrogen, such as positive ions (N_2^+) produced by direct electron impact ionization of the neutral molecules from the ground state $X^1\sum_g$, which is predominant in the gas. However, depending on the energy of the electron impact, the ions may be knocked into their vibrational ground state $X^2\sum_g$ (which could be later excited) or directly into an excited $B^2\sum_u$ state:

$$N_2(X,v=0)+e \rightarrow N_2^+(X,v')+2e \tag{2.36}$$

  where electron energy is higher than 15.6eV.

$$N_2(X,v=0)+e \rightarrow N_2^+(B,v')+2e \tag{2.37}$$

  where electron energy is higher than 18.5eV.

  Derived from this reasoning, the excited states will deca in a spontaneous way spawning an emission sprectrum with line intensities proportional to the population of the upper bands $N_2(C, v')$ or $N_2(B, v')$:

$$N_2^+(C,v') \rightarrow N_2(B,v'')+hv \tag{2.38}$$

$$N_2^+(B,v') \rightarrow N_2^+(X,v'')+hv \tag{2.39}$$

The vibronic radiative transitions occurring between various vibrational states of N_2 and N_2^+ will be recorded into a spectrum representing the emission bands in Section 4.2.

How to analyze the data from spectroscopy

Regarding how "to read" the nitrogen emission spectra, it is to be understood that this is a source of information about the potentials associated with the vibrational states of the molecules. Therefore, the spectrum transition characteristics must first be extracted and organized; for whose correct reading it is first necessary to know the selection rules that govern the transitions leading to the pattern of intensity peaks shown within each emission band progression.

The probability of transition between vibrational levels depends on the degree of overlap between the wave functions of two states, in addition to obvious contributions such as the electron occupancy of the level v_0 and the probability of electronic transition (which is constant for transitions within the same system, as for example, the second positive system $C^3\Pi_u \rightarrow B^3\Pi_g$). The overlap is quantified by Franck-Condon factors weighting the vibronic transition probability.

So, to identify the different head bands of the nitrogen, it has to be compared the wavelength of these results with the tabulated table included in Fig. 2.19[142], which represents the pattern that nitrogen (major molecule in an air plasma, easily excitable) always follows.

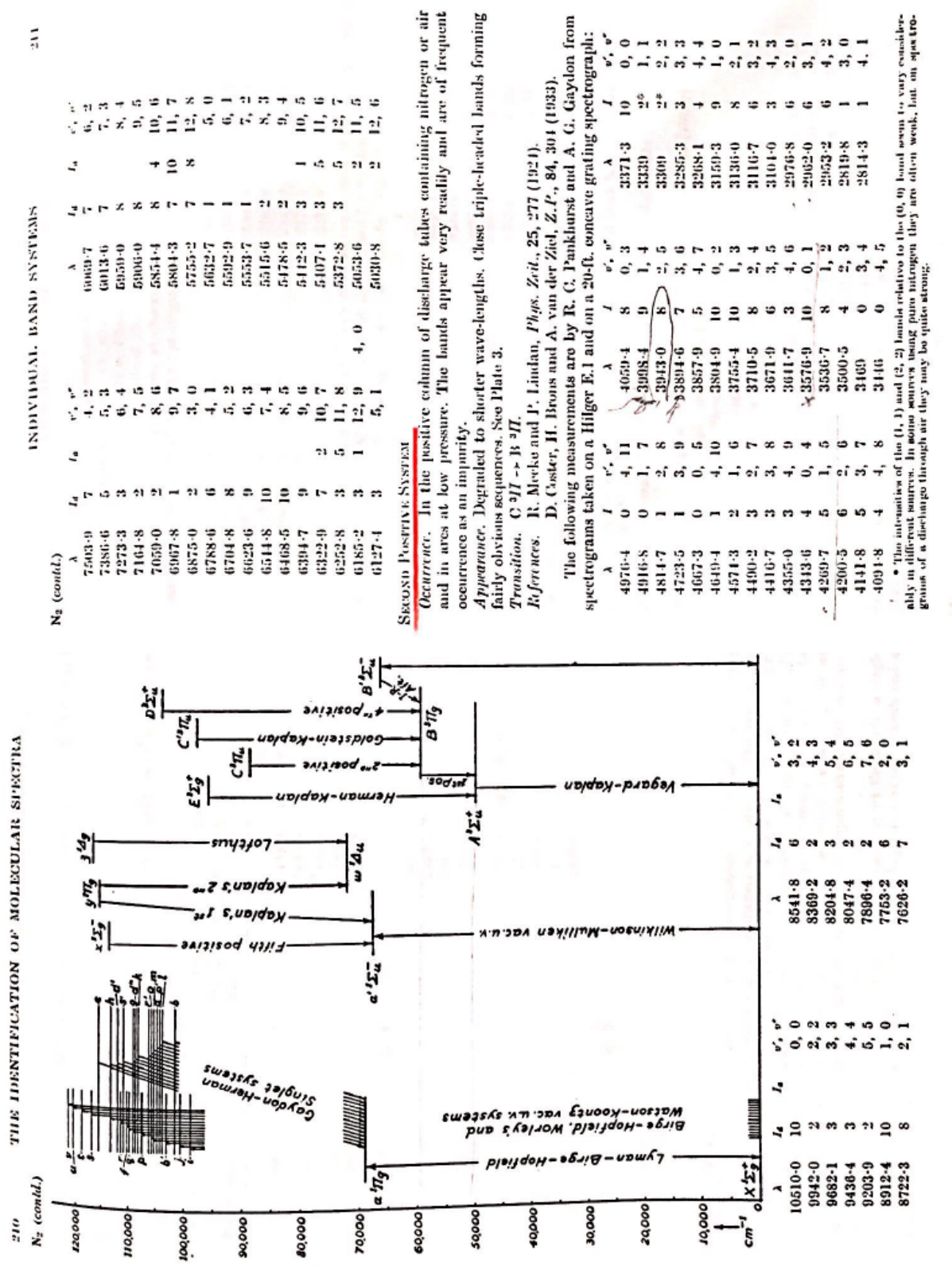

figure 2.19 **Tabulated table for Nitrogen emission spectrum for second positive system states.** *Source of the image: [142].*.

3 Design and construction of DBD plasma controllers

Different devices have been built, from which electrical and spectroscopic characterizations have been developed, in order to draw conclusions. All of them have been the result of four different phases of study, in which a series of different characteristics have been taken into account as a research subject, and whose conclusions have defined the line of action of the next phase, respectively. So, this series of devices have been designed based on the conclusions that were drawn from the previous analyzes, thus continuing with the most fruitful research line.

In this chapter, specifically in Section 3.1, are explained all the phases –and consequently, its devices– and the reasons why the different configurations were carried out; that is, the design and construction of the DBD Plasma Actuator. Each one of these devices used will be presented in order to characterize them to understand the differences between the data obtained from their analysis, which will be shown in Chapter 4. Also, in Section 3.2 and 3.3 some considerations regarding the manufacturing of the devices and about the experimentation are collected respectively, and, finally the experimental procedure and its necessary resources and considerations will be shown in Section 3.4.

3.1 Phases of the study

Four phases of study have been considered to develop this work, through which one wanted to find the most powerful and energy efficient configuration, finding the device that achieves a surface covered with plasma of greater length when it is sufficiently energized as function of the magnitudes/properties that have been studied in this project. All of them, except experiments of Phase 4, have been studied at atmospheric pressure and atmosphere in calm as general strategy. The description of these phases is presented below in the next sections.

Before presenting the mentioned enumeration of the phases, remember that the reader can go to Section 2.2.2 to know the physical characteristics of the different materials that are used in the construction of the devices. Besides, after the presentation of the different phases, in Table 3.1 all built devices are presented. Having said this, the different

phases of study are called like the following way –included in Section 3.1.1-3.1.4. –:

- **Phase 1: Basis functional study of DBD actuator with the aim of generating the largest possible amount of surface covered with plasma**
- **Phase 2: Influence of dimension of gap**
- **Phase 3: Active multi-electrode configurations**
- **Phase 4: Experimentation with airflow and reduced pressure**

The following devices included in Table 3.1 have been built, and, in general, the nomenclature used to size the devices is indicated in Fig. 3.1. The dimensions that characterize the devices built in Phase 1 and Phase 2 are detailed in Table 3.2, whose structures can be seen in the schemes contained in Fig. 3.2; dimensions of the rest are detailed in their corresponding Section.

Table 3.1 **List of experiments and its corresponding devices.**.

DEVICES				
EXPERIMENT	Substratum	Conductive	Configuration	Picture
Exp.1, Phase 1|Device 1	Quartz (SiO_2)		Type A	
Exp.2, Phase 1|Device 2	Quartz		Type B	
Exp.3, Phase 1|Device 3	Quartz	Copper (Cu)	Type C	Fig. 3.3
Exp.4, Phase 1|Device 4	lithium niobate ($LiNbO_3$)		Type A	
Exp.5, Phase 2|Device 5	Quartz		Type D, gap=5mm	
Exp.6, Phase 2|Device 6	Alumina (Al_2O_3)		Type D, gap=5mm	
Exp.7, Phase 2|Device 7	lithium niobate		Type D, gap=5mm	
Exp.8, Phase 2|Device 8	Quartz		Type D, gap=2.5mm	
Exp.9, Phase 2|Device 9	Alumina		Type D, gap=2.5mm	
Exp.10, Phase 2|Device 10	lithium niobate		Type D, gap=2.5mm	
Exp.11, Phase 2|Device 11	Quartz	Copper	Type D, gap=1mm	Fig. 3.4
Exp.12, Phase 2|Device 12	Alumina		Type D, gap=1mm	
Exp.13, Phase 2|Device 13	lithium niobate		Type D, gap=1mm	
Exp.14, Phase 2|Device 14	Quartz		Type D, gap=0mm	
Exp.15, Phase 2|Device 15	Alumina		Type D, gap=0mm	
Exp.16, Phase 2|Device 16	lithium niobate		Type D, gap=0mm	
Exp.17, Phase 3|Device 17	Quartz	TFO, Fluor tin oxide ($SnO_2 - F$)	Type E	Fig. 3.5
Exp.18, Phase 3|Device 18	Quartz	TFO	Type F	Fig. 3.5
Exp.19, Phase 3|Device 19	lithium niobate	Copper	Type G	Fig. 3.6, 3.7
Exp.20 Phase 4|Device 19	Device 19 faced with airflow			Fig. 3.8
Exp.21 Phase 4|Device 19	Device 19 at reduced pressure			Fig. 3.9

3.1.1 Phase 1: Basic functional study of DBD actuator

In this first phase it has been studied, mainly, the efficiency of different configurations of a DBD Actuator with, as explained, the aim of generating the largest possible amount of surface covered with plasma, on the dielectric layer. For this purpose, reactors with three different configurations have been powered, and in addition, the effect on two different dielectric materials has been checked: quartz (SiO_2) and lithium niobate ($LiNbO_3$).

Three types of devices (Type A, B and C –see Fig. 3.2 to know the dimensions–) have been built and powered according to the configuration of the electrodes –in all devices, has been avoided that electrodes extend to the limits of the substrate to ensure that they do not interact, creating edge effects which are not desired–. That is:

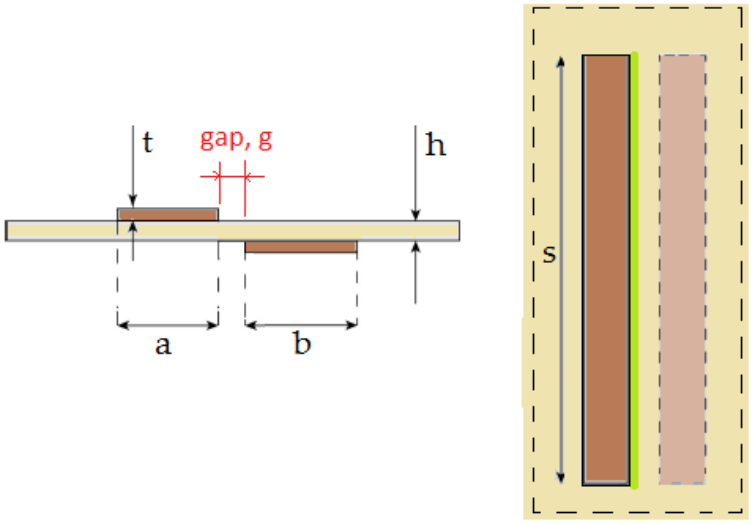

figure 3.1 **Nomenclature to size the devices.**
The green zone represents the face of the active electrode where the plasma is generated most immediately..

Table 3.2 **Dimensions of devices of Phase 1 and 2.** Thickness of the dielectric discs used (*h*) are, respectively for lithium niobate, quartz and alumina: 1mm, 1mm and 2mm. The values belong to the same order of magnitude, and their influence on the discharge has not been studied, however the influence is not believed to be significant, as it does not affect the conclusions of the trend included in this paper..

DIMENSIONS OF DEVICE CONFIGURATIONS							
Electrode material, thickness (*t*)	Copper, 0.025mm						
Configuration type	**Type A**		**Type B**	**Type C**	**Type D**		
Width of the exposed electrode(s) (*a*)	12mm	12mm	10mm	10mm,	10mm	10mm	10mm
Width of the encapsulated electrode (*b*)	R>9cm	R>9cm	R>9cm	R>9cm	10mm	10mm	10mm
Gap (*g*)	-	-	5mm	5mm	5mm,2.5mm,1mm,0mm		
Length of discharge zone (*s*)	>7cm	>7cm	6.5cm	6.5cm	7cm	7cm	7cm
Dielectric material	Quartz	lithium niobate	Quartz	Quartz	Quartz	lithium niobate	Alumina

Type A: Device with a single active electrode, located on the upper face of the substrate, centered and shaped like a rectangular strip, and the ground electrode under the circle-shaped substrate that occupies practically the entire surface –see Fig. 3.2.a–.

The objective of this configuration is, fundamentally, to verify that the discharge causes the generation of plasma around the active electrode, observing the characteristics of the same depending on the dimension of the different magnitudes that determine the energization chosen to apply to the device during the experiment.

Type B: Device with three electrodes in the form of rectangular bands on the upper face of the substrate, of which the two external bands are active and the center is a ground electrode, and a single ground electrode, with a circular shape, at the bottom of the substrate as the Type A configuration –see Fig. 3.2.b–.

The purpose of this device is to try to cover the space between the different electrodes of the upper face of the substrate, in the form of "bridges" between them. In the beginning it was decided that the electrode of the

medium should be grounded to avoid a possible short circuit.

Type C: Same configuration as Type B, but in this case the three electrodes of the upper face are active –see Fig. 3.2.c–.

The objective is the same as Type B, but trying to see if the fact that there are three active electrodes does not cause incidents, besides seeing if it maximizes the sought effect of plasma "bridges".

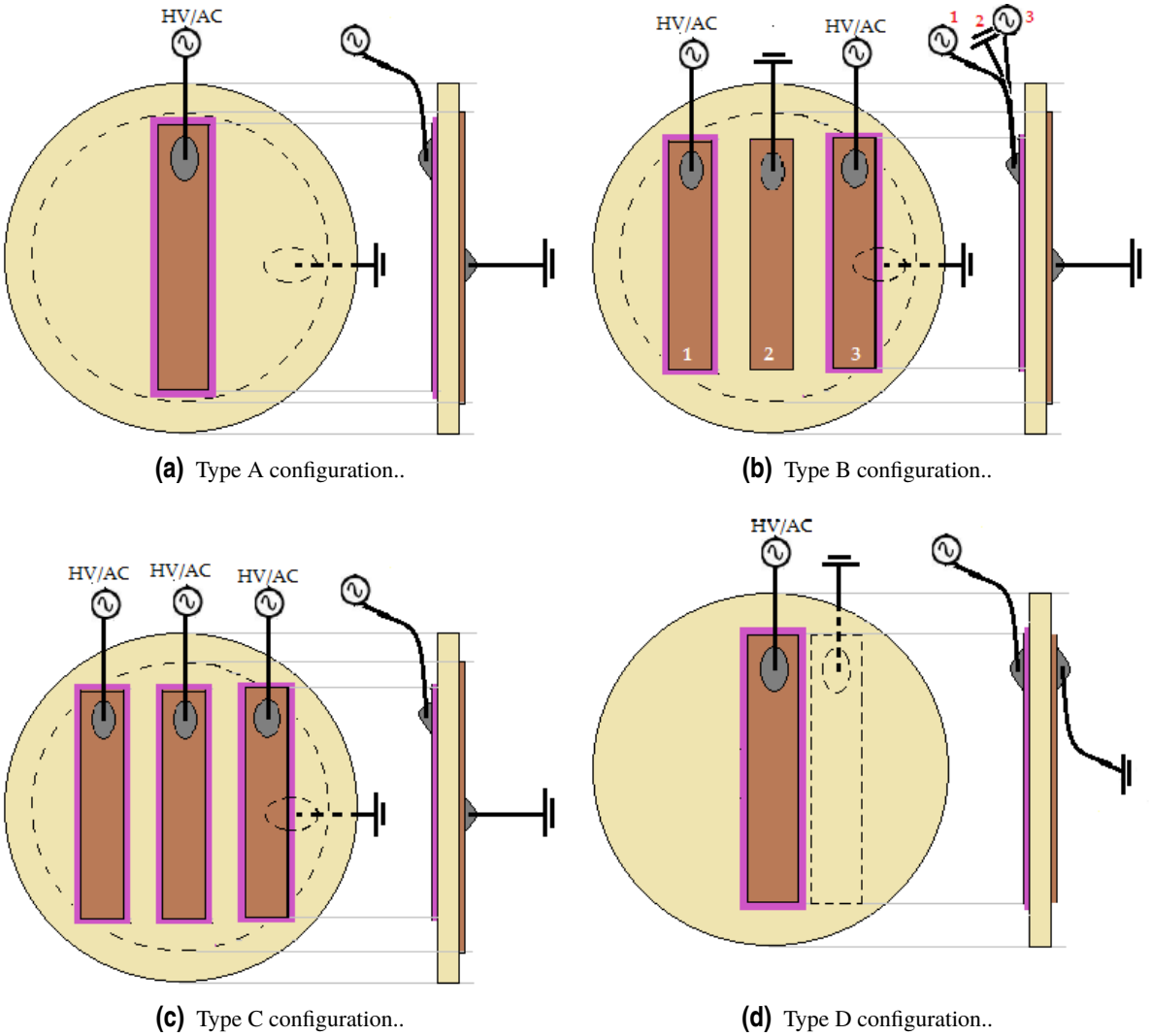

(a) Type A configuration..

(b) Type B configuration..

(c) Type C configuration..

(d) Type D configuration..

figure 3.2 **Phase 1 and 2: Type A, B, C and D DBD Plasma controller configurations.**.

Type A construction has been developed on both quartz and lithium niobate, as dielectric substrates, while configurations type B and C have been tested only on quartz. In Fig. 3.3 one can see real pictures of the devices.

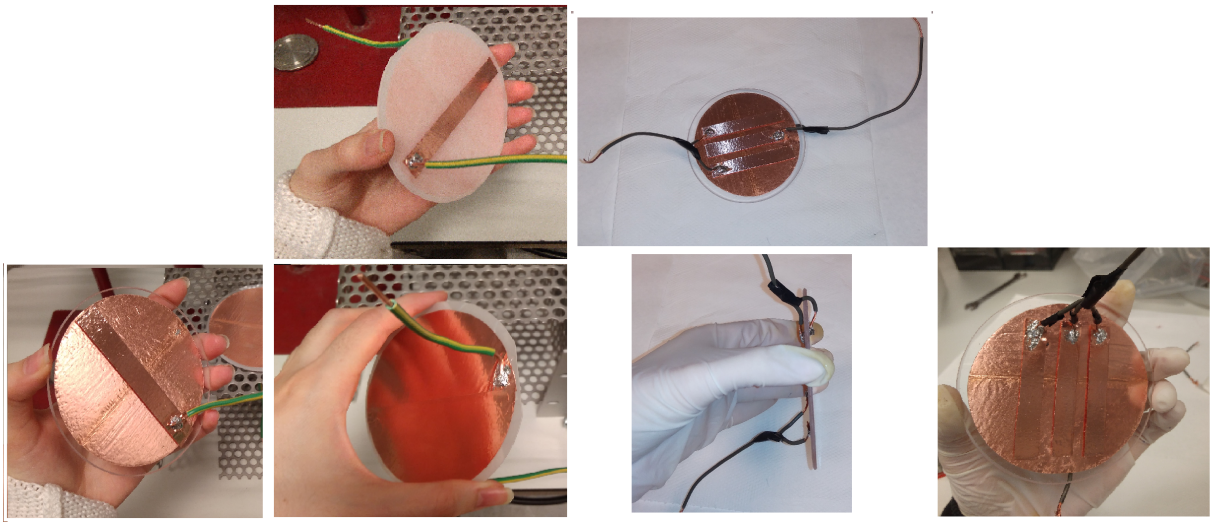

(a) **Device 1**: Type A, quartz..

(b) **Device 2**: Type A, lithium niobate..

(c) **Device 3**: Type B, quartz..

(d) **Device 4**: Type C, quartz..

figure 3.3 **Phase 1: Real pictures of the devices.**.

3.1.2 Phase 2: Influence of dimension of gap

To this goal, reactors that have been electrically fed they share the same configuration regarding: shape, number and function of the electrodes used, composed of an active electrode with a narrow band on the upper face and another with the same characteristics on the lower/overleaf face but in this case connected to ground, called Type D –see Fig. 3.2–, both developed with adhesive copper films superimposed on the surface of the substrate. This configuration of electrodes has been mounted on 3 different types of substrates, thus having 3 different device species, to which size of the gap between both electrodes has been varied. For each device, 4 measurements have been made according to the gap: 5 mm, 2.5 mm, 1 mm and canceling the gap. The substrates used were: quartz (SiO_2), alumina (Al_2O_3) and lithium niobate ($LiNbO_3$). Real pictures of some devices are in Fig. 3.4.

3.1.3 Phase 3: Active multi-electrode configurations

Phase 3 is presented as an evolution of phase 2. In it, active multi-electrode configurations are studied, as a result of a series of type D configurations adjacent to each other, that is, alternating conductive and insulating bands.

In this sense, the schematized band structures developed are shown in Fig. 3.5 (Type E, F configurations) and 3.7 (Type G configuration), since three tests were carried out. Configurations E and F were developed on quartz crystals that previously had a TFO transparent conductive oxide deposition ($SnO_2 - F$, Fluor tin oxide) on one of its surfaces, several microns thick; so that certain areas –see Fig. 3.6– of the surface have been sanded to eliminate all the conductive coating and thus achieve the structure of alternating conductive-insulator bands on said face, being this face the active electrodes side. For the ground electrode, two different geometries have been used by

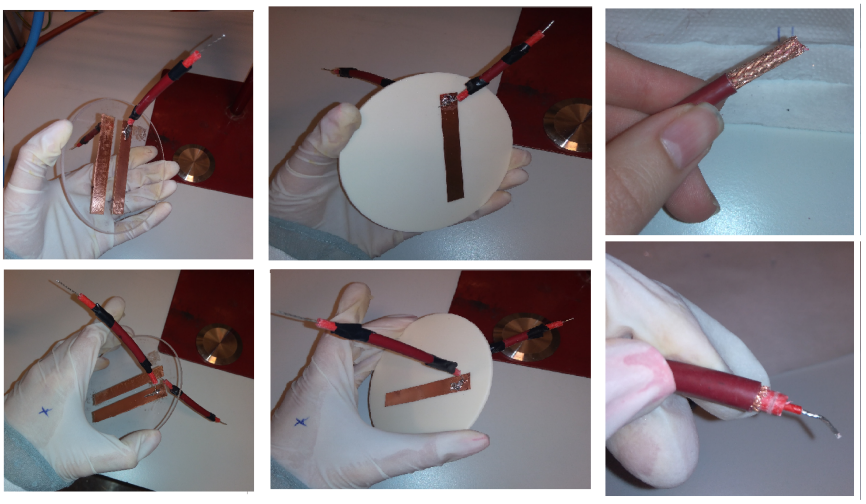

(a) **Device 5**: Type D, quartz, gap=5mm..

(b) **Device 6**: Type D, alumina, gap=5mm..

(c) High voltage cable used..

figure 3.4 **Phase 2: Real pictures of some devices.**.

placing the copper used in the previous devices on the lower face of the glass: one of them simply corresponds to covering practically the entire back surface (without reaching the limits to avoid edge effects) and the second, more meticulous, places ground electrode bands coinciding in a top view with the insulating bands that were left uncovered in the top surface after sanding the material.

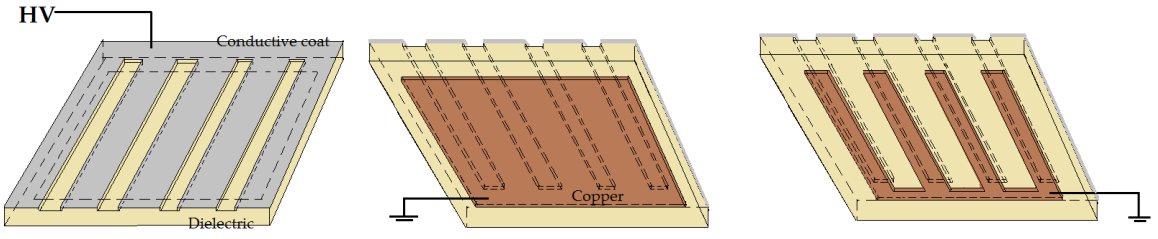

(a) Type E configuration..

(b) Type F configuration (underside)..

figure 3.5 **Phase 3: Type E and F DBD Plasma controller configurations.** Grey zone corresponds to active TFO electrodes (common for E and F), and the other two schemes represent the back face, connected to ground..

Regarding the G configuration, after the success of the previous experiment –that is, the number 18 that has the type F configuration on quartz with conductive coating–, it was proposed to advance in this proposal but being developed with a substrate-material with more power in the discharge and with a more sensitive configuration. The experiment number 19 was developed on lithium niobate since it has been the material that has provided the best results, as will be explained in Chapter 4. The same concept of geometry of the electrodes used in type F has been implemented, but decreasing both the width of each conductive band and the strips that remain uncovered between each pair of electrodes. In particular, a common width of 1mm has been used for each division. Again, electrodes have been made in copper and the active electrodes have been placed on the unpolished face of the lithium niobate

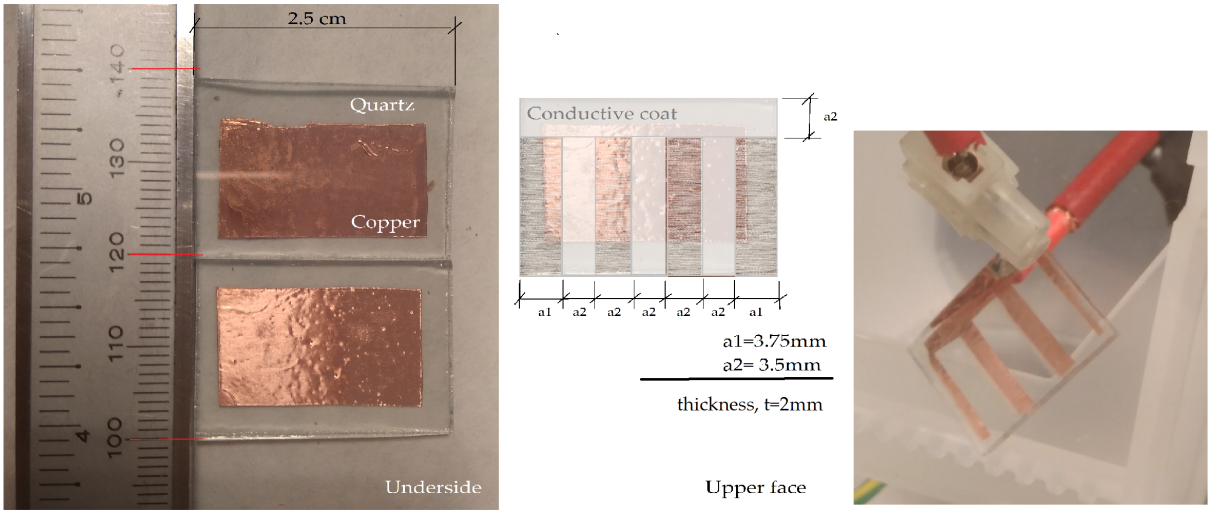

(a) Device 17..

(b) Device 18..

figure 3.6 Phase 3: Real pictures of devices E and F..

disc. In Fig. 3.7 pictures of the real device and information about its geometry are shown.

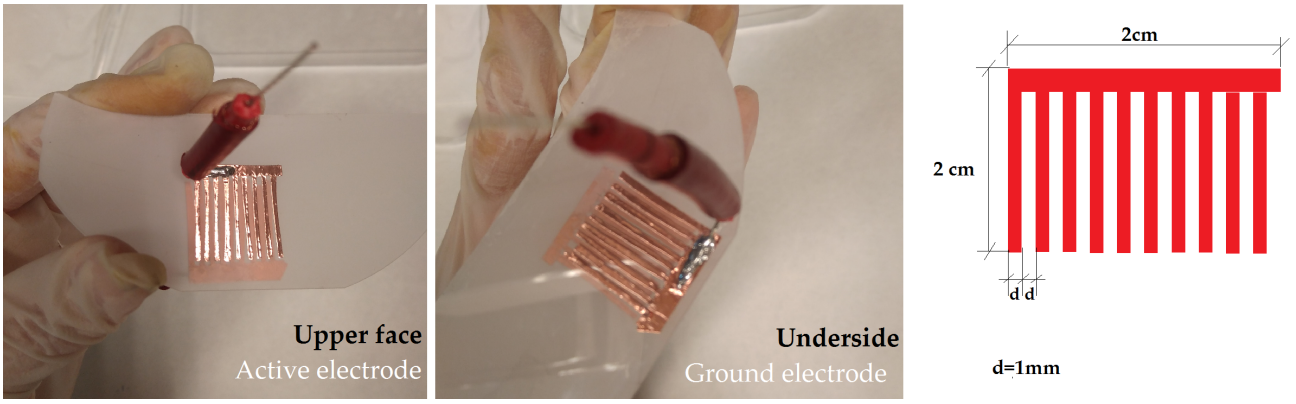

figure 3.7 Phase 3: Real pictures of device G..

3.1.4 Phase 4: Experimentation in airflow and at reduced pressure

In this phase, two experiments were carried out. First, in experiment 20, the DBD plasma actuator has been faced with a surface current of air with the plasma already generated, to test what effect the current has on the covered plasma surface as to whether the flow displaces or extends it, as well as to observe the variation in its direction that the current experiences as a result of the effect of the plasma exerts on it. The assemblage needed for the experiment that has been used is showed in Fig. 3.8. The experiment was executed at 13 kHz and 3 kV_{pp}, however it was not possible for a naked eye to perceive the effect of the current on the generated plasma due to the small order of magnitude of the lit area and the limited capacity of the device that generates the current.

Regarding the second goal of this phase, whose observation would be interesting, it would have been convenient to

develop a smoke chamber to be able to visualize the variation of the streamlines disturbed by the actuator; however, the existing safety requirements of the laboratory did not allow this type of experiment to be carried out with the means we had.

In Appendix B are included evidences as a result of this type of experiments that have been published in other studies.

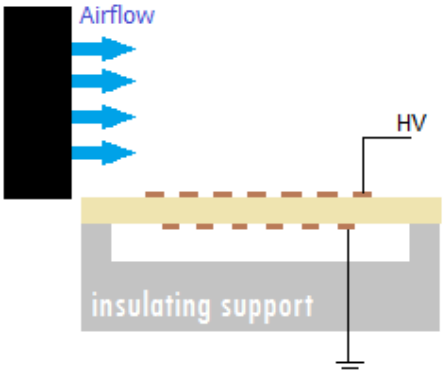

figure 3.8 **Phase 4: Scheme of experiment 20, over device 19.**.

Respect to experiment 21, correspond to device used in experiment 19 but being tested at reduced pressure (as a usual flight situation for an aircraft) inside a specific reactor, always in atmosphere in calm. The effect of the pressure on the ignition voltage and current was studied, and for that It was taken for measures: at 988 mbar (corresponding to the pressure in the laboratory[1], in order to compare this result with the result obtained in experiment 19), at 667 mbar(corresponding to 11000 ft approximately), at 301 mbar (corresponding to 30000 ft approximately) and 20 mbar. All of the measures were saved at 5 kHz of frequency because it correspond to optimum frequency, as it can be read in the section of electrical analysis results. In the Fig. 3.9 it can be seen how and where the device was placed for the development of the experiment. The spheric camera is marketed by Kurt J. Lesker Company.

[1] Possible discrepancies justified by the calibration of the high pressure meter.

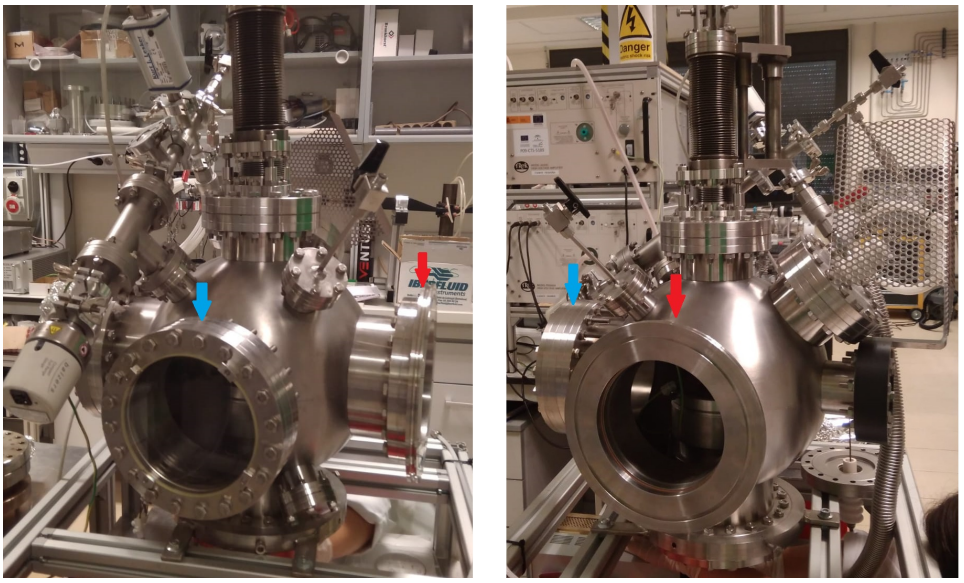

(a) Different views of the reactor..

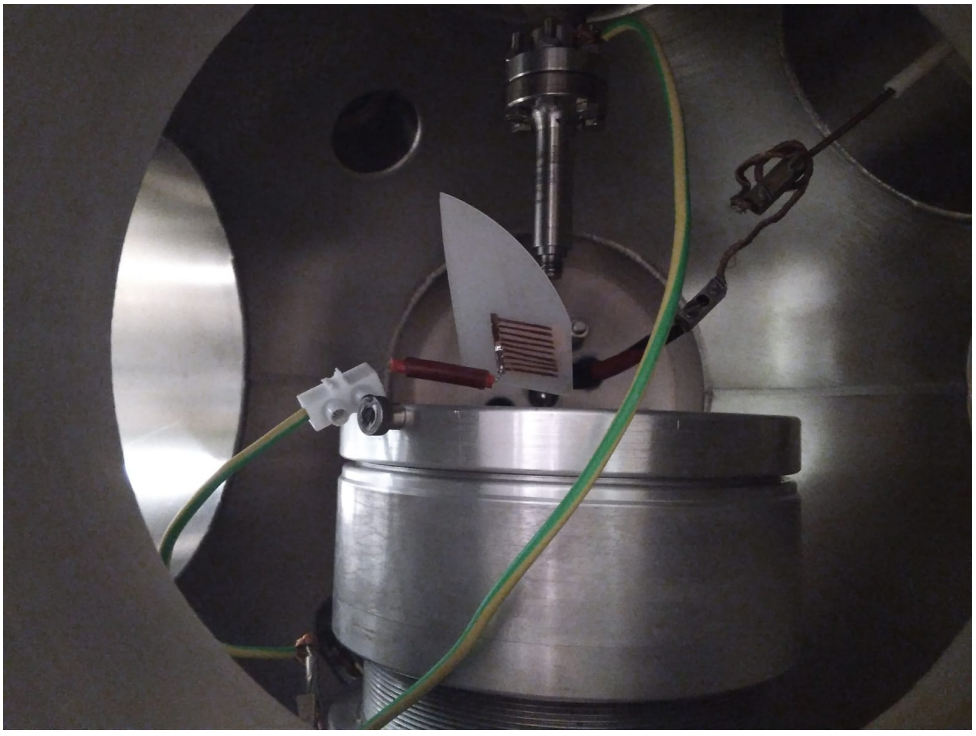

(b) Device mounted in the inner chamber of the reactor..

figure 3.9 **Experiment 21 (Phase 4): Device 19 at reduced pressure.**.

3.2 Notes about manufacturing

1. To manufacture the electrodes, the copper used corresponds to adhesive tapes by one of its faces of low thickness..
2. The cables used to make the connections have been soldered to the copper with tin. Depending on the fragility

of the dielectric, it may or may not be welded on the copper once it is already adhered to the dielectric to avoid damage; since, for example, the first time I worked on the lithium niobate, it could not withstand the thermal shock when this was done, breaking the disc and having to be replaced, so after this incident the welding was carried out on the copper prior to its assembly on these discs in question.

3. Not all the cables used have been of the same type. Within Phase 1, for the Type A device, common grounding wires were used for both electrodes, while for Type B and C devices, thinner cables were used. For Phase 2, specific cables for high voltage have been used –see Fig. 3.4.c–.
4. As I was progressing in the construction of the devices, I tried to achieve smaller welds, so that the area of contact with the high voltage was smaller, and interfere, as a result, as little as possible in the ignition of the plasma.
5. In general, the substrate discs have been reused for the different experiments.
6. The dimensions of the discs have not been strictly taken into account, since they did not necessarily have to be the same in all the materials, since this aspect did not affect the experiment.
7. The discs of dielectric material in the laboratory all have the same surface finish on both sides, with the exception of lithium niobate, in which one of the faces is polished and the other is not; for this reason, the active electrode has always been placed on the unpolished surface. Regarding the quartz discs, both faces are polished, while in alumina none of them is, although the roughness is minimal and comparable to the unpolished face of the lithium niobate discs.
8. Ground electrode is not embedded in the substrate, but adhered to the underside of the disc.
9. The electrodes never extend to the edge of the dielectric to avoid unwanted edge effects.
10. Related to nomenclature aspects, when one talks about the upper face of the substrate it refers to the face where the active electrodes are located, while the lower face or underside is the face where only the ground connection is located.

3.3 Considerations regarding the experiments

1. The generated plasma emits fluorescent light of violet color due to nitrogen mainly.

2. *Regarding how to recognize/establish the breakdown point* in which to save measures, a visual criterion has been applied to perceive a significant level of luminosity, this being the minimum to which I can perfectly perceive the discharge lines between the active electrode and the substrate if I observe the disc in profile (that is, facing the vision to the thickness of the device), since it is more difficult to try to be exact in said recognition if I observe the disc in plant (from above), especially the less translucent is the substrate material.

   It has to be commented that due to the existence of concentrators such as the corners of the electrodes, the welding zone to the high voltage cables, the possible irregularities and roughnesses that the copper film presents, fruits of the construction of the device, or the degradation of the adhesive that keeps the electrodes adhered to the discs either by overheating or by drying them during the time they remain inactive stored in the laboratory, these elements constitute uniformities in the electrodes that affect the way in which the current is distributed over them , as well as, consequently, the moment in which the plasma appears around each local point of the perimeter of the electrodes. Consequently, in all experiments it is common that approximately half a kilovolt –at least– before the breakdown point considered by my criteria, plasma appeared in very localized points of the electrodes progressively, as are the corners mentioned above. That is why these previous appearances have not been considered representative of the phenomenon studied, and were taken simply as a reference (although observed at all times to analyze its repercussion). The breakdown point was considered when a significant part of the contour was turned on, and when said parameter was repeated throughout the experiment, but logically said pattern is not the same for each configuration, but a level considered equivalent.

   In some cases this critic level corresponded almost instantaneously to practically the whole contour, but in other occasions, if one waited for the contour to fill up, there were large areas that remained long (from a relative perspective) time on, reaching greater luminosity; for what was the appreciable ignition of these concrete areas, whenever their extension was significant, the one considered as point of ignition.

   It was also thought that perhaps a finer design of the electrodes would improve the uniformity in the generation of the plasma.

   It is useful to cover the methacrylate box with an opaque material so that the reactor remains dark in the viewing angle and the discharge is easily noticeable at its minimum level of light intensity. The atmosphere of the room should be as dark as possible.This fact adds a certain degree of subjectivity to the experiment since it is not possible to maintain an ambience in the laboratory completely without light.

   Derived from the above considerations, the most complex measure to determine, for me, has always been the first one at a frequency of 1 kHz.

3. *The experiment generates ozone*, so precautions must be taken to divert this flow as much as possible and thus aspire as little as possible.

4. Due to the ionization of the gas, *there is emission of sound from the experiments from a certain level of charging*, especially intense and acute in the case of experiments with lithium niobate, but this aspect has not been considered as a useful reference as measuring tool.

5. The heating of the disc or level of polarization achieved can influence the breakdown point of the experiments when it remains energized for a long time, since the experiments extend at least one hour. That is why *the experiments should be done with the maximum agility possible.* At least, while the plasma is active, the process of discharge the device must also be slow, progressively decreasing the polarization, avoiding forcing the crystalline network of the substrate.

6. *Prior to starting each study* at a certain frequency, the device must be electrically discharged. That is why after loading the reactor for each measurement, *it must be completely discharged. The charging process must be done at a moderate speed* (with a sensitivity level in the ascent of the order of ten volts, minimum), taking care that the substrates do not suffer damage or short circuits.

7. For the development of experiments at reduced pressure it was necessary to take special care in opening the air inlet valve of the camera between experiments, to clean the atmosphere in which they were carried out, and thus avoid an atmosphere enriched in ozone.

3.4 Experimental Procedure

The performance of the process was analyzed by varying both the input voltage, $V(t)$, and the characteristic frequency, f. The experimental system used for the **electrical characterization** is showed in Fig. 3.10: a function generator (Stanford Reserach System, Model DS345) and a high voltage generator (Trek, Model 20/20 C) have been needed to power the controller, and as a reader of voltage and current signals in time, $V(t)$ e $I(t)$ respectively, an oscilloscope (Agilent Technologies Oscilloscope DSO X 3024A) was used. The DBD controller is inserted in a methacrylate box to carry out the experiments as a safety measure. Likewise, this is usually covered so that the external light of the ambient does not penetrate into the cavity and the plasma and, more specifically, the breakdown point can be appreciated (since although the discharge is perceptible to the naked eye, the necessary conditions to appreciate it in detail require an atmosphere of darkness, for which the laboratory ambience was adapted closing all possible light sources although this can not be total), moment in which the measures are saved –see Fig. 3.11–.

For the case of the experiments under reduced pressure, these were carried out inside the spheric camera which can be seen in the Fig. 3.9, marketed by Kurt J. Lesker Company.

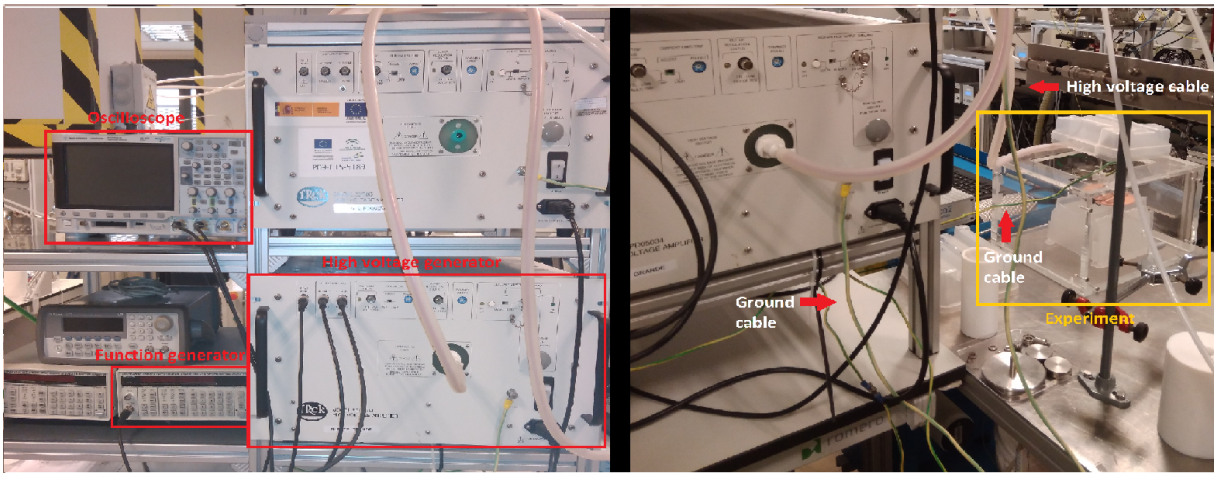

figure 3.10 **Experimental system for electrical characterization.** A function generator (Stanford Reserach System, Model DS345) and a high voltage generator (Trek, Model 20/20 C) have been needed to power the controller, and as a reader of voltage and current signals in time, $V(t)$ e $I(t)$ respectively, an oscilloscope (Agilent Technologies Oscilloscope DSO X 3024A) was used..

Following with the typical performance values of the DBD controllers –see page 32, Fig. 2.2– we have worked in a range of frequencies of 1-15 kHz taking measurements of each unit of kHz, this is, 15 measurements for each device; with a sinusoidal signal with offset and phase both null. Thus studying the influence of frequency on the electrical results of the experiments.

Considerations to take into account for the visual recognition of the breakdown point during the experiment –see Fig. 3.11 to check these tips–:

1. Ensure that the monochromator remains in a stable position and correctly pointing to the target.
2. Guarantee dark ambient, especially important to perform the spectroscopic analysis. We try to keep the

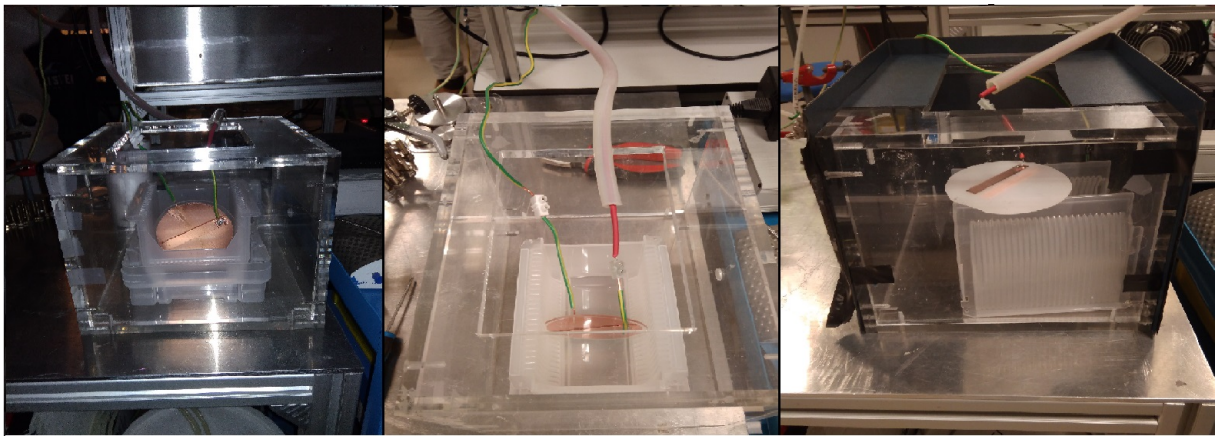

(a) Plasma off..

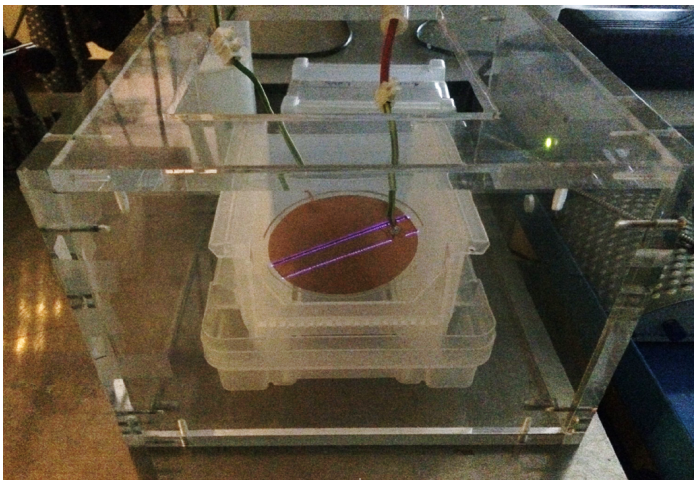

(b) Plasma on..

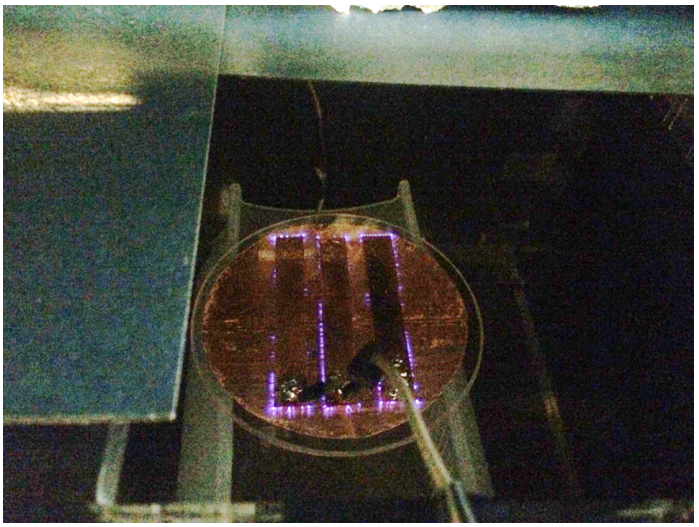

(c) Plasma on..

figure 3.11 **DBD reactor connected for the experiment in different positions.** Pictures taken in different experiments to appreciate the way in which the box was covered (in the image it is partially covered).
Likewise, the relative position occupied by the reactor inside the box is indifferent to the experiment, this depends in each case of the place where the connection cables have been placed, or the size of the device, always trying to find the more comfortable and stable position, which guarantees the correct execution of the experiment and for visual recognition of the breakdown point.
The two images starting on the left correspond to one of the experiments performed on a Type A device mounted on quartz, while the first starting on the right is a Type D configuration on lithium niobate..

laboratory dark during the experiment, using an opaque and insulating cover on the methacrylate box if necessary.

3. Position the device so that the active electrode is always visible, as well as orientate it so that the area where the plasma is most immediately generated is in front of the observer; this is, in the case of Type D devices, around the face of the active electrode that is closest to the ground electrode, from a plan view, indicated in green in Fig. 3.1.

4. Ensure that the field of vision has access to a perspective of the profile of the device in the thickness direction, so that the start of the generated discharges can be appreciated more easily, when these are not of great intensity. Especially in less translucent devices, where it is more complicated to perceive said point of ignition of the plasma.

5. One must ensure the stability of all the elements involved in each experiment, both to ensure the general safety of the experiments, and to ensure that the spectroscopy is done correctly.

Different insulating support structures have been used (not designed for this purpose but that already existed previously in the laboratory for uses unrelated to this application), to facilitate locating the device in the way that best suited each occasion based on these conditions and of the geometry of each device, as can be seen inside the methacrylate box.

Regarding the **emission optical spectroscopy** carried out in some of the experiments that have been carried out, this test was developed with a Jobin-Yvon FHR640 monochromator[2]. Respect to the resolution of the measures saved, the spectroscopy was carried out at three different levels of resolution, whose results and argumentation are reflected in Section 4.2. The degree of precision of measurement of the spectroscopy depends mainly on the configuration of these parameters, as well as on the calibration of the equipment; as well as it is recommended to do a background spectroscopy to ensure that the only thing that is captured is noise or identify possible elements that are foreign to the plasma that will later be measured –see Fig. 3.12–. For measures referred to quartz-device number 3 and lithium-niobate-device number 16 was used a diffraction network centered at 330nm and with a density of lines in the network of 1201lines/mm. The opening/gap of the entrance and exit slits was 1mm; the resolution of the monochromator (step value, i.e., how much interval in wavelength a point is referred to) was 0.5nm and the integration time was 0.5 s. For spectroscopy of lithium-niobate-device number 19 to measure the general spectra, the values were:

- Slit in, slit out: 1 mm
- Step: 0.5 nm
- Integration time: 0.5 s

[2] A **monochromator** is an optical device that transmits a mechanically selectable narrow band of wavelengths of light or other radiation chosen from a wider range of wavelengths available at the input.

and finally, with high-resolution for the 360-390λ interval (to have accurately values for calculating vibrational temperature), for the five measures of device 19 depending of voltage those parameters were:

- Slit in, slit out: 0.5 mm
- Step: 0.2 nm
- Integration time: 0.5 s

To perform the spectroscopic measurements, the different devices were placed inside a dark chamber, for this purpose it was ensured that the methacrylate box in which the experiments were developed was completely covered with opaque material. In this way it is ensured that the optical measurements of the discharge were not disturbed by external signals. It was made use of a fiber optic cable connected to the monochromator specified above; The monochromator is responsible for digitizing the signals collected with the fiber. Subsequently, using the OriginPro software, the spectroscopic graphics were represented.

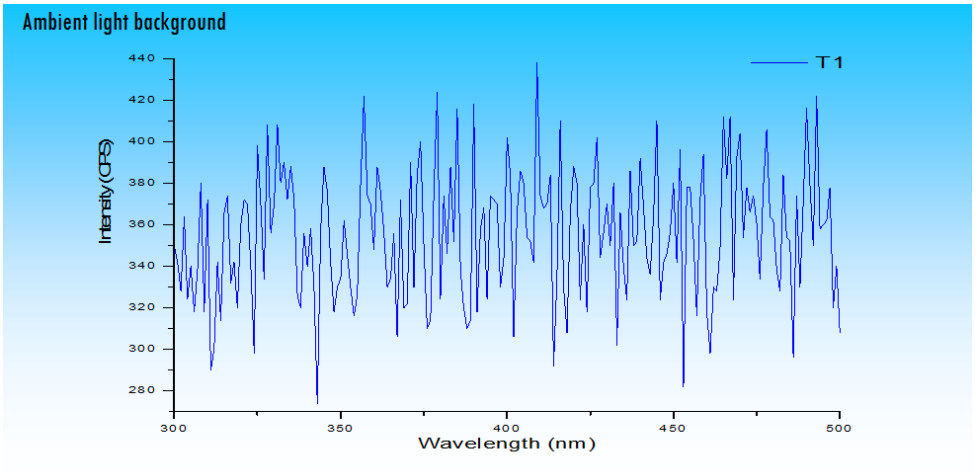

figure 3.12 **Background spectroscopy.**.

4 Analysis of the results

The oscilloscope provides two output files that contain, respectively, the discretization of the Voltage $V(t)$ and Current $I(t)$ signals at the point of choice, for as many periods as indicated on the screen at the time of saving the data. From these data, Matlab has been used to convert them to international system measurement units, treat them and obtain other significant electrical magnitudes for the experiment, and finally the output files of said data processing have been open with OriginPro, a computer program for interactive scientific graphing and data analysis produced by OriginLab Corporation, through which to build the different graphs that are shown in the document.

In this chapter, the results and conclusions of the electrical and spectroscopic characterization are presented, respectively in Section 4.1 and 4.2 –it is remembered that Table 3.1 contains an index of experiments classified by phase of study, with the main characteristics of the devices–. Finally, in Section 4.3, some things to keep in mind about the materials during the experiments was collected.

Reminding that for **electrical analysis** the measures were saved at appreciable ignition point of plasma for each selected frequency (from 1 kHz to 15 kHz). Even though an exhaustive comparative analysis of all the experiments has been carried out, in the report will show only a representative sample of them, to avoid an extremely long report. These results will be exposed differentiating by operational parameter.

In reference to the **spectroscopic analysis**, the obtained results will be exposed in the Section 4.2. These data, unlike the electrical analysis, do not necessarily had to be recorded at the point of ignition of the plasma, but at a level in which sufficient luminosity is guaranteed so that the spectroscopy can be successfully developed.

All the measures have been saved averaged and without averaging; however, for the data processing, averaged outputs have been used whenever possible. Likewise, a smoothing of said outputs has been used (through the function of matlab *smooth()*). It is recommended to see the content of Fig. 4.1 and 4.2.

It is recalled that the fact of using alternating current (AC) allows to work continuously charging and discharging the dielectric successively. According to [125], the discharge current is composed by the displacement current and conduction current, where the magnitude of the latter is smaller than that of the former in the test. Meanwhile,

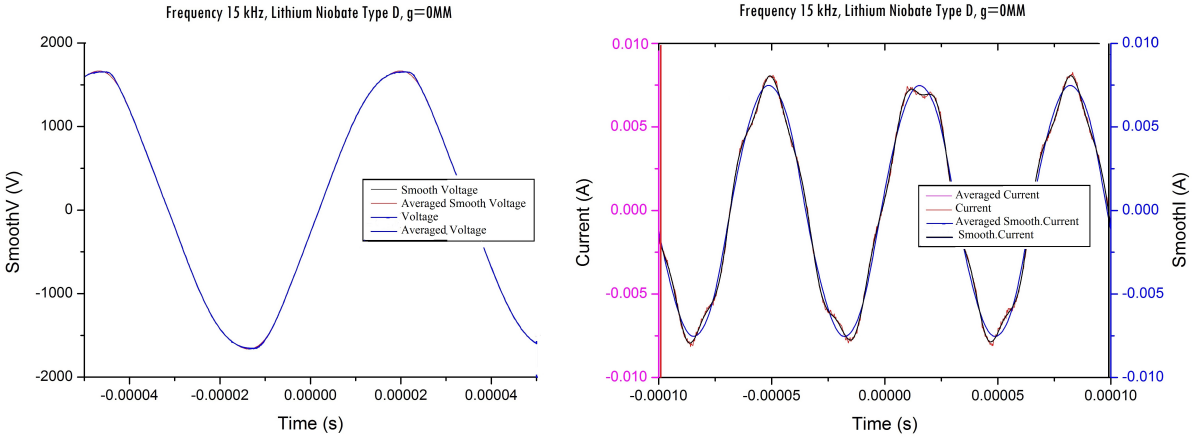

figure 4.1 **Some aspects about comparison between Voltage and Current signals I.**
Comparison of measures smoothed, averaged and without averaging. As the frequency increases, the differences decrease; but always differences are more significant for the current signal than for the voltage signal.
Table 3.1 contains an index of experiments. .

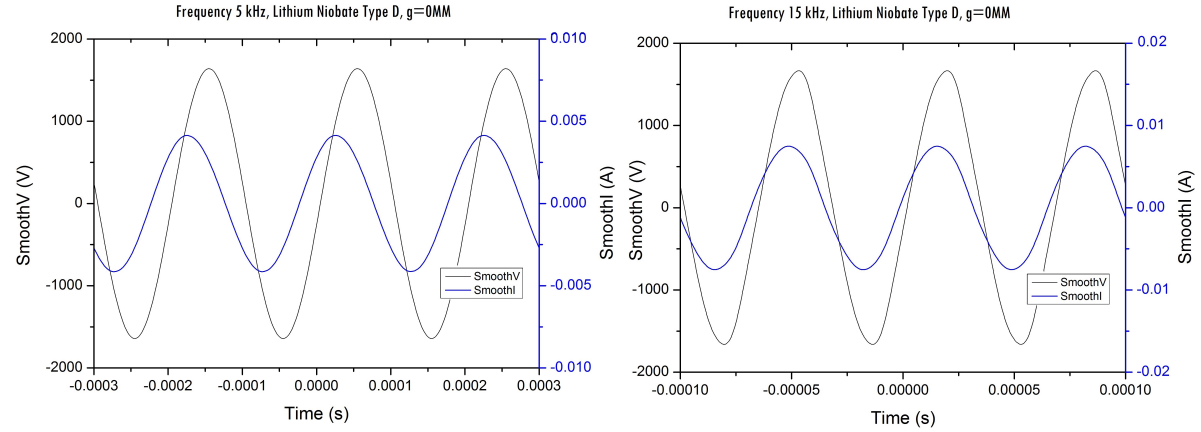

figure 4.2 **Some aspects about comparison between Voltage and Current signals I.**
Offset between $V(t)$ and $I(t)$, and variation by frequency increase.
Table 3.1 contains an index of experiments. .

intensity of the discharge is stronger during the positive half-cycle. The current leads the voltage by 90, performing a typical characteristic of the capacitive discharge.

During these experiments, the current signal does not suffer large deformations due to the characteristics of the dielectric, obtaining a more homogeneous discharge than in another bibliography –see Fig. 4.3.a–, being in our case the filaments of the current signal very small. Likewise, in these experiments there is no noise in the signal either. However, it was appreciated that the greater the efficiency of the device, the faster its shape varies, tending to get square-form. This was most noticeable especially when the experiments were carried out under reduced pressure on the multi-band configuration on lithium niobate (device 19, Experiment 21). It is recommended to see Fig. 4.3.b to verify this affirmation.

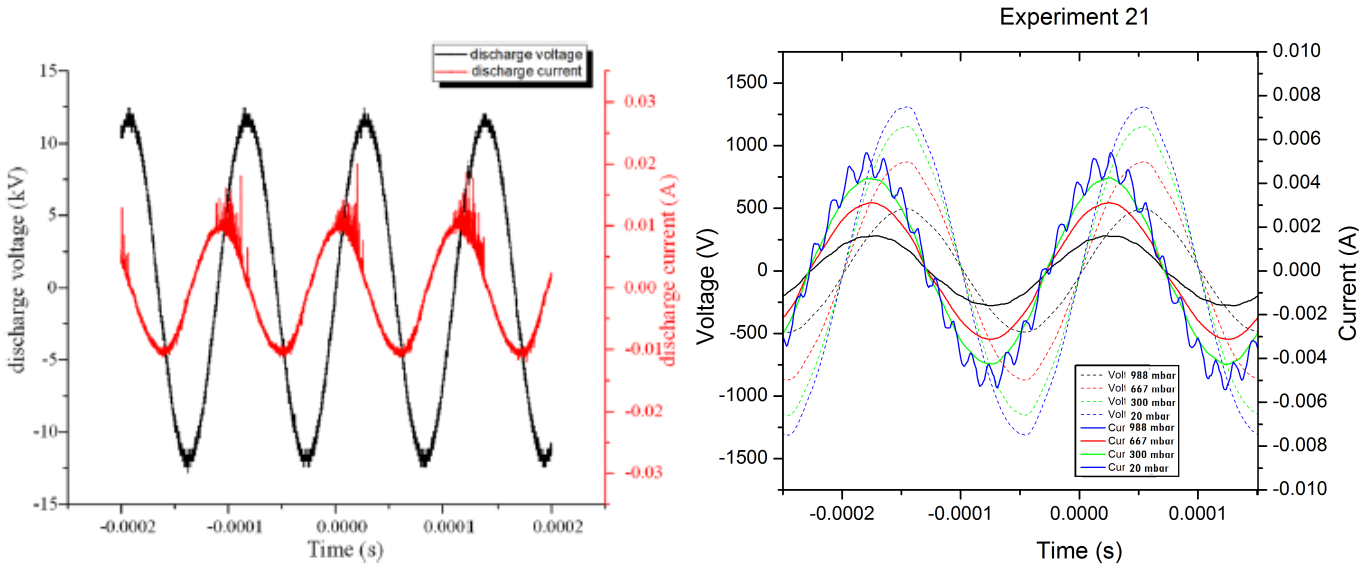

(a) Typical waveforms of discharge voltage and current. Source of the image: [125]..

(b) Comparison of deformation of Current signal by generation of plasma in different experiments..

figure 4.3 **Informtation about deformation of the Current signal.**
Table 3.1 contains an index of the experiments carried out..

4.1 Electrical analysis results

First of all, there is a section that includes a summary of the events that took place during the testing of the different devices –Section 4.1–; and after that, the results of the analysis of the obtained data can be found in the Section 4.1. Have been analyzed the following parameters/representations –they are duly explained in Section 2.3–:

- ***Lissajous curves***[1] depending on the frequency f of the signal. This includes the representation of Current $I(t)$ versus Voltage $V(t)$, but the representation of Charge $Q(t)$[2] versus Voltage $V(t)$ can also be included in this category of Lissajous figures, which provides Averaged Power $\overline{P}$ data directly due to the relation respect to its enclosed area –see equation 2.21–.
- ***Representation of significant values*** as ($V_{pp}, I_{pp}, V_{rms}, I_{rms}, \overline{P}, Q_0, Z_{real}, Z_{imag}, cos\ \phi, \phi$) have been analyzed for each experiment, to obtain results in function of operational parameters as frequency, pressure and electrode geometrical configuration, and by dielectric material.

At the end of the chapter, in Section 4.1 there is a summary table with the main results, included in Table 4.2.

4.1.1 Comments about the experiments

1. **PHASE 1: BASIC FUNCTIONAL STUDY OF DBD ACTUATOR**

   In this phase, how to get an increase of the surface covered by generated plasma was studied. To study this purpose, the following sequence of experiments was followed:

   - **Experiment 1, Type A Configuration in Quartz:** This first experiment was carried out to verify, with a basic configuration of electrodes, whether the plasma could be ignited around the active electrode and that it follow the evolution tendencies with the frequency predicted by the literature and experience of the consulted researchers. The result was satisfactory, with which, the following experiments 2, 3 and 4 are focused on achieving maximize the plasma surface with the most optimal configuration from an energy point of view.
   - **Experiment 2, Type B Configuration on Quartz:** In this second experiment, an electrode structure was built on the face where the high-voltage connection was located, leaving free channels on the substrate that extended parallel to the axial axis of the electrodes, in order to see if the generated plasma was achieved it would spread filling the surface of such spaces. For safety, a configuration of three electrodes on the upper layer was first tested, the two exteriors being active and the interior being connected to ground.

     The experiment suffered no mishap except a short circuit while the first measurement was made at 1 kHz and that did not cause damage to the device; and that was not considered caused by the configuration itself,

[1] The fact that in these representations several overlapping lines could be seen for each Lissajous figure associated with each frequency, responds to the fact that more than one period of the signal has been taken.

[2] From now on, for simplicity, I am going to use the general term *electric charge*, $Q(t)$, but it must not be forgotten that it is really *accumulated charge* and, in particular, a *cumulative centered charge*, whose formulas can be consulted in Section 2.3.

in fact after turning off the power and restart the experiment again, no other problem occurred. However, with respect to the objective pursued: the “bridges” were not filled with plasma at the breakdown or by slightly increasing the intensity, but again concentrated around the activated electrodes and extended outwards a length of order of the millimeter as much (similar to experiment 1). In consequence, the electrodes had to be approached as well as to activate all of the upper face.

- **Experiment 3, Type C Configuration on Quartz:** Due to the fact that no electric arcs between electrodes were produced in the previous experiment, the originally desired structure was developed, in which bands of active electrodes were repeated parallel to each others, giving rise to configuration C. The configuration C is the same as Type B, but in this case the three electrodes of the upper face are active. The objective is the same as Experiment 2, but trying to see if the fact that there are three active electrodes does not cause incidents, besides seeing if it maximizes the sought effect of plasma "bridges".

  Regarding the objective pursued, the experiment was developed without incident, however it was not possible to fill the free areas between active electrodes in an appreciable way. It was only perceived that the ignition was more uniform along the perimeter of the active electrodes than in Experiment 2.

- **Experiment 4, Type A Configuration on lithium niobate:** After Experiment 3, it was concluded that it was necessary to bring the electrode bands closer together in order to obtain a surface covered with plasma, so the next line of research would be to study the influence of the spacing between active electrode and encapsulated electrode (Phase 2), the gap. However, to complete the information extracted from this phase, it was decided to study the Type A configuration in a different material, in this case, in lithium niobate.

Summing up, regarding the learning obtained in this phase in relation to the behavior of the different devices tested, the one of Experiment 4 was analogous to Experiment 1; with the exception that lithium niobate has much higher efficiency values generating plasma significantly reducing the value of the ignition voltage. So, it is necessary to bring the electrode bands closer together in order to try to obtain a bigger surface covered with plasma, because the experiments of this phase were not significant for the rank of values of tension in which it was tested. This fact led to the development of **Phase 2** focused on the study of the influence of the gap between the active electrode and the ground electrode in the generation of plasma.

2. <u>PHASE 2: INFLUENCE OF DIMENSION OF GAP</u>

In this phase has been study the influence of the spacing between active electrode and encapsulated electrode, that is, the gap. To test this, reactors that have been energized they share the same configuration regarding: shape, number and function of the electrodes used, composed of an active electrode with a narrow band on the upper face and another with the same characteristics on the lower face but in this case connected to ground, Type D, both developed with adhesive copper films superimposed on the surface of the substrate. This configuration of electrodes has been mounted on 3 different types of substrates, thus having 3 different device species, to which the size of the gap between both electrodes has been varied; for each device, 4 measurements

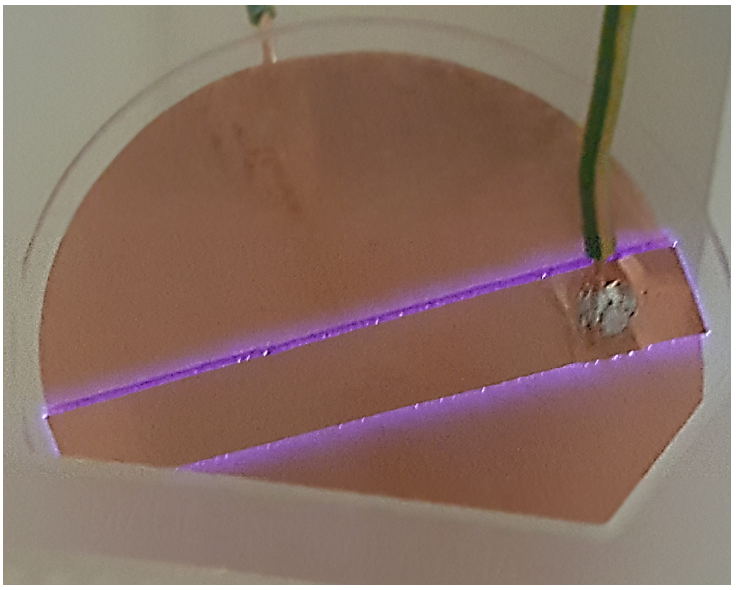

(a) Device 1..

(b) Device 1: zoom..

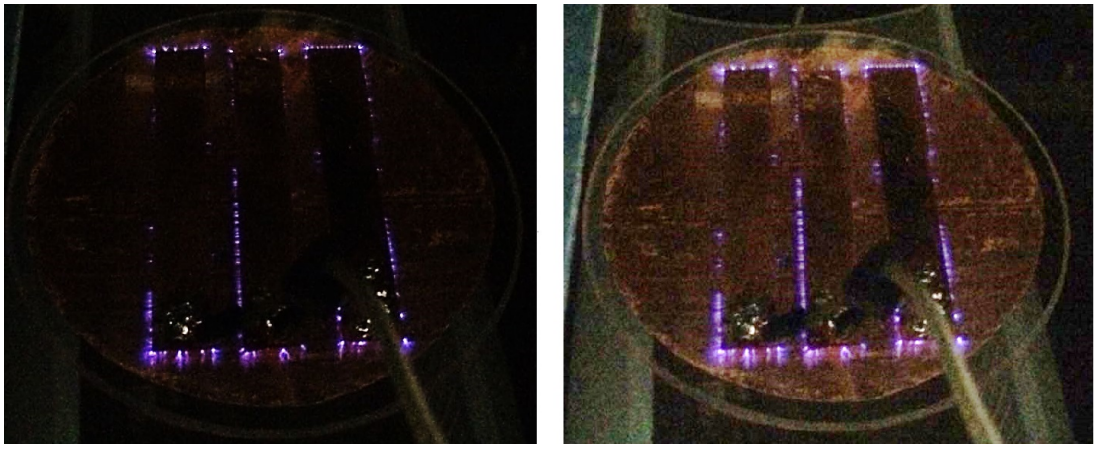

(c) Device 3..

figure 4.4 **Real pictures of plasma generated in experiments of Phase 1.**
Table 3.1 contains an index of experiments.
NOTE: The level of plasma's light intensity of the photo does not have to correspond to the breakdown values. In b) and c), as can be seen, the images are repeated, in the case of those on the right they are digitally manipulated with a different color balance, to ensure that the printing of the document allows observing the discharges..

have been made according to the gap: 5 mm, 2.5 mm, 1 mm and canceling the gap. The substrates used were: quartz (SiO2), alumina (Al2O3) and lithium niobate (LiNbO3).

The experiments that are framed in this phase are from number 5 to 16, both included; all of them with Type D configuration for 3 different dielectric substrates and 4 different gaps.

During he experimentation with a 5 mm gap there was not achieved generation of plasma for an ignition value not exceeding 12.5 kHz for quartz or alumina, considered too high from a consumption point of view; therefore, tests were made for gaps of 2.5 mm, 1 mm and 0 mm, to which the response of the devices was more tolerant as this value decreased, as well as for the case of lithium niobate substrates.

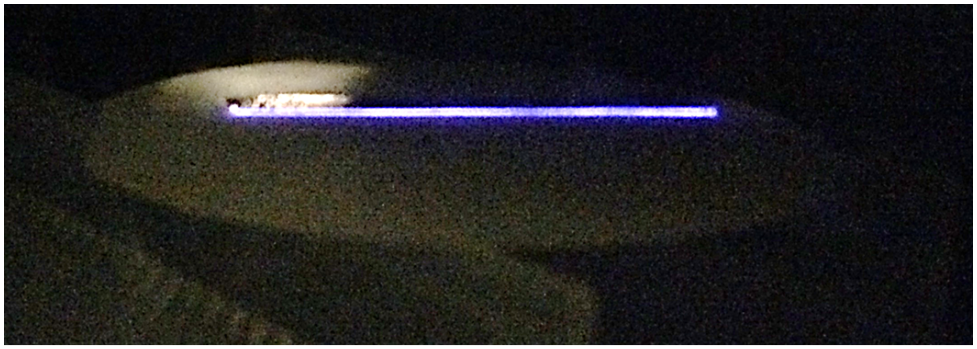

figure 4.5 **Real pictures of the plasma generated during the test with airflow applied to Device 16, in Phase 2.** Type D, lithium niobate with 0 mm of gap.
Table 3.1 contains an index of experiments.
NOTE: The level of plasma's light intensity of the photo does not have to correspond to the breakdown values. .

3. **PHASE 3: ACTIVE MULTI-ELECTRODE CONFIGURATIONS**

Phase 3 is presented as an evolution of phase 2. In it, active multi-electrode configurations are studied, as a result of a series of D configurations adjacent to each other, that is, alternating conductive and insulating bands. Devices 17, 18 and 19 were built; being the first two test models of the concept developed in 19, which will present the results below. Regarding experiment 17, the plasma was unfortunately generated around the ground electrode, so it was decided to develop a band structure also on the face of the "encapsulated electrode", giving rise to device 18. In this case, it was generated Plasma around the perimeter of both faces of electrodes, but as the free surfaces between the bands could not be covered with plasma, so the electrical characterization was not saved again and it was decided to develop the definitive structure with a band width of 1 mm, this being device 19, mounted on a disc of lithium niobate, since it has been the material that has presented the best efficiency. It was appreciated that the space between the strips, all of them of 1 mm of width, was covered with plasma for both sides of the disc.

Regarding the results achieved with the device 19, these follow the same tendencies than the previous phases, with the lower ignition voltages. In addition it was appreciated that the space between the strips, all of them of 1 mm of width, was covered with plasma. The images of some of the experiments cited can be watched below

in figure 4.6.

Summarizing, for this phase of experimentation with a 5 mm gap, there was not achieved generation of plasma for an ignition value not exceeding 12.5 kHz for quartz or alumina, considered too high from a consumption point of view; therefore, tests were made for gaps of 2.5 mm, 1 mm and 0 mm, to which the response of the devices was more tolerant as this value decreased, as well as for the case of lithium niobate substrates.[3]
In summary, the repetitive band structures of Phase 3 were carried out, reaching for the experiment 19 (on lithium niobate) successful results in terms of covering the spaces between electrode bands with plasma, as well as plasma appeared around both active electrodes and ground electrodes.

4. PHASE 4: EXPERIMENTATION IN AIRFLOW AND AT REDUCED PRESSURE

In this phase, two experiments were carried out. First, experiment 20, the DBD plasma actuator has been faced with a surface current of air with the plasma already generated, to test what effect the current has on the covered plasma surface as to whether the flow displaces or extends it, as well as to observe the variation in its direction that the current experiences as a result of the effect of the plasma exerts on it. However, it was not possible for a naked eye to perceive the effect of the current on the generated plasma.

Respect to experiment 21, correspond to device used in experiment 19 but being tested at reduced pressure inside a specific reactor, always in atmosphere in calm. It was taken for measures: at 988 mbar (corresponding to the pressure in the laboratory[4], in order to compare this result with the result obtained in experiment 19), at 667 mbar(corresponding to 11000 ft approximately), at 301 mbar (corresponding to 30000 ft approximately) and 20 mbar. All of the measures were saved at 5 kHz of frequency because it correspond to optimum frequency, as it can be read in the next section. and as always, at the breakdown voltage. Respect to perceive the breakdown point, it was more difficult due to the device had to be observed through the window of the reactor.

For the development of these experiments it was necessary to take special care in opening the air inlet valve between experiments, to clean the atmosphere in which they were carried out, and thus avoid an atmosphere enriched in ozone.
Indeed, the results were as expected, the decrease in pressure reduces the ignition voltage considerably, since it favors the ionization of the gas. In addition, the laboratory pressure results were practically identical to those obtained during the experiment 19. Again, it was appreciated that the space between the strips, all of them of 1 mm of width, was covered with plasma for both sides. So, summing up, in Phase 4, after not being able to appreciate with the naked eye the displacement of the plasma with the passage of the current, as well as the impossibility of developing experiments with smoke chamber that showed the deformation of the current lines of the incident flow emitted by a fan, no more information regarding that experiment is included.

[3] In the case of alumina, problems happened in achieving ignition at a 2.5 mm gap, because the breakdown value exceeded 14 kV peak-peak at 1 kHz frequency, too high for our criteria, and it was decided to abandon this experiment, the number 9.
[4] Possible discrepancies justified by the calibration of the high pressure meter.

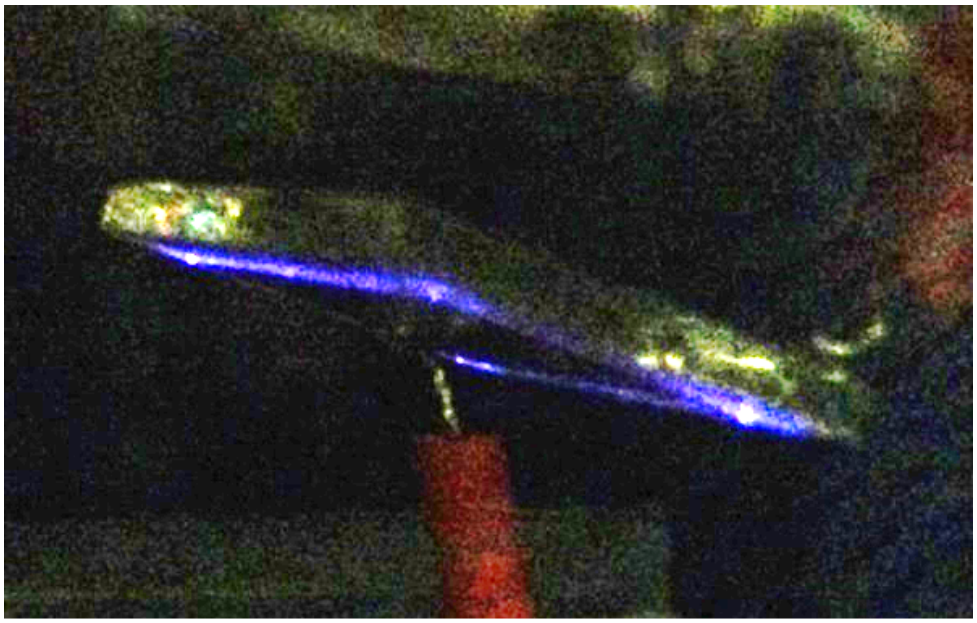

(a) Plasma generated around ground electrode in device 16..

(b) Plasma appear around active and ground electrodes..

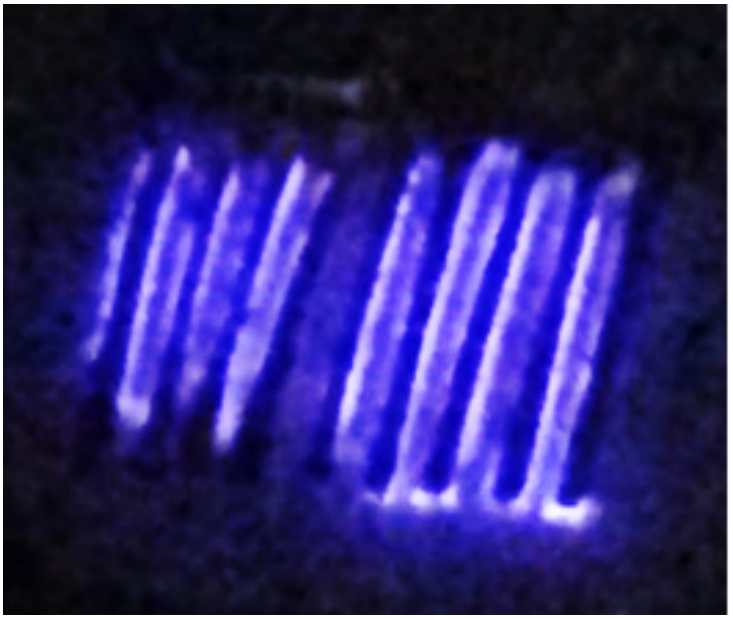

(c) Zoom of Device 19..

figure 4.6 **Real pictures of plasma generated with devices of Phase 3.**
Table 3.1 contains an index of experiments.
NOTE: The level of plasma's light intensity of the photo does not have to correspond to the breakdown values. .

4.1.2 Results

Next, in the following sections, the behavior patterns that are extracted from analyzing all the operating parameters found in Table 4.1 are exposed. It has been discovered that there is an **optimum frequency around 5 kHz, for which the accumulated charge is maximum**, and that can be inferred from the electrical behavior of the devices for each parameter studied.

Table 4.1 A. Operational parameters analyzed with the electric analysis.

Parameters			
Frequency	V	Power factor	PF
Voltage	V	Phase difference	ϕ
Current	I	Gap	g
Accumulated charge	Q_c	Dielectric material	-
Consumed power	P	Number of electrodes	-
Effective capacitance	C	Pressure	p
Impedance	Z		

A. Behavior of Voltage and Current with frequency

Ignition **voltage**[5] decreases when frequency of the signal that is applied to the experiment increases. The decrease is more pronounced between low frequencies and ends up drastically decreasing its slope around 5 kHz for all the cases studied, reaching a zone of apparent stabilization.

Voltage and current have a proportional behavior. The ignition **current** increases when frequency of the signal that is applied to the experiment increases. The increase more pronounced between low frequencies and ends up slightly decreasing its slope around 5 kHz. It must be remembered that the electric current value shown corresponds to a total value and not a real value; since, as we saw in the theory of Chapter 2, electric current has two components, a conductive due to the movement of electrons (known as real) and another of displacement $\partial E/\partial t$ due to polarization.

The lithium niobate presents a much more efficient behavior from the point of view of the voltage consumed at the time of ignition. However, the generated plasma is located around the same current values for the three dielectrics studied.

That is, voltage and current increase with frequency until reaching a saturation value, and around 5 kHz its variation slope changes. These trends occur independent of the type of device. Below, in Fig. 4.7- 4.9, are figures that corroborate this conclusion for phase 1 –showing the peak-to-peak values of both parameters– 0mm-of-gap

[5] The measurement of the signals tends to be more stable as the frequency of the experiments increases, since the appreciable breakdown point appears more intense and abrupt.

differentiating by material, and lithium niobate differentiating by gap, respectively.

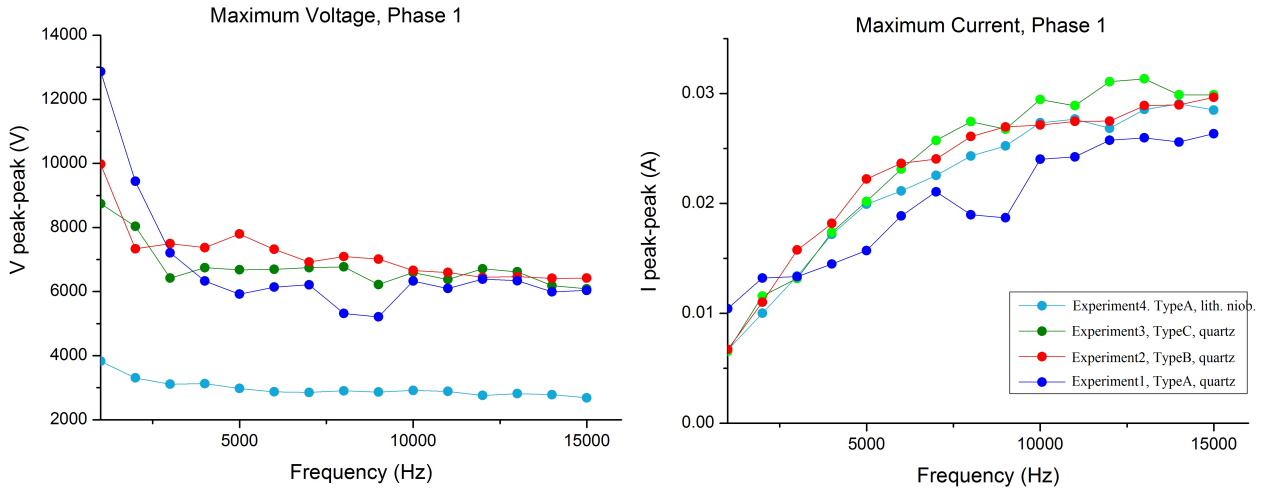

figure 4.7 **Voltage and Current results: example with Phase 1 outputs.**
Table 3.1 contains an index of experiments..

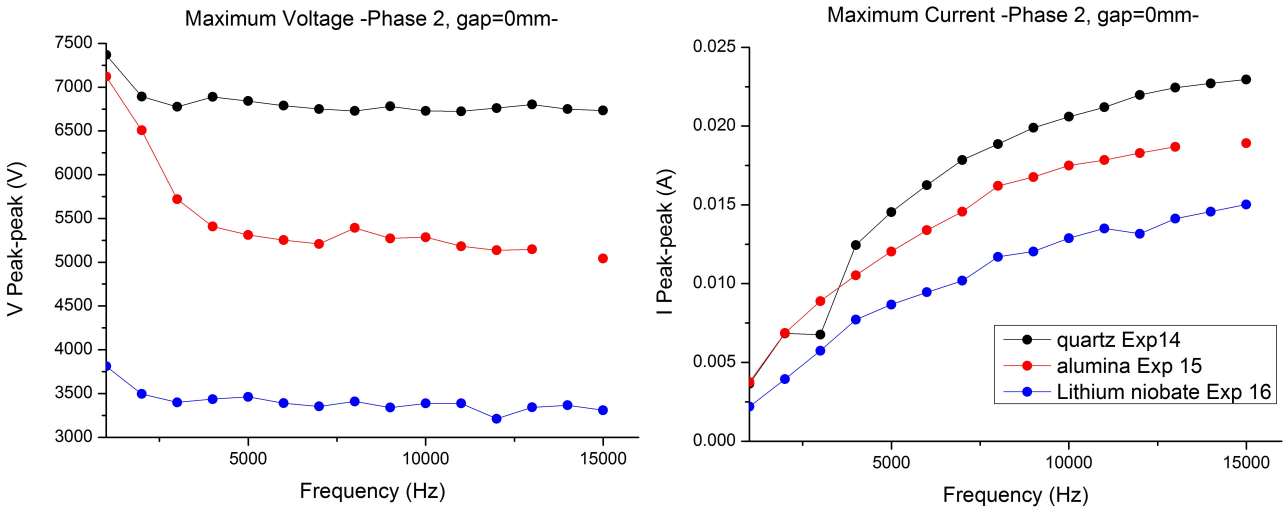

figure 4.8 **Voltage and Current results: example with Phase 2 outputs for 0 mm of gap, differentiating by material: quartz, alumina and lithium niobate.**
Table 3.1 contains an index of experiments..

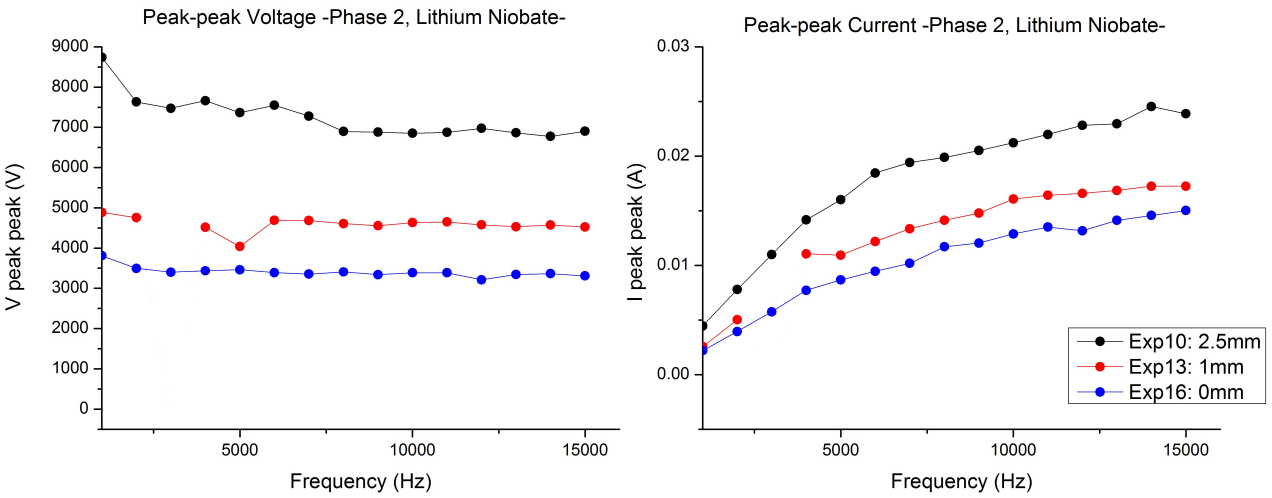

figure 4.9 **Voltage and Current results: example with Phase 2 outputs for lithium niobate.**
Table 3.1 contains an index of experiments..

B. Lissajous figures. Behaviour of Accumulated charge and Capacitance with frequency

The shape of the Lissajous figures varies with frequency in a pattern that is repeated throughout the rest of the experiments; in general, they have an elliptical appearance. For representations of $I(t)$ vs. $V(t)$, the shape of the figure is more flattened in the direction of the current and more elongated along the horizontal axis representing the voltage for low frequency values, which is equivalent to higher ignition voltages and low currents, and this appearance is gradually reversed as the frequency increases, becoming more energy efficient as the current through the device grows and the ignition voltage decreases.

Regarding the representation of $Q(t)$ vs. $V(t)$, although the shape of the figure is still approximately elliptical, the evolution with the frequency is different from the previous representation due to the fact that the accumulated load decreases as frequency increases, thus also corroborating an efficient growth in the performance of the device, which means that the area enclosed by these figures –and equivalent to, being multiplied by frequency, the average power $\overline{P}$– grows with frequency increase. Also, as a consequence of the behavior of the electric current, it is noticeable that as the frequency increases, the maximum accumulated electric charge points are not presented for the maximum voltage amplitude of said signal.

The variations between the different figures with the frequency is more prominent for low frequencies, while it tends to adopt a more similar behavior starting from, approximately, 5 kHz. And respect to the **zero-charge**[6], it has a trend of increasing-decreasing when frequency increases, and the turning point (a maximum) is located around 5 kHz for all the cases. So, it is clear that said frequency is the optimum frequency from a point of view of energy consumption because the accumulated charge in the device is maximum when there is no applied voltage, on this way less voltage is needed to generate plasma. To illustrate these comments, Fig. 4.10 shows a representative selection of Lissajous figures that have been built from the electrical signals saved from the experiment. The trend of zero-charge, Q_0 can be also checked in Fig. 4.11-4.12.

This fact is significant since the accumulated charge is the factor that decreases the ignition voltage. In this way, although the ferroelectrics have a dielectric constant that varies with the voltage-dependent $\varepsilon(V)$ (which leads therefore to a **capacitance** also dependent on the voltage $C(V)$), it takes place a maximum charge capacity reached with this optimum frequency, around 5 kHz –see equation 4.1–. The devices have a maximum value of accumulated charge when the device is off (called zero charge Q_0), that is, they present a maximum capacitance at the optimum frequency value, and in consequence they need less voltage to generate plasma when the discharge cycle starts again.

$$C = \frac{Q}{V}; \qquad C = \varepsilon_0 \varepsilon_r \frac{S}{d} \tag{4.1}$$

where C is capacitance, Q is electric charge, V is voltage, ε_0 is the vacuum dielectric constant, ε_r is the dielectric constant, d is the thickness of the dielectric and S is the dielectric surface/area.

[6] Referred to zero-accumulated charge, charge when voltage is null.

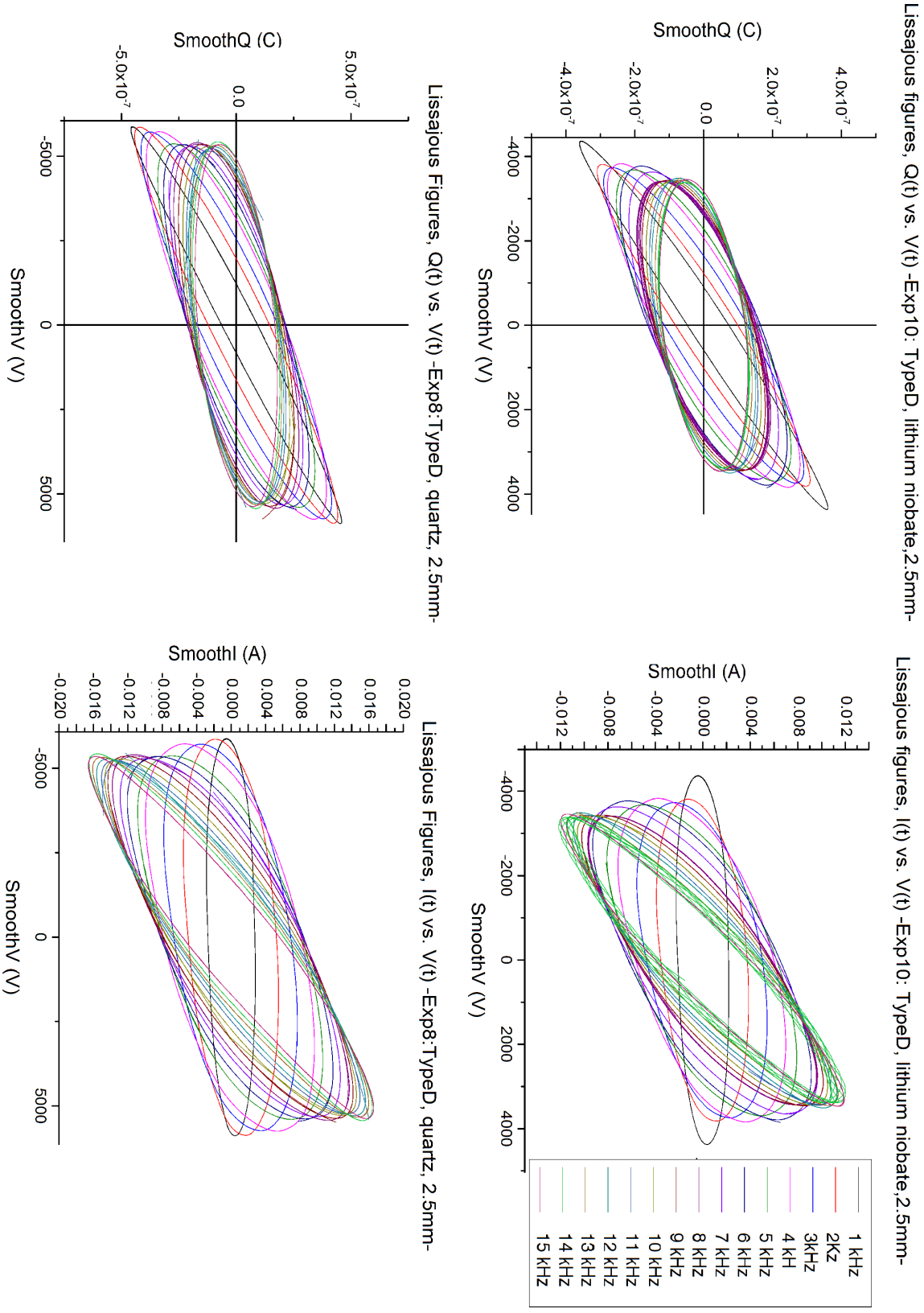

figure 4.10 **Lissajous figures. Representative results.** Experiments 8 and 10 for all the frequencies tested. The figures of Lissajous are collected for a range of frequencies f of 1 to 15 kHz. The representation of Charge $Q(t)$ vs. Voltage $V(t)$ has vital importance since its enclosed area offers directly the value of the Average Power $\overline{P}$ of the period for each frequency if this area is multiplied by frequency.
Table 3.1 contains an index of experiments..

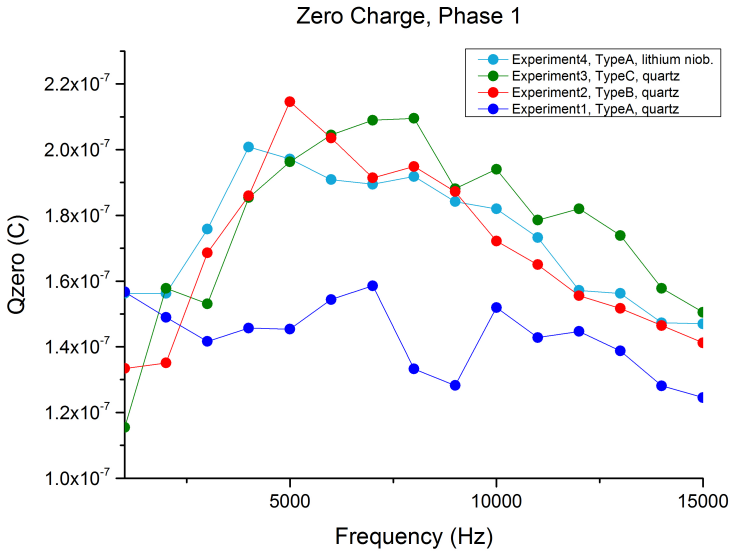

figure 4.11 **Zero Charge results: Phase 1 sample.**
Table 3.1 contains an index of experiments..

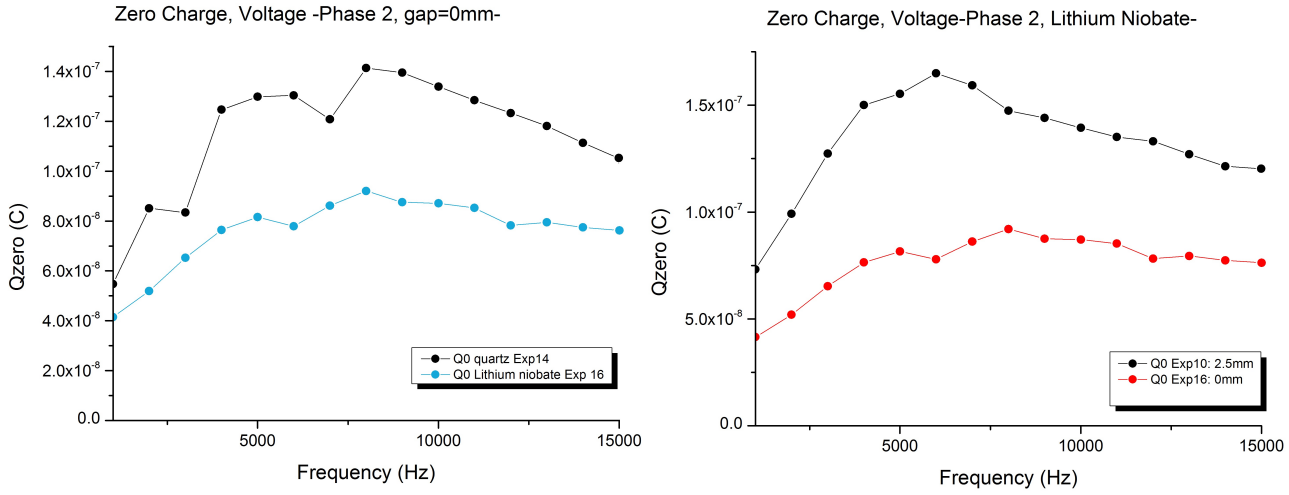

figure 4.12 **Zero Charge results: Examples of Phase 2 results –0 mm-gap sample in function of dielectric and lithium niobate sample in function of gap.**
Table 3.1 contains an index of experiments..

C. Behavior of Impedance and Consumed Power with frequency

The devices act as capacitors, in this way it has already been said that there are two types of current, one due to the polarization of the dielectric and another corresponding to the current of electrons in the circuit. **Consumed power** is presented as a monotonically increasing parameter with the increase in frequency, and responds to the fact that, like the current values shown, it represents the total power that passes through the circuit, not to the real component (IR ^{2}), since this total consumed power contains the sum of both components. That is to say, the part of power associated to the displacement current due to polarization ($\partial E/\partial t$) –and not to the electrons– that travel the circuit is the responsible for this result, since it is translated in terms of power as reactive power.

It can also be verified how correct experimental results have been obtained since the power extracted from the area enclosed in the Lissajous figures coincides practically in full for all the experiments developed with the integral way to obtain the power.

Both aspects can be checked in Fig. 4.13 and 4.14. Obviously, although the trends are repeated for all the experiments, the values are different according to the experiment, the lower the dielectric constant, the higher the power consumption, as well as the power consumed the lower the gap for the same material –see Fig. 4.14–.

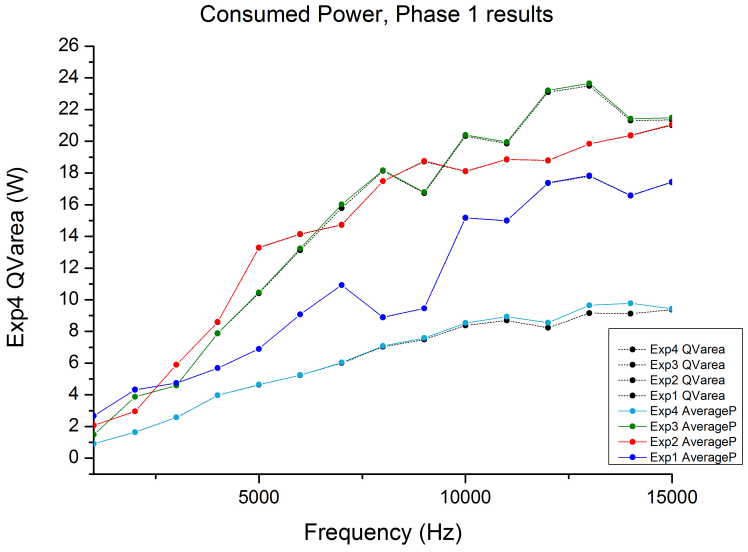

figure 4.13 **Consumed power: Integral process vs. Lissajous figure's area enclosed multiplied by frequency.** Phase 1. Table 3.1 contains an index of experiments..

The behaviors with the frequency of the voltage, current and power studied do not allow to see so clearly the existence of an optimal operating point in terms of the frequency of ignition, in comparison to other study parameters. However, the behavior of the impedance makes it possible to know the existence of an optimum frequency value according to the evolution of its real and imaginary components with frequency, that in this occasion they can be studied individually, and reflect the behaviour of the components of the current. While the real component of the **impedance** remains practically stable regardless of the frequency value, the imaginary component that has a high value at low frequencies decreases sharply (with a high value of the slope for the lower frequencies), until both

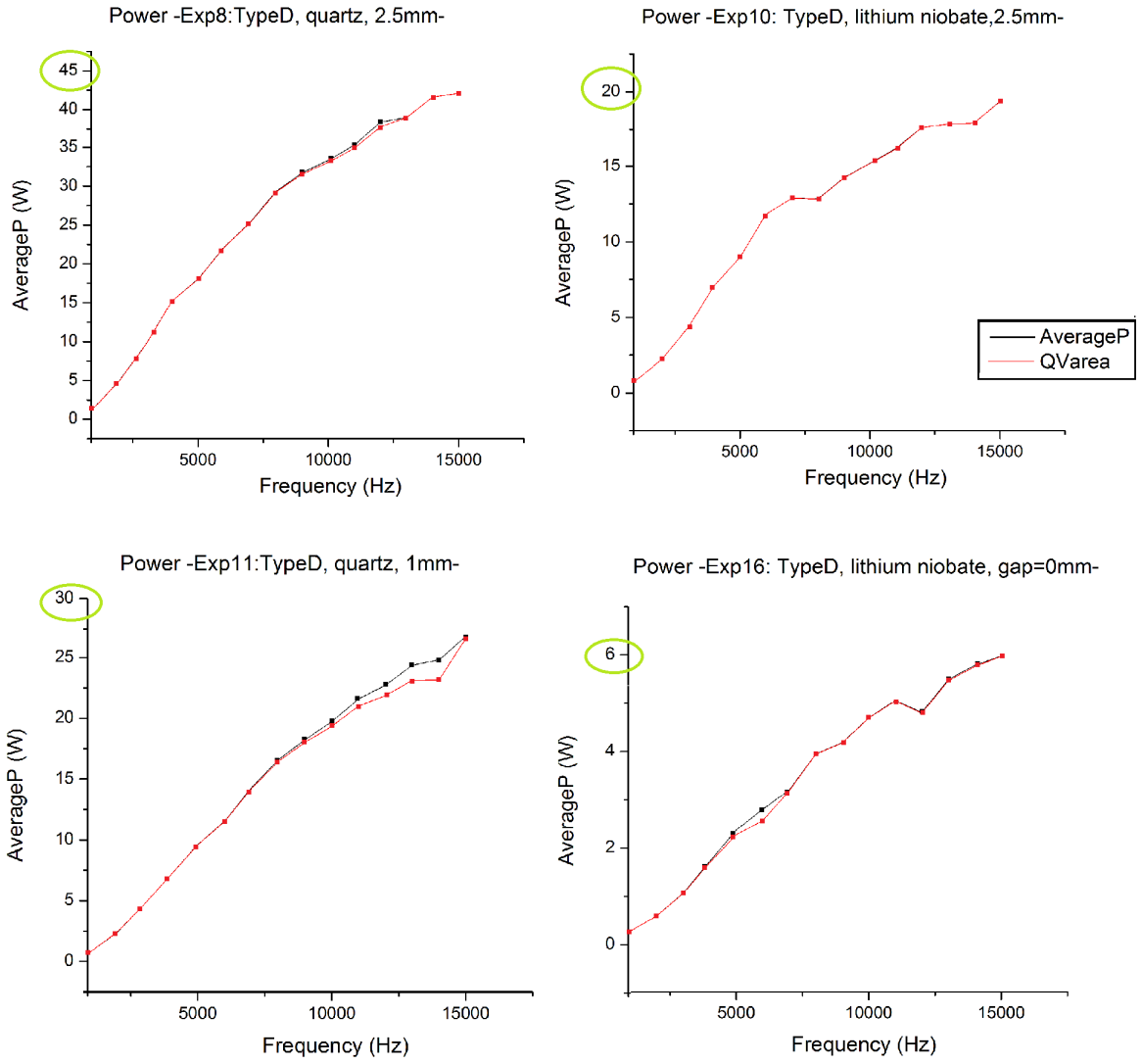

figure 4.14 **Consumed power: Integral process vs. Lissajous figure's area enclosed multiplied by frequency.** Some examples of Phase 2.
Table 3.1 contains an index of experiments..

impedance components of the impedance are crossed around 5 kHz of frequency, the optimum frequency. From this point on, the real component has a higher value than the imaginary one, and the variation of both is practically zero during the rest of the tested frequency range up to 15 kHz. This fact tells about an increase in the efficiency of the device in generating plasma from a certain frequency value. See Fig. 4.15 and 4.16, for results of Phase 1 and 0mm-gap-devices of Phase 2 respectively, to check this affirmation in a representative sample of the experiments. From an energy efficiency point of view, this event is tremendously positive, since from the optimum frequency, the device works mainly with real and not imaginary impedance.

Regarding the **power factor**, it is as representative as the impedance, since they come from the same, it simply constitutes a different way of showing the results. That is why it has finally been decided to include a single example of representation, contained in Fig. 4.15. it increases progressively but it has a slope change around 5 kHz, from

which its growth begins to approximate towards a horizontal asymptote. The closer that value is to the unit, the more efficient the device will be, because it implies that the number of watts of consumed power is the same as the number of volt-amperes consumed –that is, a unit value for the power factor is equivalent to a percentage of 100 % in which there are no energy losses–.

At 5 kHz, there is an inflection point where also the "crossing" occurs with the representation of the phase shift, which decreases with frequency increase, change its slope at 5kHz, and logically to become practically zero for frequencies around 15 kHz.

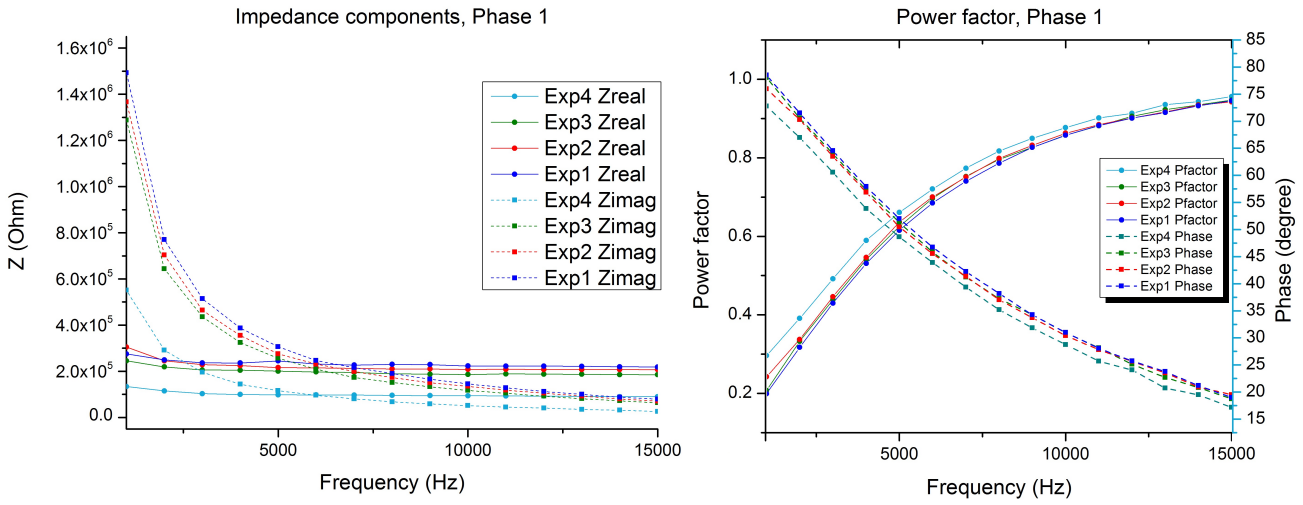

figure 4.15 **Impedance and Power factor results: Phase 1 sample.**
Table 3.1 contains an index of experiments..

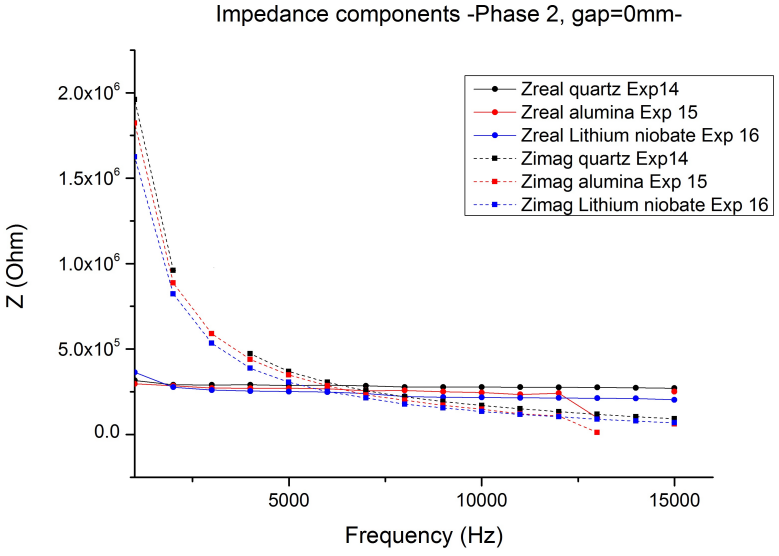

figure 4.16 **Impedance results: Phase 2 sample on 0mm-gap-devices.**
Table 3.1 contains an index of experiments..

D. Influence of Gap

Gap significantly affects the ignition values, being the experiments developed at null gap those of greater electrical efficiency. This tendency is reflected in all the data analyzed, breakdown voltage sharply decreases as gap decrease –see Fig. 4.17 representing this influence at optimum frequency sample–. So, a decrease of gap favors more capacitance for the device, because capacitance is obtained as indicated by expression 4.1.

Likewise, it has not been successful for the conditions of the study to generate plasma surface greater than approximately one millimeter.

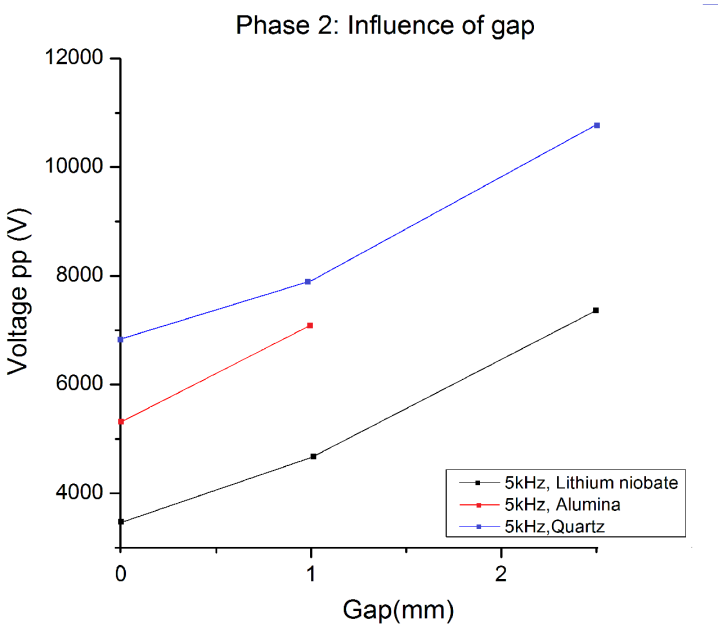

figure 4.17 **Influence of gap in the ignition voltage.**Example at optimum frequency of 5 kHz..

E. Behaviour of Single DBD vs. Multi DBD

To analyze this purpose, the data from Multi-band Experiment 19 (Phase 3) and from Single-band Experiment 16 (Phase 2) have been studied; both have been built on lithium niobate and with a gap of 0 mm between its corresponding pair active-ground electrodes. The electrodes have different width and length in these two devices, so the conclusions drawn have to be qualitative, especially in the case of the consumed power. In Fig. 4.18 it can be checked how similar values of current are obtained at the ignition point of plasma but at much lower voltage in the case of the single-band configuration. Also, since 5 kHz, the the single-band device generates a higher amount of current of the plasma ignited when frequency increases comparing to the multi-band device.

Also, the single band device consumes more power, but one has to consider the dimensions are different and larger than multi-band electrodes –see Fig. 4.18–.

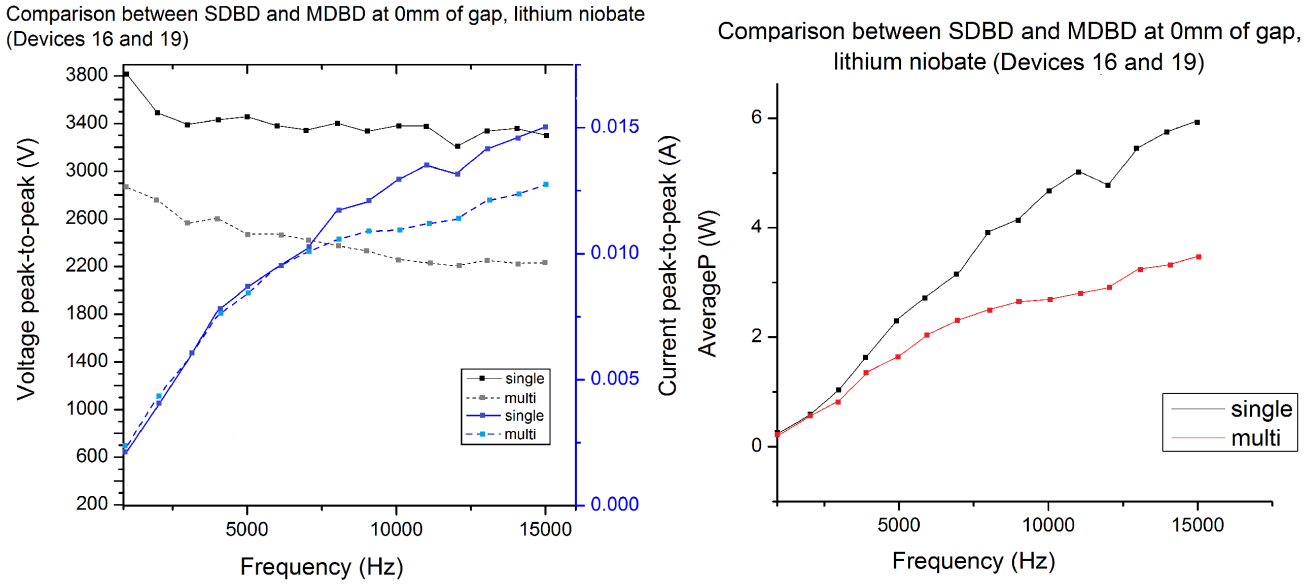

figure 4.18 **Comparison between single and multi DBD device (Devices 16 and 19): Voltage, Current and Consumed Power.** Both in lithium niobate and 0 mm of gap.
Table 3.1 contains an index of experiments .

An estimation of the capacitance of the dielectric used in the device can be made from the Lissajous Figure Q vs. V applying the expression 4.1, understanding that capacitance is the slope of the curve at each point. That is, to obtain a value that gives us a qualitative idea (effective capacitance) on the behavior of its capacitance. 4.2–.

$$C_{eff} = \frac{Q_0}{V_0} \approx \frac{Q_0}{V_{ignition,pp}} \tag{4.2}$$

where C_{eff} is an effective capacitance, Q_0 is charge when the voltage is null, V_0 is voltage when charge is null, and $V_ignition$ is in this case the break-down or ignition voltage referred during the document, that is, the appreciable voltage by naked eye in lab conditions that ignites the plasma.

Consequently, observing Fig. 4.19 and 4.20, respectively contain Lissajous figures and a representation of

capacitance, it is verified that there is an optimum point of charge (and therefore capacitance) when the frequency is 5 kHz. Likewise, the maximum accumulated charge value in the device is a little higher for the multi-band device until reaching the optimum frequency point, from which the trend changes since the charge fall for it is harder than the single-band. As expected, given the difference in ignition voltage between both configurations, the capacitance is greater for the multi-band device.

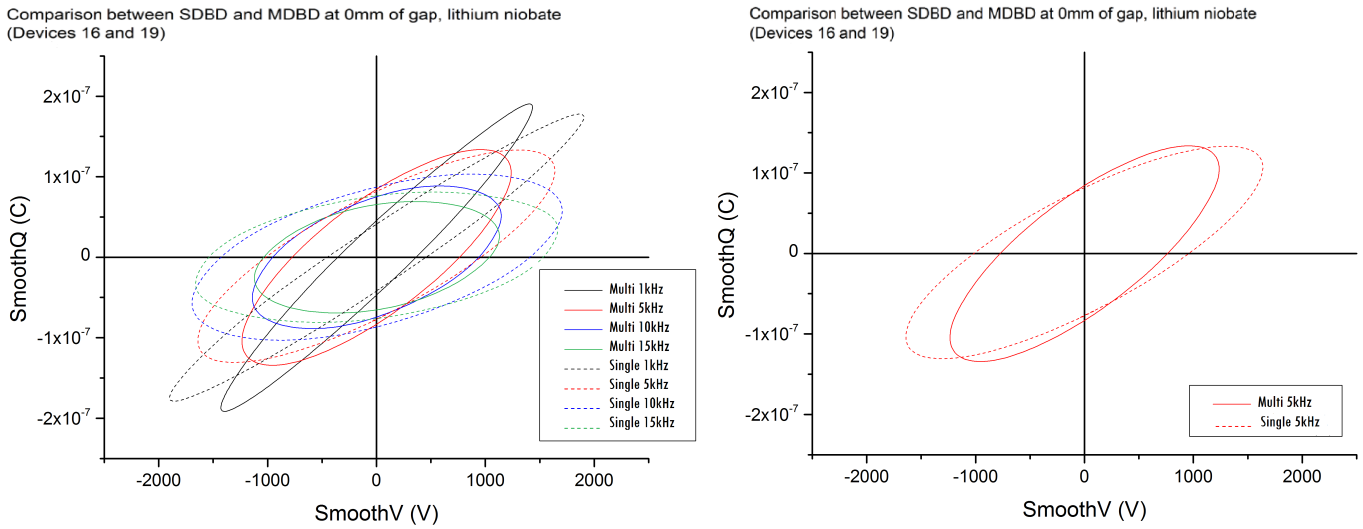

figure 4.19 **Comparison between single and multi DBD device (Devices 16 and 19): Accumulated Charge** Both in lithium niobate and 0 mm of gap.
Table 3.1 contains an index of experiments. .

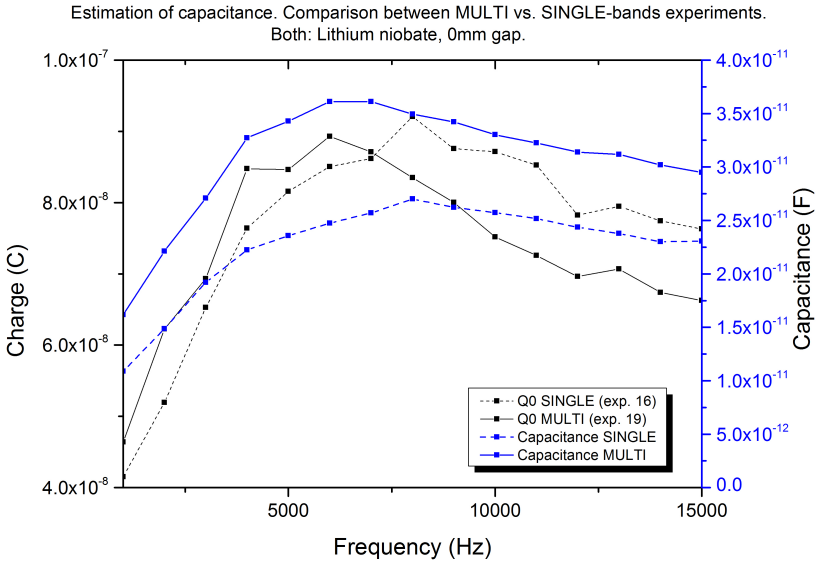

figure 4.20 **Comparison between single and multi DBD device (Devices 16 and 19): Capacitance.** Both in lithium niobate and 0 mm of gap.
Capacitance is calculated dividing accumulated charge by amplitude voltage (not peak-to-peak voltage).
Table 3.1 contains an index of experiments. .

F. Influence of Pressure

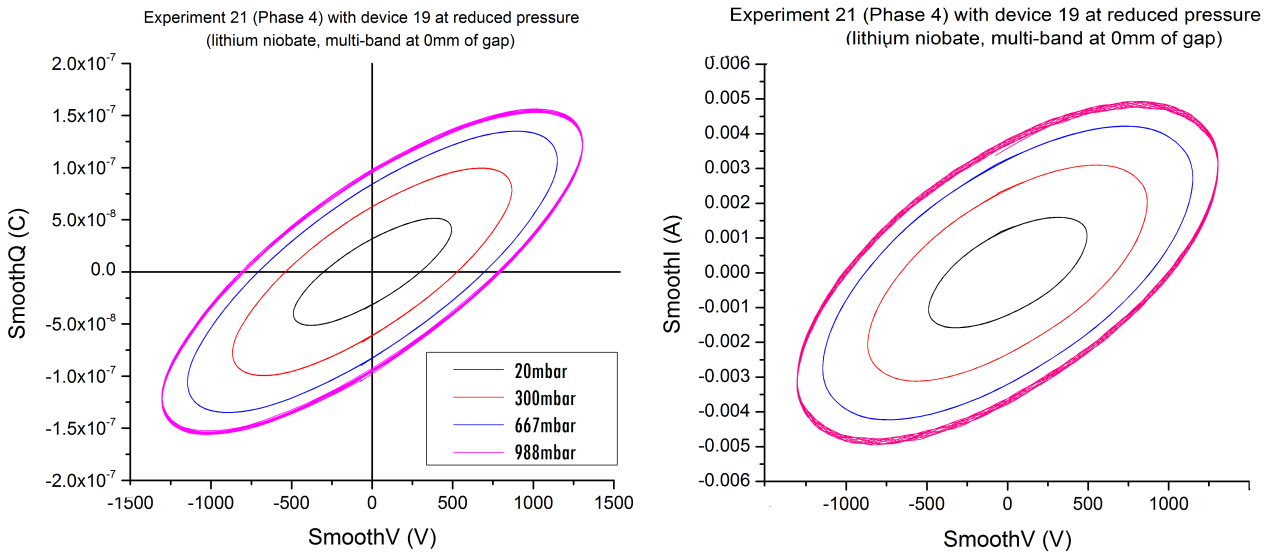

figure 4.21 **Phase 4, Experiment 21 at reduced pressure: Lissajous Figures.** Device 19 on lithium niobate and multi-band configuration with 0 mm of gap.
Table 3.1 contains an index of experiments. .

Reducing the pressure favors the ionization process –see Fig. 4.21 and 4.23, all of them measured at the optimum frequency of 5 kHz–. It was found that a reduction in pressure facilitates the generation of plasma, notably decreasing the ignition voltage, as well as, consequently, the impedance and power consumed by the experiment; which would favor the use of these devices in flight.

Respect to the impedance, given that the data has been saved at 5 kHz (the value around which the optimum frequency is) in this zone the crossing between the imaginary and real components takes place, so that in Fig. 4.22 one can check the closeness between these two components for all measurements compared to the usual impedance values.

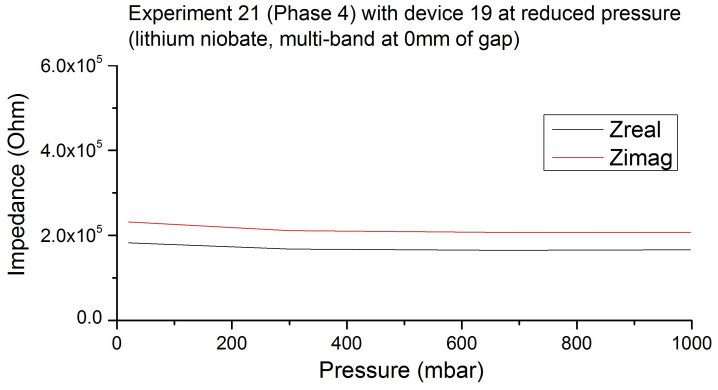

figure 4.22 **Phase 4, Experiment 21 at reduced pressure: Impedance components.** Device 19 on lithium niobate and multi-band configuration with 0 mm of gap.
Table 3.1 contains an index of experiments. .

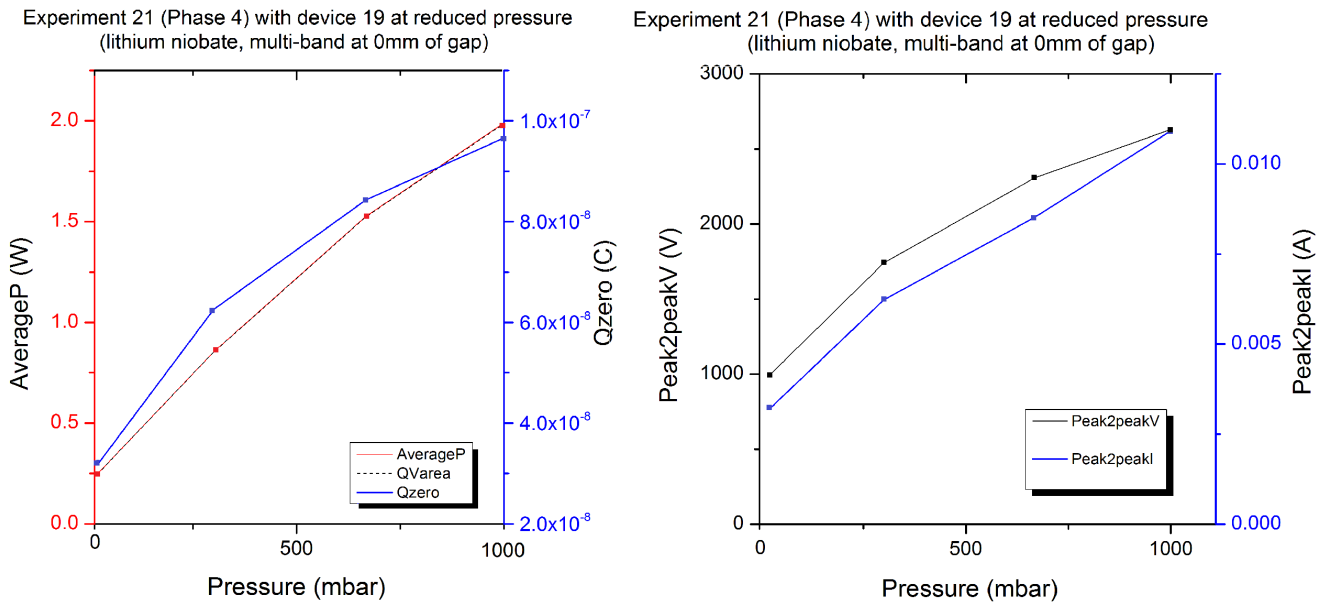

figure 4.23 **Phase 4, Experiment 21 at reduced pressure: Power and Zero Charge.** Device 19 on lithium niobate and multi-band configuration with 0 mm of gap.
Table 3.1 contains an index of experiments. .

G. Influence of dielectric

Regarding the **dielectric**, lithium niobate represents the most efficient alternative for the development of the actuator, since from an electrical perspective, it allows to obtain higher values of current at ignition voltages much lower than the rest of the materials with which it has been experimented, so, even the current generated is in a range similar than others, the breakdown voltage associated is considerably lower. Related to alumina and quartz, quartz is the one that shows the greatest resistance to current flow.

This fact is directly related to the value of the dielectric constant of the material, since in the case of the ferroelectric such as lithium niobate, it increases by two orders of magnitude with respect quartz or alumina –see Table 2.1–; and in elements such as these devices where the capacitive effect (capacitor) is very important, this property has a great influence. The greater the dielectric constant, the greater the accumulated charge in the material, and therefore the greater the current flowing through it. The fact that a material increases a large amount of charge due to a high dielectric constant is reflected in that it needs much less amount of voltage for a second ignition, as can be verified for the results of the niobate throughout all the experiments made during this work. In addition, ferroelectric is a material with a polar structure whose polarity can be reversed (switched) by applying an electric field, and this also intensifies the previous effect. [7].

To illustrate this example graphically, beyond being able to be verified in all the results that appear in this chapter,

[7] The ferroelectric phenomenon appears in certain dielectric materials and consists in the retention of the polarization induced by an external electric field, once it has disappeared. In ferroelectrics, polarization is not a linear function of the field, since neither is the dielectric constant.
For more information, go to Section 2.2.

a type of specific graphs have been developed in which the value of the capacitance of the device is shown. This decision has been made because, although the ignition voltages are much lower for the lithium niobate compared with quartz or alumina, the current ranges are similar. So, Fig. 4.24 shows that the capacitance is much higher in lithium niobate devices due to its high dielectric constant in comparison with the others.

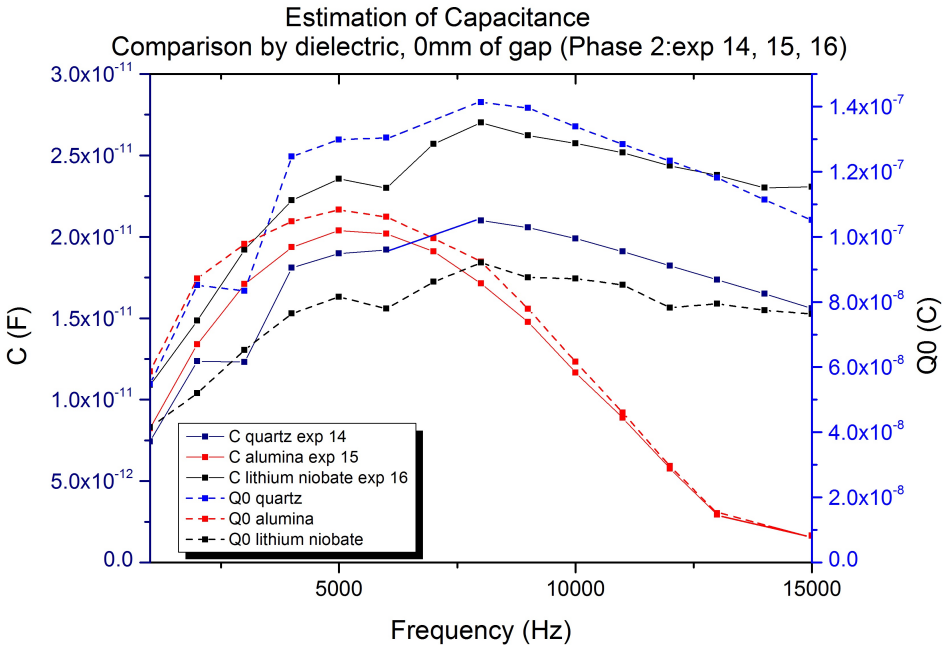

figure 4.24 **Comparison by material, 0 mm of gap (Phase 4: Experiments 14,15 and 16): Charge and Capacitante.** Capacitance is calculated dividing accumulated charge by amplitude voltage (not peak-to-peak voltage)..

Main electrical results: summary

Table 4.2 **Summary of main Electrical results.**.

MAIN RESULTS OF ELECTRICAL ANALYSIS		
Measures saved at appreciable ignition point of plasma.		
Existence of an optimum frequency around 5 kHz.		
Parameter	Behavior with frequency	Page
Voltage (V)	Voltage decreases with frequency increase to a saturation value, with a change in its slope at the optimum frequency.	80
Current (I)	Current increases with frequency increase to a saturation value, with a change in its slope at the optimum frequency. One can not see a maximum in the current representation with the optimal frequency because it has been analyzed a global value that does not differentiate between its real and displacement components.	80
Accumulated Charge (Q)	There is a maximum value of accumulated charge in the device at the optimum frequency. Zero-charge ($Q_0 = Q(V = 0)$ within the cycle of the discharge) is a significant parameter.	83
Capacitance (C)	In consequence, capacitance also has a maximum with optimal frequency, even for ferroelectrics, which have a voltage-dependent dielectric constant, and in consequence a voltage-dependent capacitance.	83
Impedance (Z)	The imaginary component of the impedance decreases with the frequency increase and from the optimum point of frequency it becomes smaller than the real component, which remains practically constant with the frequency.	86
Power factor (PF)	The imaginary component of the impedance decreases with the frequency increase and from the optimum point of frequency it becomes smaller than the real component, which remains practically constant with the frequency.	86
Power (P)	The power presents a monotonous growth with the frequency, but it has to be taken into account that, as with the current, a value of the real component is not reflected, but global.	86
Influence of Gap (g)	The decrease in gap favors a lower ignition voltage. No ignitions were achieved at gap = 5 mm in a range of V_{pp} applied less than 12.5 kV.	89
Influence of Pressure (p)	The decrease in pressure favors ionization, and therefore the ignition voltage decreases considerably.	90
Influence of number of electrode bands	The multiband device requires lower ignition voltage. Both devices generate similar current values up to the optimum frequency value.	92
Influence of dielectric	The greater the dielectric constant, the lower the ignition voltage is required. Lithium niobate presents the best capacitance results.	93

4.2 Spectroscopic analysis results

As for why optical emission spectroscopy (OES) is useful, as we have already read in Section 2.3 it allows to directly obtain the composition of the plasma from its "bands or lines" of intensity. In addition, if more exhaustive analyzes are applied, as mentioned, it offers information about the excitation or ionization processes and plasma temperatures. Thus, depending on the type or value of temperature that is established, different properties of the plasma can be characterized.

The objective of this spectroscopic analysis is not to develop a complete study of the field, but to demonstrate the existence of active species, generated by the plasma, in the air surrounding the device; allowing thus to develop a deeper characterization of the generated plasma; as long as air plasma has been generated, and therefore it must be obtained nitrogen spectra, because N_2 species are, mostly, easy to excite.

Each device generates a different plasma that can be characterized with spectroscopy. At atmospheric pressure, in a dark ambient and at a plasma intensity level considered high enough for the fiber make a correct measurement, spectroscopic measurements were taken of the emission spectra of devices number 3, 16, and 19. In the case of Experiment 3, measurements were taken at 7, 8, 9 and 10 kHz; in the case of Experiment 16 the measurement took place at 15 kHz frequency; and for the last case spectroscopy was carried out at five different voltages for the same frequency, the optimum frequency (5 kHz).

In the optical emission spectrum, the band heads associated with the element constituting the plasma are to be observed[8].

4.2.1 Results

At the end of the spectroscopic analysis, Section 4.2 contains the Table 4.4 with the main results obtained.

As a representative sample, is included in Fig. 4.25 the optical emission spectrum[9] of the plasma generated with device 19, indicating in it the corresponding assignment to each nitrogen's vibrational transition[10]. In this figure, there is the spectra corresponding to device 19 at optimum frequency. The vibrational quantum numbers $v' - v''$ of each transition are indicated above the band head. Under the spectrum is the diagram of the transitions observed in it between the vibrational levels of N2.

[8] What is really observed is the envelope of a considerable number of bands of smaller size representing both the vertical and rotational displacements of the electrons, because both (and especially the latter, the rotational ones) are very complicated to observe with greater degree of detail with a usual monochromator. To get an idea, we would have to have a monochromator of measurement characteristic of around a minimum of two meters, to obtain a resolution at that level with respect to rotational vibrations. This is why we usually work with band heads.

[9] To know the resolution data of measuring of each spectroscopy showed in this section, it is recommended to go to page 69.

[10] It is important to say that the values contained in the tables included in Fig. 2.19 correspond to the equilibrium, so they are only useful for comparative purposes.

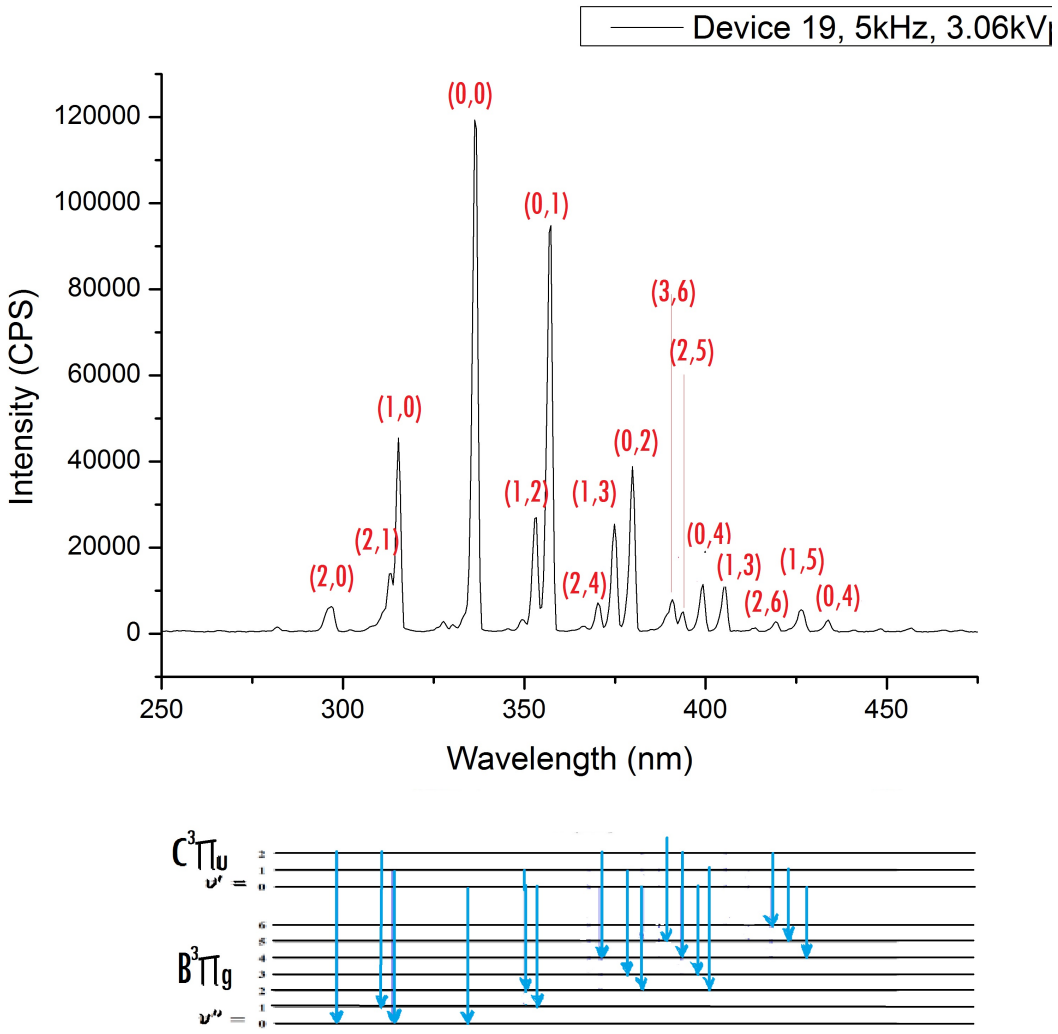

figure 4.25 **Assigned head bands for Nitrogen second positive system states in the plasma's emission spectrum.**
Device 19: lithium niobate, type G.
Table 3.1 contains an index of experiments..

In Fig. 4.26 and 4.27, a study is collected according to the voltage for that same device and optimum frequency with an increase in resolution of the measure in order to, also, to calculate the vibrational temperature according to Section 4.2. It has been found that the pattern of placement of the band heads with respect to the wavelength never varies, since it is characteristic of the element in question, in this case, nitrogen. Likewise, the increase in frequency or voltage translates into a significant increase in the intensity of emission.

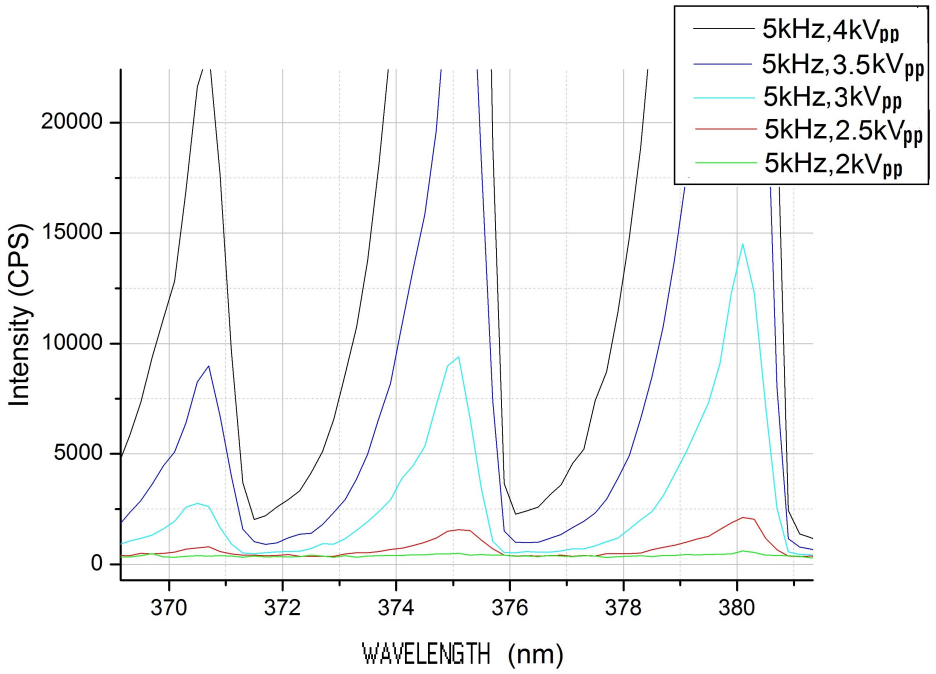

(a) Device 19. Zoom of b)..

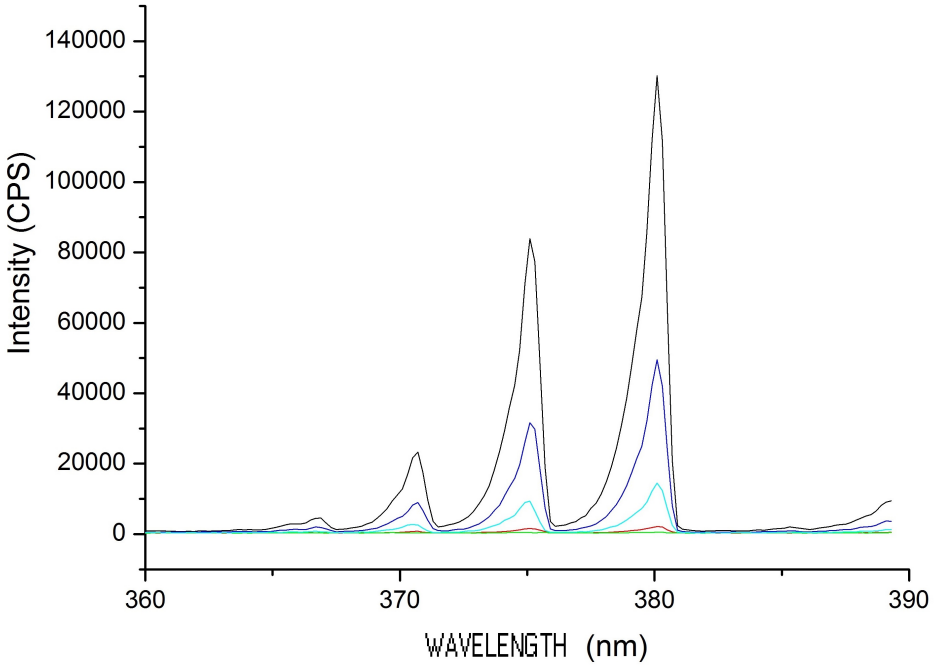

(b) Device 19. 370-390nm..

figure 4.26 **Head bands for Nitrogen second positive system states in the plasma's emission spectrum: Detail in function of voltage at high-resolution (370-390nm of wavelength).**
Device 19: lithium niobate, type G.
Electrical value for saved measures collected in Fig. 4.27.
Table 3.1 contains an index of experiments..

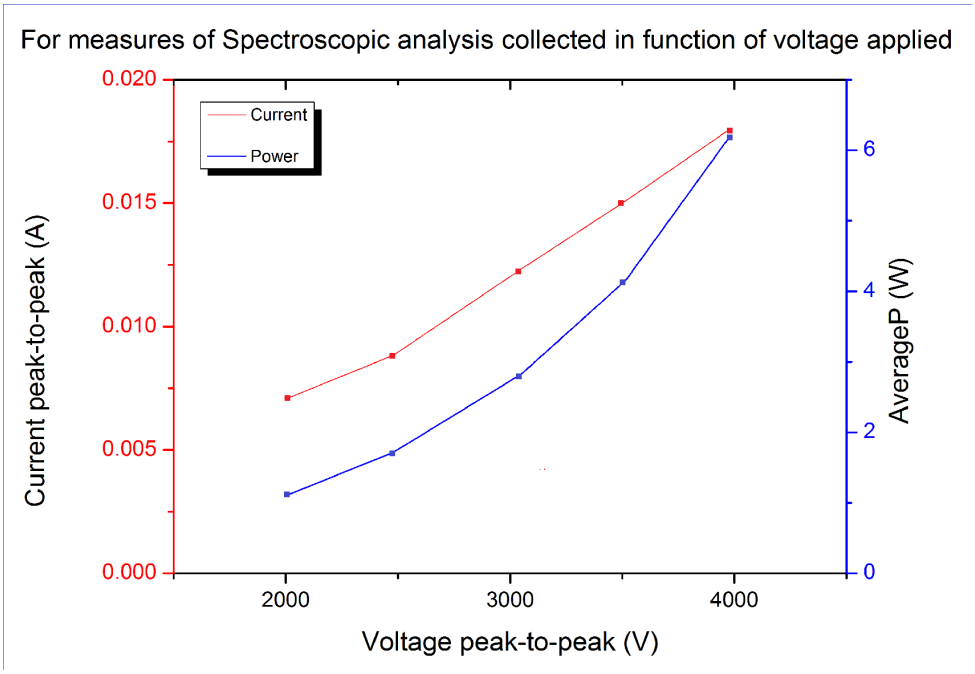

figure 4.27 **Head bands for Nitrogen second positive system states in the plasma's emission spectrum: Electrical value for saved measures of Fig. 4.26.**
Device 19: lithium niobate, type G.
Table 3.1 contains an index of experiments..

Examples of the influence of frequency that corroborate the previous statement (an increase in frequency results in an increase in intensity) can be found in Fig. 4.28 developed from measurements taken on device 3 (quartz, type C) for different values of frequency and voltage.

It is important to know that in this case the experiments were not performed at the same voltage but at a similar level of brightness that would allow obtaining the spectroscopy correctly. That is why the results must be studied qualitatively. Because, in addition, this spectroscopic analysis, unlike those contained in Fig. 4.25 and 4.26, in which the device was only turned on for that purpose, were instead made throughout the electrical characterization experiment of the device in question, so that the device was on for a considerable time as well as subjected to many charges and discharges in a short time. The voltage data to which each measurement was saved are included in the caption of the figure.

Finally, Fig. 4.29, which compares the spectra obtained for different devices (19 and 16) that both use lithium niobate for the barrier. Regarding the influence of material of the barrier, lithium niobate presents greater intensity for same values of voltage than quartz, due to it gets more current for same voltage; and in an analogous way, Fig. 4.29 shows the influence of the electrode configuration regarding said reasoning.

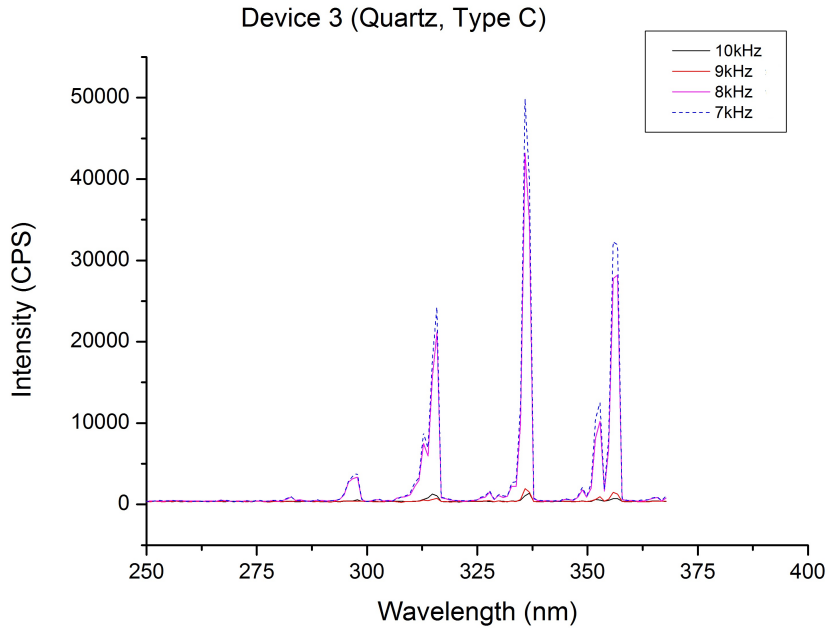

figure 4.28 **Head bands for Nitrogen second positive system states in the plasma's emission spectrum: Detail in function of frequency at low-resolution.**

Device 3: quartz, type C. Table 3.1 contains an index of experiments.

The voltage data to which each measurement was saved are the following: 6.844 kV_{pp}-0.0305A_{pp}(measured at 10 kHz), 6.91 kV_{pp}-0.02975A_{pp} (measured at 9 kHz), 8.256 kV_{pp}-0.03372A_{pp} (measured at 8 kHz) and 8.332 kV_{pp}-0.03186A_{pp} (measured at 7 kHz)..

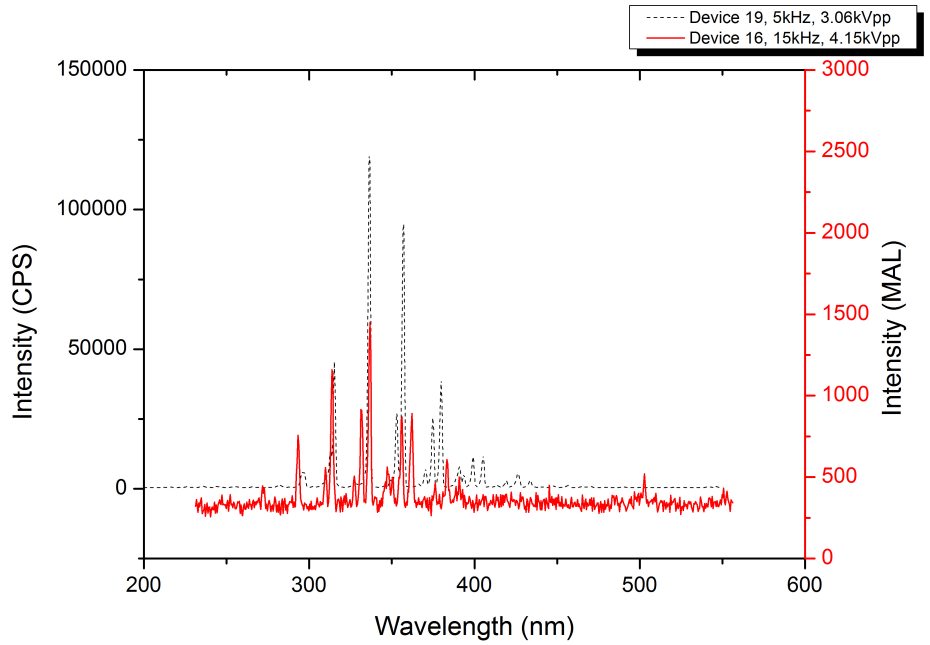

figure 4.29 **Head bands for Nitrogen second positive system states in the plasma's emission spectrum: Comparison between different electrode configurations, both in lithium niobate.**
Device 16 and 19. Table 3.1 contains an index of experiments.
It is important to know that in this case the experiments were not performed at the same current conditions. That is why the results must be studied qualitatively. .

Vibrational Temperature

According to the study found in the reference [143], under conditions of atmospheric discharge, the temperature of the gas can be estimated through the rotational temperature of a molecule, because rotational energy levels are closely spaced ($10^{-3} eV$) and they allow quick transfers of energy between two energy modes. This article tells *"The population distribution inthe rotational energy level of N_2 is also believed to fit Boltzmann distribution due to the dense collisions between molecules. [...] By assuming a rotational temperature and considering the dipole radiation probability and the response function of the monochrometer, one can calculate the profile of a certain emission band. The actual rotational temperature (T_r) can be determined through comparing the experimental measurement and theoretical calculation.[...] Here, in surface discharge, the vibrational excitation of nitrofen seems to be the most important. $N_2(C^3\Pi_u)$, which is not a metastable state, is generated from the ground-state electron impact excitation an the cascading effect is not important for the $N_2(C^3\Pi_u)$ state population. Therefore, the vibrational temperature can be determined according to the ratio of two lines in the $N_2(C)$ second positive system. The spectra lines at 371.1nm and 380.5nm are selected to calculate the vibrational temperature (t_V), as follows in equation 4.3.´´*

For this reason a series of spectroscopy was measured with an increase in resolution, to obtain data contained in Table 4.3 used to build Fig. 4.30. In it, for the case of lithium niobate device 19, it can be verified how, from a certain voltage, the electronic vibrational temperature associated with the second positive state of the nitrogen states

remains approximately stable with the voltage growth (although with a slight decrease, which means a decrease in the movement –energy– of the electrons), which corroborates the conclusions presented in other studies consulted [0][143].

The consulted bibliography tells us that the rotational temperature is very sensitive to both: applied voltage and frequency. In addition, some bibliography teaches that the electronic vibrational temperature is independent of the material used as a barrier[0].

It is important to bear in mind that the calculated temperatures are an effective temperature measurement, with the aim of qualitative analysis, since the plasma we have is out of equilibrium.

$$1.1384 \cdot e^{-0.4952eV/T_e'} = \frac{I_{371.1}}{I_{380.5}} \tag{4.3}$$

Table 4.3 Vibrational temperature data for air plasma according to [143]. Results extracted from Fig. 4.26, and these data are represented in Fig. 4.30..

	Intensity [CPS]			**Vibrational temperature** [eV]
Voltage [kV]	$I_{371.1nm}$	$I_{380.5nm}$	$A = \frac{I_{371.1}}{I_{380.5}}$	$T = -0.4952/ln(A/1.1384)$
2	372	416	0.89423077	2.05123809
2.5	472	1190	0.39663866	0.469671758
3	920	7204	0.12770683	0.226362469
3.5	3974	23902	0.16626224	0.257405507
4	9614	64096	0.14999376	0.244327796

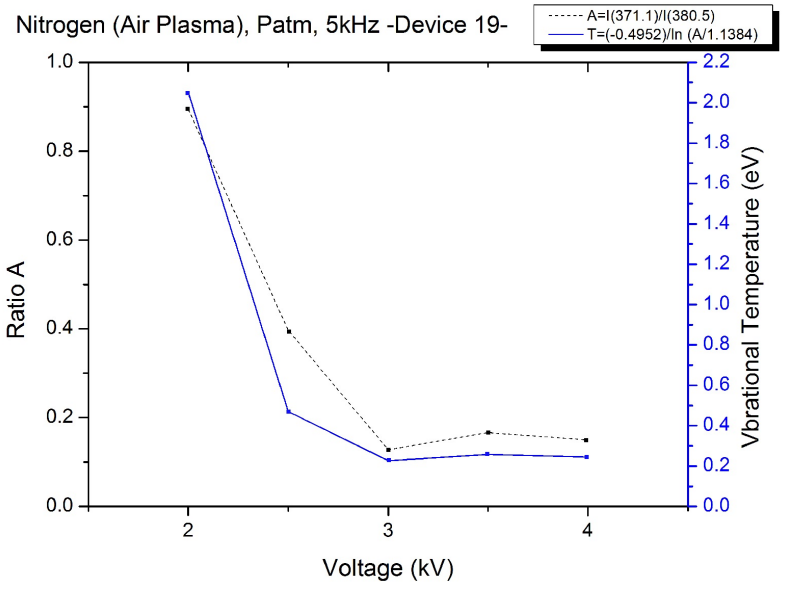

figure 4.30 Vibrational temperature for nitrogen of a air plasma, at 5 kHz and atmospheric pressure. Generated with device 19. Data from Table 4.3, including what is Ratio A referred to.
Table 3.1 contains an index of experiments.

.

Main spectroscopy results: summary

After analyzing the emission bands of the generated surface plasma, one has the main results included in Table 4.4.

Table 4.4 **Summary of main spectroscopy results.**.

MAIN RESULTS OF SPECTROSCOPIC ANALYSIS		
	The head bands optical spectrum of the nitrogen molecule are perfectly identified, corresponding to the vibrational transitions associated with the first and second positive states –Fig. 4.26–.	
Parameter	Behavior with intensity	Figure
Voltage (V)	The increase in voltage translates into a significant increase in the intensity of emission.	99
Frequency (f)	The increase in frequency translates into a significant increase in the intensity of emission.	100
Behavior of Vibrational temperature with voltage	From a certain value of voltage, the electronic vibrational temperature associated with the second positive state of the nitrogen states remains approximately stable with the voltage growth,although with a slight decrease, which means a decrease in energy of the electron.	102

4.3 Things to keep in mind about the materials during the experiments

During the course of this experimental work have taken place the following facts or appreciations regarding the materials of discharge barrier, such as wear or degradation and even breakage. It is important to know how the materials used as a substrate respond, in order to choose the most appropriate material to develop a device to market, where the operating conditions can be, in addition to prolonged, more extreme than those carried out in this experimental work . The most notable observations are listed below:

1. It is necessary to be careful with the realization of welds on the copper already adhered to the dielectric discs, especially for the case of lithium niobate, avoiding in this case if it is possible to carry them out on it. This has to do with the thermal shock that the material receives, which together with the pressure of the welder, can cause the material to break, as happened on one occasion with one of the devices on lithium niobate while it was being manufactured. In addition, in general, special care must be taken in the handling of lithium niobate discs due to their fragility.

2. The discs do not show a great deal of degradation after the experiments, at least not enough to alter the results of the experiments excessively. Although we must be aware that we must always try to ensure that the measurements are taken correctly the first time (for example, avoiding repeating a measurement or having to discharge the disc to return to a breakdown point that we would not have realized), since the heating of the disc as well as the accumulation of charge in ferroelectrics would introduce new variables that would not correspond with the rest of the measurements taken in the rest of the experiments.

3. In order to preserve the subtracts of the devices in the best possible state, the experiments must be carried out as quickly as possible, although always carrying out the electric charge process in a moderate and controlled manner. It is as much about avoiding the excessive heating of the disc as of the excessive accumulation of charge in the case of ferroelectrics, which leads to an affectation in the results introducing other parameters of influence to the study.

   Regarding the electric arcs, only two short circuits were experienced during this work: one of them took place at the beginning of experiment 2 and it was considered that the reasons had nothing to do with the device itself, and during the development of the study of the influence of the voltage in the spectroscopy performed on device 19, which broke during the application of a peak-to-peak voltage of 4.5 kV at 5 kHz of frequency (twice its breakdown voltage approximately at this frequency), because it had been on for a long time and probably would have a high value of accumulated charge.

   After the mentioned breaks of the lithium niobate discs, they were unusable. Regarding its break during the spectroscopy experiment, the reasons can be based on the fact that when applying such a high voltage and due to its crystalline structure, a piezoelectric effect appears. As the frequency increases, this effect becomes

increasingly greater until the crystals do not support the stresses that are produced and therefore break; said ruptures may be due to defects of the crystalline network produced during the manufacture of the material.

It was not the object of this study to bring the materials to a limit state.

5 Conclusions

In the present work, consistent with the objectives set out in Section 1.1, a series of flow control devices have been developed and characterized electrically and spectroscopically, studying the influence of the geometrical configuration of their electrodes, the dielectric material used as substrate, the pressure and the frequency in the ignition of superficial plasma generated by Dielectric Barrier Discharge. In Chapter 4, there were exposed the results of the analyzes carried out, and in Fig. 4.2 and 4.4 respectivelly one can find a summary of the main results. Now, as conclusion, briefly, the following is expressed:

- **About ignition voltage and current**

  The ignition voltage of this surface plasma decreases with frequency increase to a saturation value.

  The current shows a behavior proportional to the voltage, in this case the frequency increases as does the current to a saturation value.

- **Existence of an optimal frequency**

  There is an optimal point of operation with respect to the frequency, which is around 5 kHz. Operating around said value, a maximum of accumulated charge (and in capacitance) is obtained in the devices regardless of the dielectric material used, the air pressure value, or the geometrical configuration of the electrodes. All the operational parameters studied reflect a turning point in said frequency value, widely discussed in Chapter 4.

  Related to the current generated, it was found that as the ignition voltage decreased when frequency increases, the current at that breakdown point grew, thus achieving more efficient devices. Likewise, logically, the lithium niobate was the material that offered the most behavior since although the current ranges in which it is located are similar to the rest of materials, this current was achieved at much lower voltage.

- **About influence of pressure**

  it is demonstrated that the decrease in pressure favors ionization, thus decreasing the ignition voltage values.

- **About geometrical configuration of electrodes**

  It is verified that decreasing the distance between the active electrode and the ground electrode favors the ignition, in such a way that it diminishes the necessary voltages. Likewise, the use of multi-band electrode configurations also increases this advantage.

  Different configurations of electrodes have been tried in an attempt to increase the plasma-covered surface, reaching a maximum around one millimeter wide at the ignition time.

- **About dielectric material**

  The greater the dielectric constant, the lower the ignition voltages despite being around similar values of generated current, so that the power consumption is lower –this difference in power consumption increases as the frequency increases–. The best results regarding this definition of energy efficiency have been obtained for lithium niobate; this is due to the fact that it has more capacity to accumulate electric charge and therefore requires less voltage to generate the discharge again.

- **About spectroscopy**:

  All the nitrogen emission head bands of the second positive system have been successfully identified, since there is an air plasma; verifying that the pattern matches for the different operational and geometrical parameters studied, being independent the pattern with frequency or applied voltage. The intensity of the emission bands increases with voltage and frequency.

  As the applied voltage increases, the vibrational temperature decreases although stabilized around a saturation value from a certain voltage value.

List of figures

List of Tables

A. In relation to Paschen curves

Related to the theory exposed in Subsection “Breakdown voltage and Paschen curves” in Page 22 a similar representation has been made with data extracted from experiments of Phase 2 on lithium niobate in function of frequency. The representations, Voltage vs. *pg*, are included in Fig. 1 and 2.

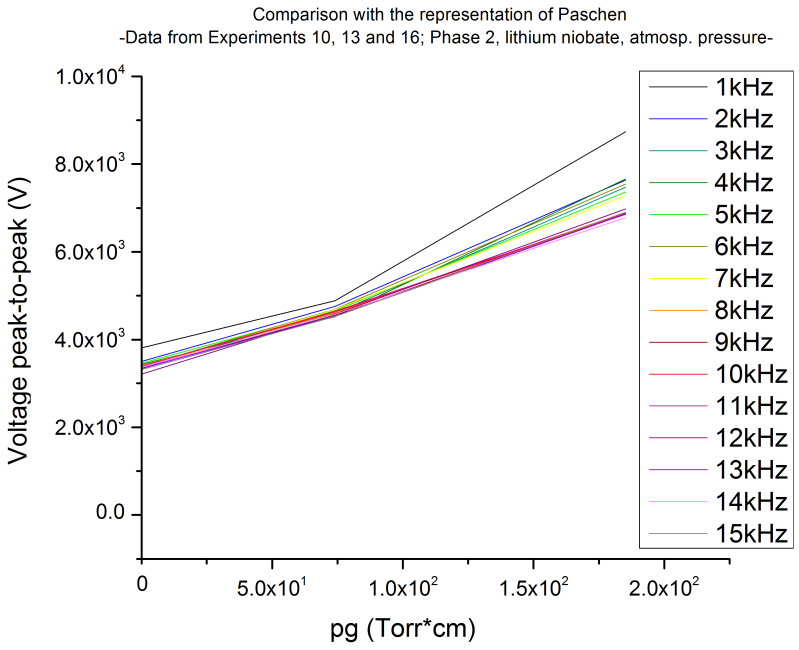

(a) Phase 2-Lithium niobate for different gaps and frequencies, at atmospheric pressure. Type D configuration, Experiments 10, 13 and 16..

figure 1 **Representations related to Paschen curves I. Examples with lithium niobate.** Table 3.1 contains an index of experiments..

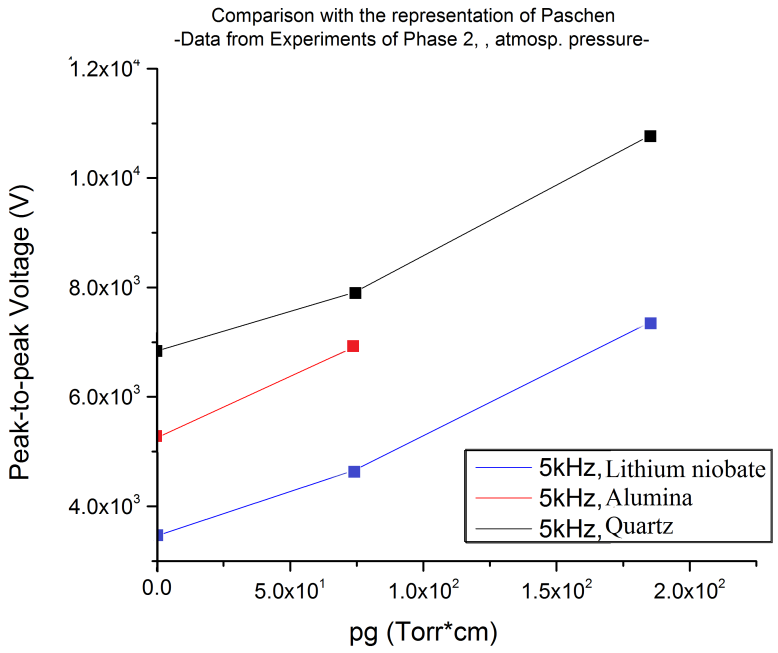

(a) Figure a) compare to quartz (Exp. 8, 11 and 14) and alumina (Exp. 9, 12 and 15) for 5 kHz..

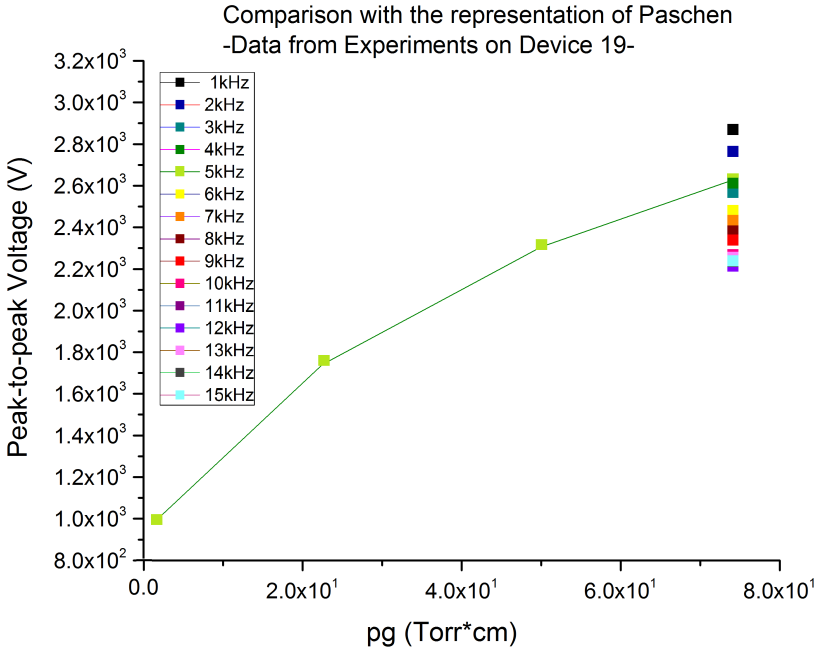

(b) Comparison between device 19 in function of pressure and frequency (Exp.19 and 21)..

figure 2 **Representations related to Paschen curves II. Examples with lithium niobate.** Table 3.1 contains an index of experiments..

B. Other thesis about DBD actuators

Respect to conclusions extracted from works about SDBD actuators (not necessary referred to breakdown values), is interesting to know that it has been verified the following:

- The power consumption increases with the increasing applied voltage [124] –see Fig. 1–.

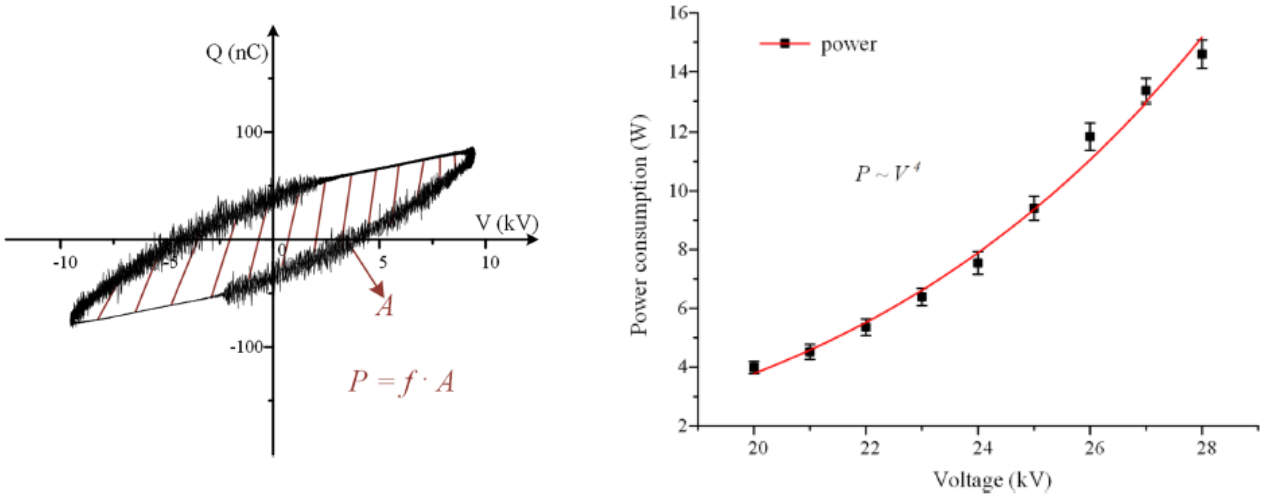

(a) *Q-V* Lissajous Figure.. **(b)** Power..

figure 1 **Power consumption of SDBD actuator with different applied voltage.**
Source of the image: [124]..

- The surface temperature of dielectric increases with the increasing applied voltage [124] –see Fig. 2–.
- The induced flow velocity increases and then decreases with the widening gap between two electrodes. With the increase in voltage, the induced airflow velocity has also an increasing tendency [124] –see Fig. 3 and 4–.
- The SDBD plasma actuator can effectively suppres the flow separation[124] [0] –see Fig. 5 and 6–.

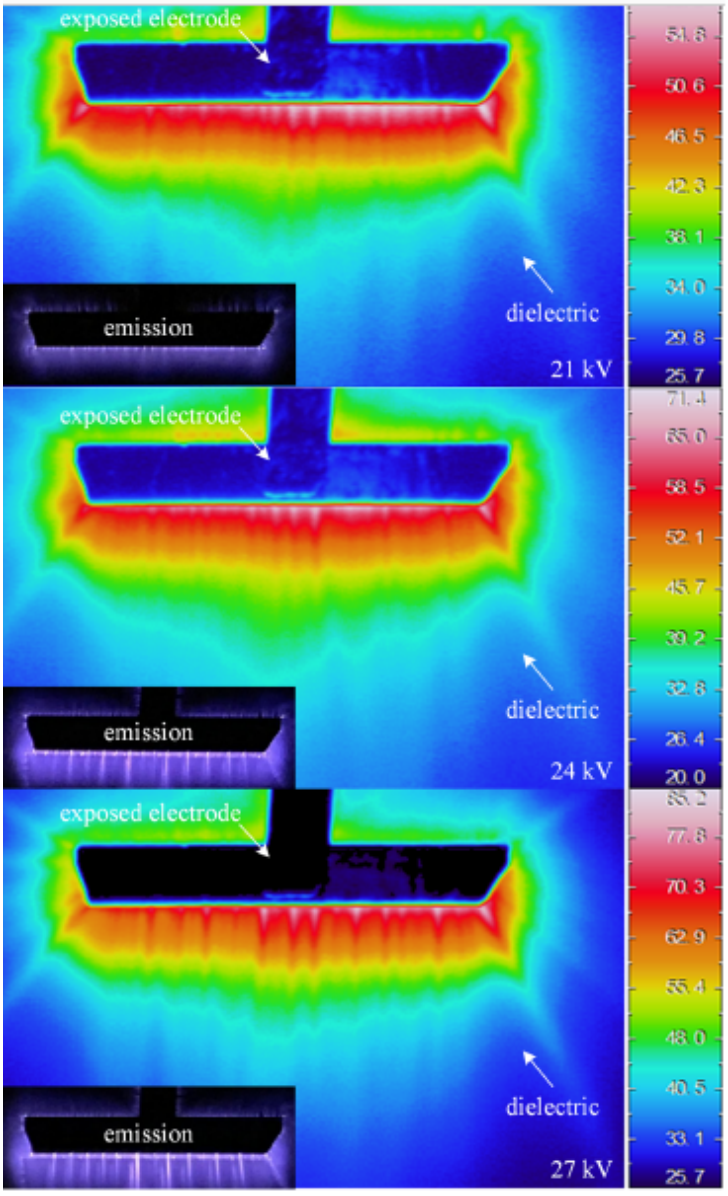

figure 2 **Temperature distribution of dielectric surface with different applied voltages.**
Source of the image: [124]..

- With the enlargement of the electrode gap, the discharge voltage increases slightly as a result of the increasing actuator impedance; while the discharge current increases first and then decreases by the combined effects of applied voltage and electrode gap [125] –see Fig. 7 and 8–.
- Variation of electric power consumption with the electrode gap shows a similar trend with that of discharge current. As for a fixed applied voltage, the critical electrode gap corresponding to the maximum power is slightly larger than that of the maximum current [125] –see Fig. 9–.
- Variations of the velocity of induced flow are in accordance with that of the discharge power. Optimal electrode gaps corresponding to the maximum induced flow velocity are obtained, related with the different applied voltage [125].

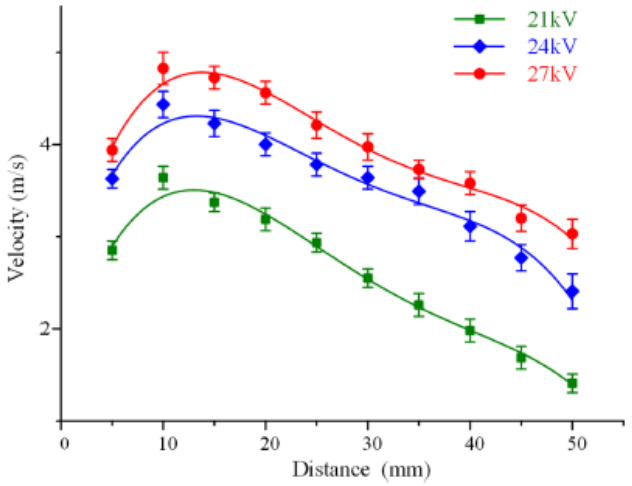

(a) Induced flow velocity with the widening gap between two electrodes..

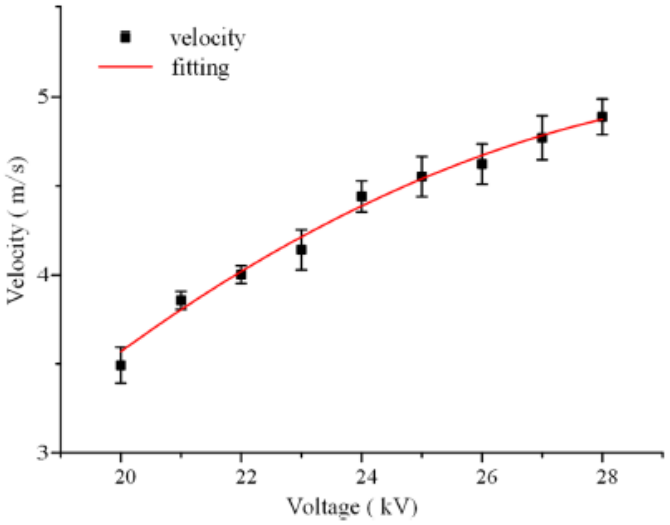

(b) Induced flow velocity with different applied voltages..

figure 3 **Induced flow velocity.**
Source of the images: [124]..

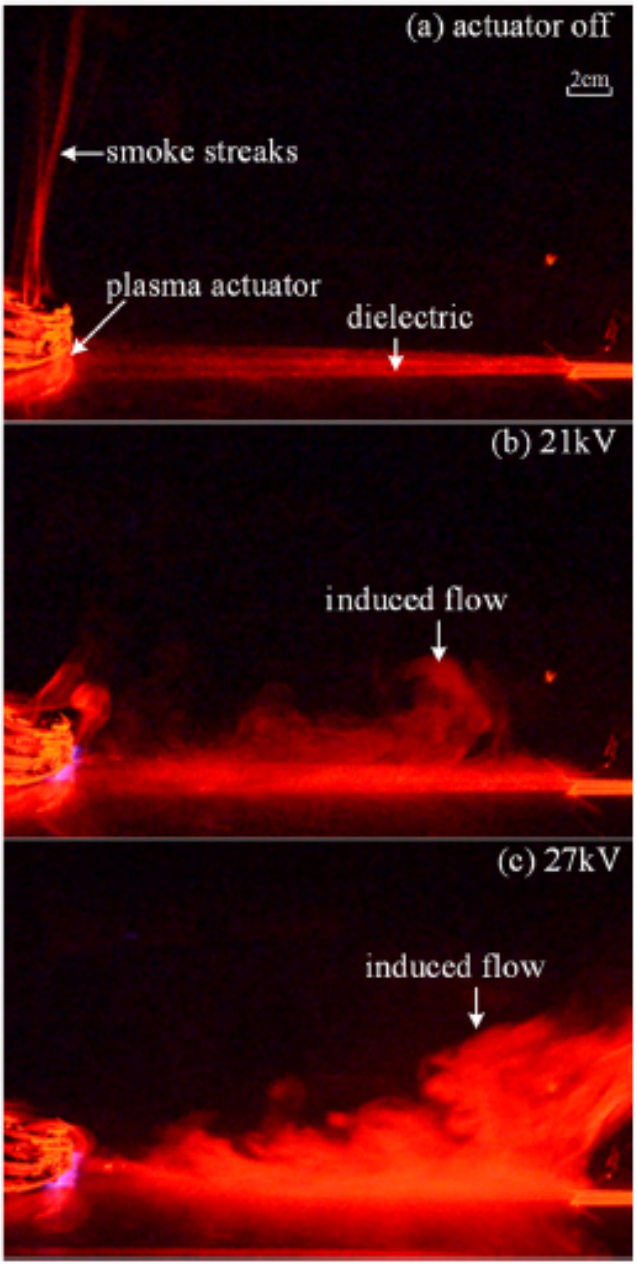

figure 4 **Smoke visualization of induced flow with different applied voltages.**
Source of the image: [124]..

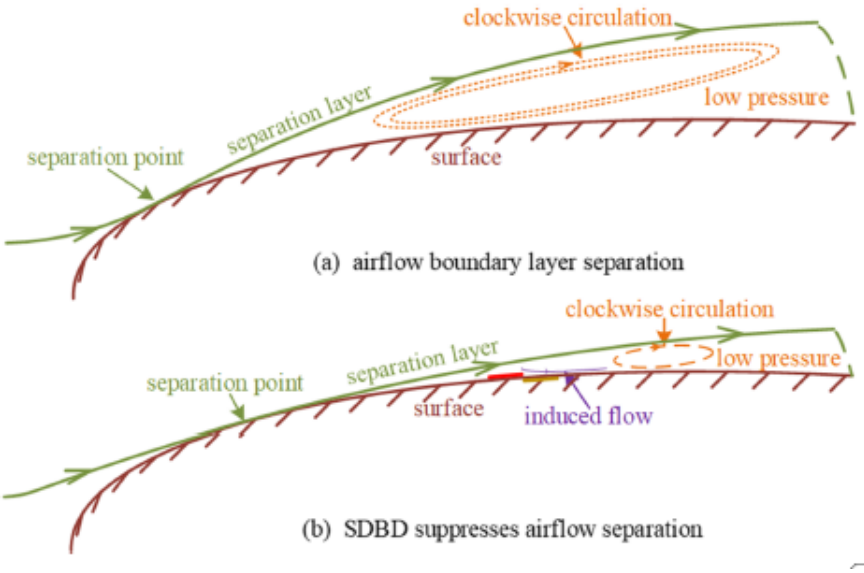

(a) Schematic of SDBD flow control..

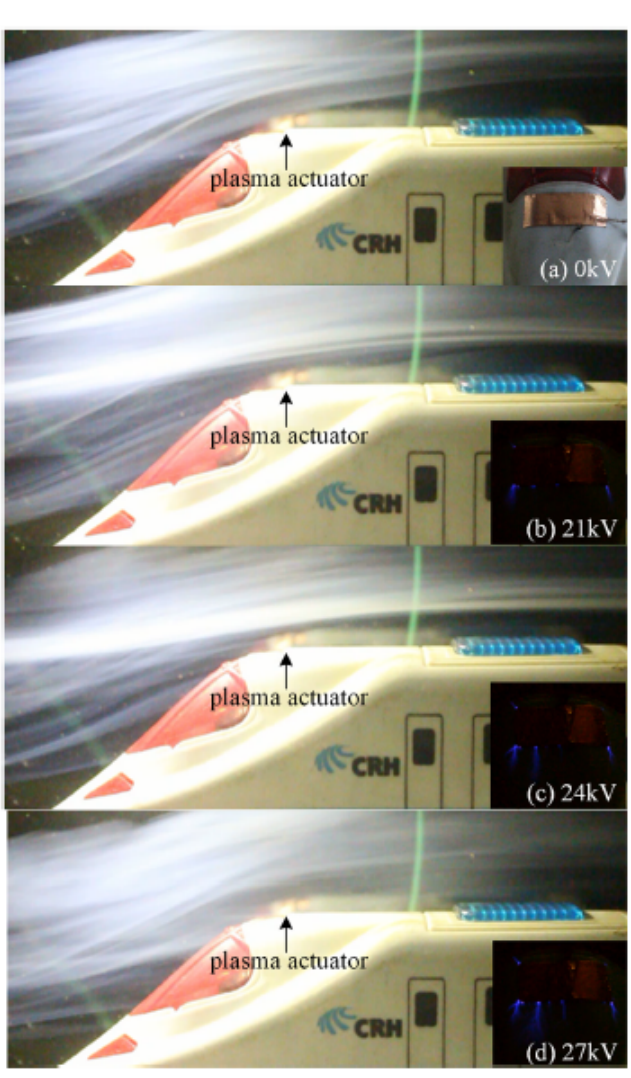

(b) Train head..

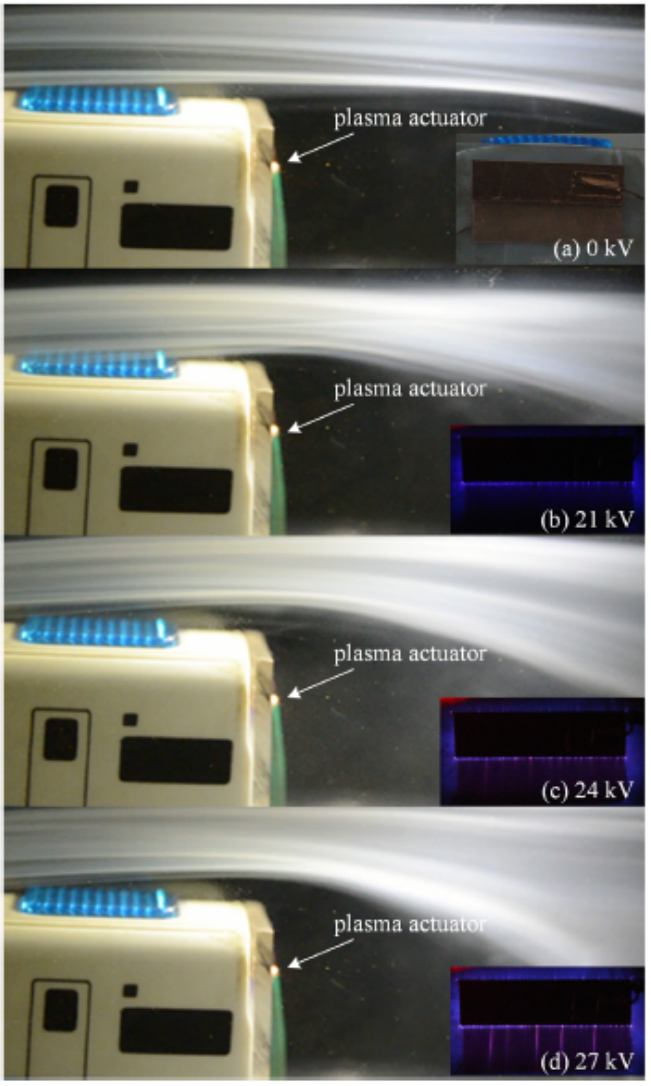

(c) Train rear..

figure 5 **Smoke visualization of gas flow around the train head/rear (with the SDBD installed) with different applied voltages.**
Source of the images: [124]..

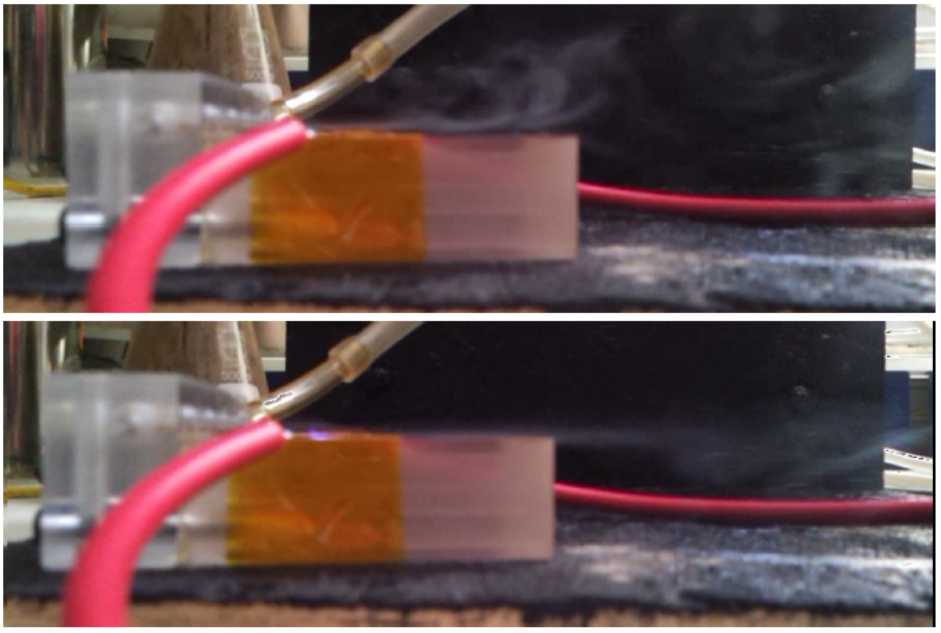

figure 6 **Pictures of the device designed to the demonstration of flow control.** In the upper image the discharge is off, and in the second the plasma the discharge is on. *Source of the images: [0].*.

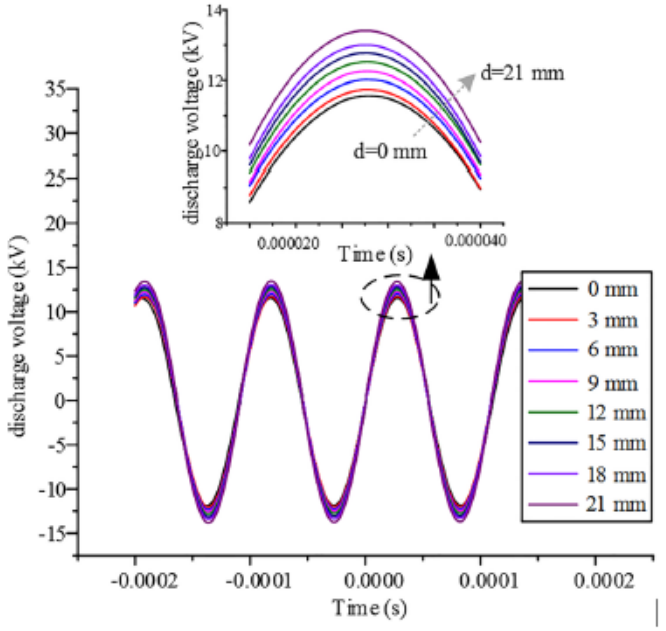

(a) Variations of discharge voltage with time at different electrode gaps..

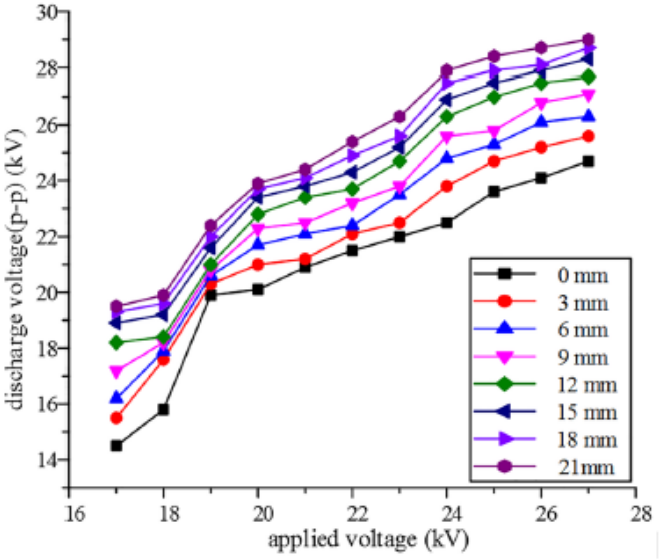

(b) Peak-peak value of discharge voltage under different conditions..

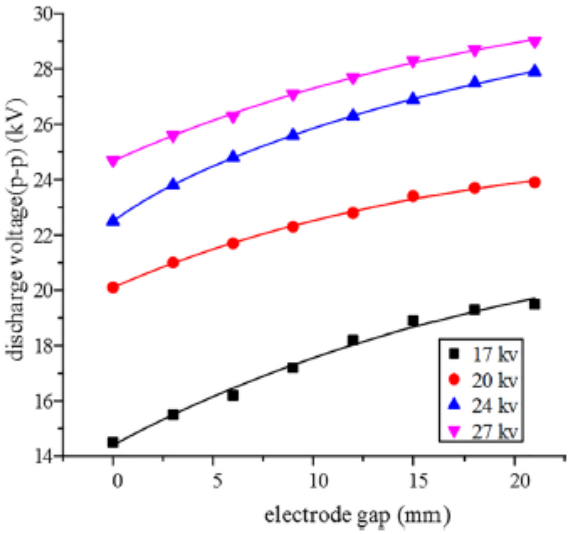

(c) Variation of discharge voltage with the electrode gap..

figure 7 **Discharge voltage with the electrode gap.** In the upper image the discharge is off, and in the second the plasma the discharge is on. *Source of the images: [125].*.

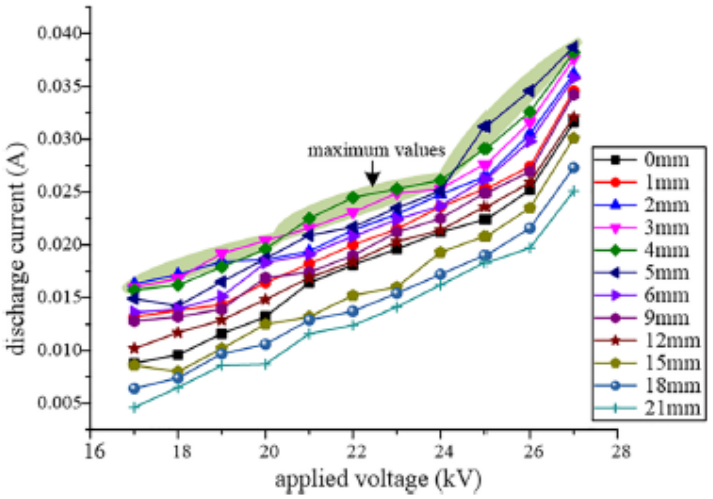

figure 8 **Variations of the discharge current with the applied voltage under different electrode gaps.**
Source of the images: [125]..

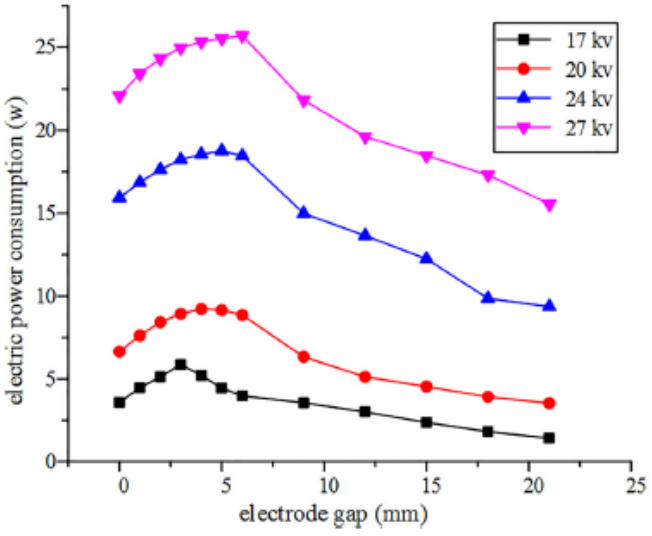

figure 9 **Variation of discharge power with the electrode gap.**
Source of the images: [125]..

C. Possible future line of reserach

Regarding possible lines with which to continue the work developed in this study with interest for aeronautical industry, the following proposals have been thought about the generation of plasma by dielectric barrier surface discharge:

- Study of the effect of humidity
- Study of the effect of temperature
- Study of the thickness of the dielectric (height)
- Limit study of devices
- Study with different types of air currents
- Research with more materials
- Research with ferroelectric materials or high dielectric constant
- Development of devices in which the dielectric is embedded
- Development of devices in which part of the electrodes are encapsulated in the substrate
- Different ways of developing the electrodes, for example, by deposition of microns thick conductive coatings through plasma
- To develop multi-band devices with microns of thickness between the bands through high accuracy manufacturing systems such as lasers
- Study of the influence of the shape of the dielectric, adapting it, for example to the curve of the part of the aerodynamic profile in which it could be placed, and to study efficiency
- Ionic wind measurement
- etc.

Bibliography

[0] García Camacho, Miguel. Control de flujo aerodinámico con descarga de barrera dieléctrica. Facultad de Física. Universidad de Sevilla. 2016.

[1] Robin Pul. Dielectric Barrier Discharge Plasma Actuators for Unsteady Aerodynamic Load Control. Master of Science Thesis. Delft University of Technology. 2013.

[2] Langmuir, I. Oscillations in Ionized Gases. Proceedings of the National Academy of Sciences. 14 (8): 627–637. 1928.

[3] E. Nasser. Fundamentals of gaseous ionization and Plasma Electronic. Wiley-Interscience. 1971.

[4] José Antonio Vallés Abarca. Descargas eléctricas en gases y plasmas: aplicaciones.

[5] Greaves, R. G.; Tinkle, M. D.; Surko, C. M. Creation and uses of positron plasmas. Physics of Plasmas. 1994.

[6] J. R. Hollahan. Techniques and Applications of Plasma Chemistry. John Wiley & Sons Inc. 1974.

[7] Chen, Francis F. Introduction to Plasma Physics and controlled fusion. Springer International Publishing. PP. 2-3. ISBN 9781475755954. 1984.

[8] Freidberg, Jeffrey P. Plasma Physics and Fusion Energy. Cambridge University Press. P. 121. ISBN 9781139462150. 2008.

[9] Hazeltine, R.D.; Waelbroeck, F.L. The Framework of Plasma Physics. Westview Press. ISBN 978-0-7382-0047-7. 2004.

[10] Morfill, G. E.; Ivlev, Alexei V. Complex plasmas: An interdisciplinary research field. Reviews of Modern Physics. 2009.

[11] Plasma, the fourth state of matter. Plasma, Ion and Electron Beam Technologies (Company). www.piescientific.com/Resource_pages/Resource_Introduction_to_plasma

[12] Kizilyalli, M.; Corish, J.; Metselaar, R. Definitions of terms for diffusion in the solid state (IUPAC Recommendations 1999). Pure Appl. Chem. 71 (7):1307-1325. doi:10.1351/pac199971071307. 1999.

[13] Langmuir, Irving. Positive Ion Currents from the Positive Column of Mercury Arcs. Volume 58. Issue 1502. pp. 290-291. Science. 1923.

[14] Albert W. Hull and Irving Langmuir. Control of an Arc Discharge by Means of a Grid. Proc Natl Acad Sci USA. 15(3):218-225. 1929.

[15] J. R. Hollahan. Techniques and Applications of Plasma Chemistry. John Wiley & Sons Inc. 1974.

[16] Nuclear Engineering Course Notes. Massachusetts Institute of Technology.

[17] Temerin, M.; Mozer, F. S. Double Layers Above the Aurora. NASA Conference Publication, #2469. 1987.

[18] Block, L. P. A double layer review. Astrophysics and Space Science, vol. 55. no.1. pp. 59-83. 1978.

[19] Bulgakova, Nadezhda M. et al. Double layer effects in laser-ablation plasma plumes. Physical Review E (Statistical Physics, Plasmas, Fluids, and Related Interdisciplinary Topics), Volume 62. Issue4. pp. 5624-5635. 2000.

[20] Joos, G. Theoretical Physics. London & Glasgow: Blackie & Son Ltd. p. 271. 1951

[22] Peter Andrew Sturrock. Plasma Physics: An Introduction to the Theory of Astrophysical, Geophysical and Laboratory Plasmas. Stanford University, California. 1994.

[23] Chen, Francis.F. Introduction to Plasma Physics and Controlled Fusion. Springer, New York. ISBN 0306413329- 0CLC 9852700. 2016. p. 2. doi:10.1007/978-3-319-22309-4. ISBN 978-3-319-22309-4.

[24] M. Rodríguez Vidal y J. A. Vallés Abarca. Curso Electromagnetismo, Unidad Didáctica 3, Ondas electromagnéticas libres, Temas X y XI. UNED. 1977.

[25] P. C. Clemmow y J. P. Dougherty. Electrodynamics of Particles and Plasmas. Addison-Wesley. 1969.

[27] Quasi-neutrality - The Plasma Universe theory. www.plasma-universe.com.

[28] Ajay Peter Manuel. Numerical Investigations of the Plasma Actuator Flow Problem.

[29] Merlino, Robert L. Plasma Oscillations— An application of electrostatics and classical mechanics. University of Iowa. omepage.physics.uiowa.edu. 2012.

[30] J. R. Reitz, F. J. Milford y R. W. Christy. Fundamentos de la teoría electromagnética, 4º ed, Cap. 14. Addison-Wesley Iberoamericana. 1996.

[31] Nicholson, Dwight R. Introduction to Plasma Theory. John Wiley & Sons. ISBN 978-0-471-09045-8. 1983.

[32] J. P. Boeuf, Y. Lagmich, T. Challegari, and L. Pitchford. Electrohydrodynamic force and acceleration in surfaces discharges. AIAA 2006-3574; 37th AIAA Plasmadynamics and Lasers Conference, San Francisco, California, USA. 2006.

[33] Y. P. Raizer. Gas Discharge Physics. Springer. 1991.

[34] E. E. Kunhardt. Generation of large-volume, atmospheric-pressure, non-equilibrium plasmas. IEEE Transactions on Plasma Science. 28:189200. 2000.

[35] P. C. Clemmow y J. P. Dougherty. Electrodynamics of Particles and Plasmas. Addison-Wesley. 1969.

[36] N. S. J. Braithwaite. Plasma Sources Science and Technology. Introduction to gas discharges. 9(4):517527, 2000.

[37] J. Jolibois. Etude et développement dún actionneur plasma à décharge à barrière diélectrique application au contrôle d'écoulement sur prol dáile. PhD thesis. Université de Poitiers. 2008.

[38] B. M. Smirnov. Physics of Ionized Gases. Wiley Interscience. 2001.

[39] Alexander A. Fridman. Plasma Chemistry. Cambridge, UK: Cambridge University Press. p. 94. ISBN 0-521-84735-4. 2008.

[41] F. Delobeau. The environment of the earth. Reidel. 1972.

[42] Chapman, Brian. Chapter 3: Plasmas. Glow Discharge Processes: Sputtering and Plasma Etching. New York: John Wiley & Sons. p. 49. ISBN 978-0471078289. 1980.

[43] J. P. Boeuf. Applications and modeling of non-equilibrium plasmas. In Mathematical.

[44] Introduction to Plasma Physics and controlled fusion. Chen, Francis F. Springer International Publishing. pp. 2–3. ISBN 9781475755954. 1984.

[45] Freidberg, Jeffrey P. Plasma Physics and Fusion Energy. Cambridge University Press. p. 121. ISBN 9781139462150. 2008.

[46] Robinson M. Movement of air in the electric wind of the corona discharge. AIEE Trans. 1961.

[47] Slater, J. C.Atomic Shielding Constant. Phys. Rev. 36 (1): 57-64. doi:10.1103/PhysRev.36.57. 1930.

[48] PC Clemmow & JP Dougherty. Electrodynamics of particles and plasmas. Redwood City CA: Addison-Wesley. pp. § 7.6.7, p. 236 ff. ISBN 0-201-47986-9. 1969.

[49] Alexander A. Fridman. Plasma Chemistry. Cambridge, UK: Cambridge University Press. p. 94. ISBN 0-521-84735-4. 2008.

[50] L. G. Christophorou and J. K. Oltho. Fundamental Electron Interactions with Plasma Processing Gases. Physics of Atoms and Molecules. Kluwer Academic/Plenum Publishers. 2004.

[51] B. Smirnov. Physics of weakly ionized gases. Mir Publishers Moscow. 1981.

[52] Hippler, R.; Kersten, H.; Schmidt, M.; Schoenbach, K.M. Plasma Sources. Low Temperature Plasmas: Fundamentals, Technologies, and Techniques (2nd ed.). Wiley-VCH. Wiley-VCH. ISBN 978-3-527-40673-9. 2008.

[53] S. FlüggeThe glow discharge at low pressure. G. Francis. Encyclopedia of Physics, volume Volume 22: Gas Discharges 2, pages 53-61. Editor: Springer. 1956.

[54] R. Gadri and J. Roth. Glow discharge-like characteristics of a oaugdp revealed by computer modeling. 25th Anniversary. IEEE Conference Record Abstracts. 1998 IEEE International on Plasma Science, page 288, 1998.

[55] Thornhill, W. The Z-Pinch Morphology of Supernova 1987A and Electric Stars. IEEE Transactions on Plasma Science, vol. 35, issue 4, pp. 832-844. 2007.

[56] Structure of a Glow Discharge. Princeton Plasma Physics Laboratory.

[57] L. B. Loeb. Electrical breakdown of gases with steady or direct current impulse potentials.

[58] C. Stees. Erste Ansätze einer neuen Strategie zur ezienten Modellierung eines Plasma Aktuators auf Basis des Verständnisses bestehender Modelle. Master's thesis. TU Darmstadt. 2008. 2008.

[59] F. Paschen. Ueber die zum funkenübergang in luft, wassersto und kohlensäure bei verschiedenen drucken erforderliche potentialdierenz. Annalen der Physik. 273(5):6996. 1889.

[60] K. Vollrath and G. Thomer. Funkenlichtquellen und Hochfrequenz- Funkenkinematographie. K. Vollrath. Editors: Kurzzeitphysik. Springer. pages 76-165. 1967.

[61] Friedrich Paschen. Ueber die zum Funkenübergang in Luft, Wassersto und Kohlensäure bei verschiedenen Drucken erforderliche Potentialdierenz. Annalen der Physik. 273 (5): 69-75. 1889.

[62] F. Paschen. Ueber die zum funkenübergang in luft, wassersto und kohlensäure bei verschiedenen drucken erforderliche potentialdierenz. Annalen der Physik. 273(5):69-96, 1889. 1889.

[63] Y. P. Raizer, M. N. Shneider, and N. A. Yatsenko. Radio-Frequency Capacitive Discharges. CRC Press. 1995.

[64] W. Siemens. Ueber die elektrostatische Induction und die Verzögerung des Stroms in Flaschendrähten. Annalen der Physik. 178(9):66-122, 1857.

[65] Matsuno, Hiromitsu, Nobuyuki Hishinuma, Kenichi Hirose, Kunio Kasagi, Fumitoshi Takemoto, Yoshinori Aiura, and TatsushiIgarashi. Dielectric Barrier Discharge lamp. United States Patent 5757132.

[66] Dhali, S.K. and I. Sardja. Dielectric-barrier discharge for the removal of SO2 fromflue gas. IEEE International Conference on Plasma Science. IEEE Conference Record - Abstracts, 1989.

[67] Kogelschatz, Ulrich, Baldur Eliasson, and Walter Egli. From ozone generators to flat television screens: history and future potential of dielectric-barrier discharges. Pure Applied Chemistry, Vol. 71. No. 10, pp. 1819-1828, 1999.

[68] U. Kogelschatz. Dielectric-Barrier Discharges: Their History, Discharge Physics, and Industrial Applications. Plasma Chemistry and Plasma Processing. 23:146, 2003.

[69] Leroux, F.; Perwuelz, A.; Campagne, C.; Behary, N. Atmospheric air-plasma treatments of polyester textile structures. Journal of Adhesion Science and Technology. 20 (9): 939–957. 2006.

[70] Leroux, F. D. R.; Campagne, C.; Perwuelz, A.; Gengembre, L. O. Polypropylene film chemical and physical modifications by Dielectric Barrier Discharge plasma treatment at atmospheric pressure. Journal of Colloid and Interface Science. 328 (2): 412–420. 2008.

[71] Leroux, F. D. R.; Campagne, C.; Perwuelz, A.; Gengembre, L. O. Polypropylene film chemical and physical modifications by Dielectric Barrier Discharge plasma treatment at atmospheric pressure. Journal of Colloid and Interface Science. 328 (2): 412–420. 2008.

[72] Laroussi, M. Sterilization of contaminated matter with an atmospheric pressure plasma. IEEE Transactions on Plasma Science. 24 (3): 1188. 1996.

[73] Lu, X.; Naidis, G.V.; Laroussi, M.; Ostrikov, K. Guided ionization waves: Theory and experiments. Physics Reports. 540 (3): 123. 2014.

[74] V. I. Gibalov and G. J. Pietsch. The Development of Dielectric Barrier Discharges in Gas Gaps and on Surfaces. Journal of Physics D: Applied Physics. 33(20):2618, 2000. 2000.

[75] Aerosol charge distributions in Dielectric Barrier Discharges. European Aerosol Conference 2009 Karlsruhe. 2009.

[76] M. Laroussi, I. Alexeff, J. P. Richardson, and F. F. Dyer. The Resistive Barrier Discharge. IEEE Trans. Plasma Sci. 30, 158. 2002.

[77] Roth, J. Reece. Chapter 15.3 Atmospheric Dielectric Barrier Discharges (DBDs). Industrial Plasma Engineering: Volume 2: Applications to Nonthermal Plasma Processing (1st ed.). CRC Press. ISBN 978-0750305440. 2001.

[78] Source of the image: en.wikipedia.org/wiki/File:Filamentous_Dielectric_Barrier_Discharge.JPG

[79] Kao, Kwan Chi. Dielectric Phenomena in Solids. London: Elsevier Academic Press. 2004.

[80] Source of the image: https://en.wikipedia.org/wiki/File:Capacitor_schematic_with_dielectric.svg

[81] Daintith, J. Biographical Encyclopedia of Scientists. CRC Press. p. 943. ISBN 0-7503-0287-9. 1994.

[82] William Whewell. The Correspondence of Michael Faraday, Volume 3. Letter. William Whewell to Faraday. 1798. James, Frank A.J.L. The Institution of Electrical Engineers. London, United Kingdom. 996. ISBN 0-86341-250-5. 1996.

[83] Frederick Seitz; T. P. Das; David Turnbull; E. L. Hahn.Ferroelectrics and Antiferroelectrics. Werner Känzig. Solid State Physics. 4. Academic Press. p. 5. ISBN 0-12-607704-5. 1957.

[84] M. Lines; A. Glass. Principles and applications of ferroelectrics and related materials. Clarendon Press, Oxford. ISBN 0-19-851286-4. 1979.

[85] Enloe, C., McLaughlin, T., VanDyken, R., and Fuscher, J. Plasma structure in the aerodynamic plasma actuator. AIAA Paper 2004-0844, 2004.

[86] http://www.lambdaphoto.co.uk/pdfs/Inrad_datasheet_LNB.pdf

[88] Dmitriy M. Orlov. Modelling and Simulation of Single Dielectric Barrier Discharge Plasma Actuators. PhD thesis. University of Notre Dame, Graduate School of Aerospace, and Mechanical Engineering. 2006.

[89] Gad el Hak. Flow Control: Passive, Active, and Reactive Flow Management. Cambridge University Press, New York. 2000.

[90] Stephen P. Wilkison Thomas C. Corke, C. Lon Enloe. Dielectric barrier discharge plasma actuators for flow control. Annu. Rev. Fluid Mech. 42:505– 529, 2010.

[91] Adil Bouchmal. Modeling of Dielectric Barrier Discharge actuator - implementation, validation, and generalization of an electrostatic model. Master's thesis. Delft University of Technology. 2011.

[92] http://www.moreelectricaircraft.com/

[93] G. Touchard. Plasma actuators for aeronautics applications - state of art review. I.J. PEST, 2:1–25, 2008.

[94] Eric Moreau. Airflow control by non-thermal plasma actuators. J. Phys. D: Appl. Phys, 40:605–636, 2007.

[95] Dmitriy M. Orlov. Thomas C. Corke, Martiqua L. Single dielectric barrier discharge plasma enhanced aerodynamics: physics, modeling, and applications. Post. Exp Fluids, 46:1–26, 2009. 2009.

[96] Wei Shyy Balaji Jayaraman. Modeling of Dielectric Barrier Discharge-induced fluid dynamics and heat transfer. Progress in Aerospace Sciences, 44:139– 191, Progress in Aerospace Sciences. 2008.

[97] Zyga, Lisa. What causes ionic wind? Phys.org. 2018.

[98] N. Bénard, N. Balcon, and E. Moreau. Electric wind produced by a surface dielectric barrier discharge operating in air at dierent pressures: aeronautical control insights. Journal of Physics D: Applied Physics. 41(4):042002 (5pp). 2008.

[99] Enloe, C., McLaughlin, T., VanDyken, R., and Fuscher, J. Plasma structure in the aerodynamic plasma actuator. AIAA Paper 2004-0844, 2004.

[100] P. Versailles, V. Gingras-Gosselin, and H. Vo. Impact of Pressure and Temperature on the Performance of Plasma Actuators. AIAA Journal. 48:859863. 2010.

[101] Al-Khazali, Hisham A. H.; Askari, Mohamad R. Geometrical and Graphical Representations Analysis of Lissajous Figures in Rotor Dynamic System. IOSR Journal of Engineering.2 (5): 971–978. 2012.

[102] Sozer, E.B. Gaseous Discharges and Their Applications as High Power Plasma Switches. 2008.

[103] Ge Lei and Zhang Yuantao. A Simple Model for the Calculation of Plasma Impedance in Atmospheric Radio Frequency Discharges.

Plasma Science and Technology, Volume 16, Number 10.

[104] Demetrius T. Paris and F. Kenneth Hurd. Basic Electromagnetic Theory. McGraw-Hill, New York. ISBN 0-07-048470-8, pp. 512, 546. 1969.

[105] Electromagnetism for Engineers. P. Hammond. Pergamon Press. OCLC 854336.1969.

[106] Bagotskii, Vladimir Sergeevich. Fundamentals of electrochemistry.p. 22. ISBN 978-0-471-70058-6. 2006.

[107] Horowitz, Paul; Hill, Winfield.The art of electronics (3rd ed.). Cambridge University Press. ISBN 978-0-521-80926-9. 2015.

[108] www.electronics-tutorials.ws/accircuits/phase-difference.html

[109] Croft, Terrell; Summers, Wilford I. Reports on August 2003 Blackout, North American Electric Reliability Council website.

[110] American Electricians'Handbook (Eleventh ed.). New York: McGraw Hill. SBN 0-07-013932-6. 1987.

[111] Fink, Donald G.; Beaty, H. Wayne. Standard Handbook for Electrical Engineers (Eleventh ed.). New York: McGraw Hill. ISBN 0-07-020974-X. 1978.

[112] www.electronics-tutorials.ws

[113] www.uco.es/organiza/departamentos/quimica-fisica/quimica-fisica/QuiFis/L14_QF_10_11.pdf

[114] https://www.lenntech.es/periodica/elementos/n.htm

[115] What are Homonuclear Molecules and Hetero-nuclear Molecules? TheBigger.com

[116] A. Lofthus and P. H. Krupenie. J. Phys. Chem. The spectrum of molecular nitrogen. Data 6, 113307. 1977.

[117] G. Herzberg. Spectra of Diatomic Molecules. Molecular Spectra and Molecular Structure. Van Nostrand, Princeton. 1950.

[118] Kennelly, Arthur. Impedance. AIEE, 1893.

[119] Ortega, Manuel R. Lecciones de Física (4 volúmenes). Monytex. ISBN 84-404-4290-4, ISBN 84-398-9218-7, ISBN 84-398-9219-5, ISBN 84-604-4445-7. 1989-2006.

[120] Resnick,Robert & Krane, Kenneth S. Physics. Nueva York: John Wiley & Sons. ISBN 0-471-32057-9. 2001.

[121] Guoqiang Gao, Lei Dong, Kaisheng Peng, Wenfu Wei, Chunmao Li, and Guangning Wu. Comparison of the surface Dielectric Barrier Discharge characteristics under different cond.

[122] J. P. Richardson M. Laroussi, I. Alexeff and F. F. Dyer. The resistive barrier discharge. IEEE Trans. Plasma Sci, 30, 2002.

[123] D.D. Sijacic U. Ebert, I.R. Rafatov. Structure formation in a dc-driven ”barrier” discharge stability analysis and numerical solutions. 28th ICPIG. 2007.

[124] Lei Dong, Guoqiang Gao, Kaisheng Peng, Wenfu Wei, Chunmao Li, and Guangning Wu. Effects of surface Dielectric Barrier Discharge on aerodynamic characteristic of train. AIP Advances 7, 075112 (2017); doi: 10.1063/1.4995985. 2017.

[125] Guoqiang Gao, Lei Dong, Kaisheng Peng, Wenfu Wei, Chunmao Li, and Guangning Wu. Comparison of the surface Dielectric Barrier Discharge characteristics under different electrode gaps. Physics of Plasmas 24, 013510; doi: 10.1063/1.4974037. 2017

[126] P. Hammond. Electromagnetism for Engineers. Pergamon Press 1969 OCLC 854336.

[127] Purcell, E. M. Electricidad y Magnetismo. Reverté. p. 141. ISBN 9788429143195. 1988.

[128] Física general. Burbano de Ercilla, Santiago y Carlos Gracía Muñoz

[129] Regents of the University of California. Universe of Light: What is the Amplitude of a Wave? 1996.

[130] The development of the concept of electric charge: Electricity from the Greeks to Coulomb. Roller, Duane; Roller, D.H.D. Cambridge, MA: Harvard University Press. 1954.

[131] Feynman, Richard; Leighton, Robert; Sands, Matthew. Section 2-5: energy levels, 19: hydrogen atom. The Feynman Lectures on Physics 3. 1965.

[132] Fundamentos de Espectroscopía Raman. Capítulo 1. UPC Universitat Politècnica de Catalunya.

[133] S. B. Bayrama and M. V. Freamatb. Vibrational spectra of N_2: An advanced undergraduate laboratory in atomic and molecular spectroscopy.

Physics Department, Miami University, Oxford, Ohio 45056. 2012.

[134] G. Herzberg. Molecular Spectra and Molecular Structure, I. Spectra of Diatomic Molecules. Van Nostrand, Princeton. 1950.

[135] Friedrich Paschen. Ueber die zum Funkenubergang in Luft, Wassersto und Kohlensaure bei verschiedenen Drucken erforderliche Potentialdifferenz. Annalen der Physik 273 (5): 69-75.. 1889.

[136] H. R. Velkoff and J. Ketcham. Effect of an Electrostatic Field on Boundary-Layer Transition. AIAA. 6:1381-1383, 1968.

[137] J. R. Roth, D. Sherman, and S. P. Wilkinson. Boundary Layer Flow Control with a One Atmosphere Uniform Glow Discharge Surface Plasma. 1998-0328; 36th AIAA Aerospace Science Meeting and Exhibit; Reno, Nevada, USA. AIAA. 1998.

[138] Huang, J., Corke, T., and Thomas, F. Separation control over low pressure turbine blades. American Physical Society Division of Fluid Dynamics. vol. 47. 2002.

[139] Morris, S. C., Corke, T. C., VanNess, D., Stephens, J., and Dou- ville, T. Tip Clearance Control Using Plasma Actuators. AIAA Paper 2005-0782, 2005.

[140] Visbal, M. R., and Gaitonde, D. V. Control of Vortical Flows Using Simulated Plasma Actuators. AIAA Paper 2006-505, 2006.

[141] Corke, T. C., He, C., and Patel, M. Plasma aps and slats: an application of weaklyionized plasma actuators. AIAA Paper 2004-2127, 2004.

[142] The Identification of Molecular Spectra. R.W.B. Pearse and A.G. Gaydon. Third Edition. Chapman & Hall LTD. 1965.

[143] Max Mulder. Ying-hong Li, Yun Wu, Hui-min Song, Hua Liang and Min Jia. Plasma Flow Control, Aeronautics and Astronautics, Prof. 473-3, InTech.2011.

[144] A Short History of Ferroelectricity. Talari. 2009.

[145] Ferroelectridad y piezoelectricidad. Universidad de Navarra. Lesson 7. www4.tecnun.es/asignaturas/PFM_Mat/Prog/Ferroelecv2.pdf

[146] Source: http://iopscience.iop.org/article/10.1088/1009-0630/16/10/05/pdf

[147] Roth J R. Electrohydrodynamically induced airflow in a one atmosphere uniform glow discharge surface plasma. 25th IEEE Int. Conf. Plasma Science (Raleigh, USA). 1998.

[148] Roth J R, Sherman D M and Wilkinson S. P. Electrohydrodynamic flow control with a glow discharge surface plasma. AIAA. 2000.

[149] Roth J R, Sherman D M and Wilkinson S. P. Boundary layer flow control with a one atmosphere uniform glow discharge surface plasma. AIAA Meeting (Reno, USA) 1998.

[150] Chuan He, Thomas C. Corke, and Mehul P. Patel. Plasma Flaps and Slats: An Application of Weakly Ionized Plasma Actuators. Plas, Journal of Aircraft, Vol. 46. 2009.

[151] Sebastian Bürkle. Environmental Impacts on Dielectric Barrier Discharge Plasma Actuators. Master-Thesis. 2013.

[152] Yongqiang TIAN, Zhengke ZHANG, Jinsheng CAI, Leilei YANG Lei KANG. Experimental study of an anti-icing method over an airfoil based on pulsed dielectric barrier discharge plasma. Chinese Journal of Aeronautics Volume 31. 2018.

[153] Jinsheng Cai, Xuanshi Meng, Yongqiang Tian, Xuzhao Han. An experimental study of icing control using DBD plasma actuator. Article in Experiments in Fluids 58(8). August 2017.

[154] Nicole M. Houser. Manufacturing of DBD plasma actuators for degradation resistance. Dissertation. University of Toronto. 2013.

[155] Martina L. Post. Plasma actuators for separation control in stationary and oscillating airfoils. Dissertation. M.S.M.E. Notre Dame, Indiana. 2004.